NEURONAL BASIS OF V1 BINOCULAR NORMALIZATION

By

Blake Austin Mitchell

Dissertation

Submitted to the Faculty of the

Graduate School of Vanderbilt University

in partial fulfillment of the requirements

for the degree of

DOCTOR OF PHILOSOPHY

In

Psychology

August 9th, 2024

Nashville, Tennessee

Approved:

Alexander Maier, Ph.D.

Randolph Blake, Ph.D.

Mark Wallace, Ph.D.

Nicholas Priebe, Ph.D.

DEDICATION

To my family and Katelyn Mase

Thank you for being my anchor and my sail

ACKNOWLEDGMENTS

I extend my deepest gratitude to my advisor, Alexander Maier, whose guidance and support have been instrumental throughout this journey. I am also thankful to my committee members—Dr. Randolph Blake, Dr. Nicholas Priebe, and Dr. Mark Wallace—for their expert advice, constructive feedback, and continuous encouragement.

I am immensely grateful to Brock Carlson for his partnership in the trenches of data collection and experimentation. His meticulous approach, hands-on expertise, and unwavering positivity were fundamental to our success. Brock, you have got a friend in me for life.

I would also like to express my gratitude to my research collaborators—L. Daumail, M. Cox, K. Dougherty, B. Calrson, and J. Westerberg. Their contributions were pivotal in developing the publications that underpin Chapters 1 and 2 of this dissertation.

Heartfelt thanks are due to A. Bastos, D. Heeger, F. Tong, and J. Kaas for their advice and stimulating discussions that enriched my research experience. In a similar vein, my acknowledgment extends to M. Feurtado, I. Haniff, Dr. C. Jones, M. Maddox, Dr. S. Motorny, D. Richardson, M. Schall, Dr. K. Shuster, L. Toy, B. Williams, and R. Williams for their technical expertise and assistance, which proved to be crucial in navigating complex research challenges.

Special thanks to my sister, Skyler, for her artistic talent and graphic design skills, which brought to life several of the illustrations in this dissertation. Your creativity has added a unique and personal touch to my scientific narrative, making this journey all the more special.

Lastly, I acknowledge the financial support from National Eye Institute (1R01EY027402-03) and National Eye Institute Training Grant (5T32 EY007135-23) without which this research would not have been possible.

TABLE OF CONTENTS

LIST OF TABLES

LIST OF FIGURES

Summary

Our current understanding of how the brain merges input from the two eyes to manufacture binocular vision stems from a culmination of neurophysiological investigations. Through experimentation employing techniques such as autoradiographic tracers, researchers have been able to trace and visualize the convergence of inputs from both eyes within the primary visual cortex (V1) (Barton, 2004). These studies have revealed the existence of specialized *binocular* neurons that integrate signals from the two eyes, forming the foundation of binocular fusion and stereoscopic vision. Yet, it remains unclear precisely *how* binocular neurons in V1 achieve combination of each eye's input. That is, the rules and operations underlying binocular convergence in visual cortex have yet to be fully elucidated. In this thesis, three outstanding questions are addressed: (1) What sort of gain-control processes control V1 excitation when input is raised by a factor of two (opening and closing one eye), (2) What role, if any, does cell-to-cell variation in response properties play during the binocular integration process, and (3) How are processes of binocular integration distributed across the canonical cortical microcircuit in V1?

Introduction

Our brain's visual processing system demonstrates impressive capability in converting incoming light signals into a three-dimensional representation of our environment. In primates, including humans, the presence of two forward-facing eyes results in binocular vision (Barton, 2004). An essential function of the early visual centers in mammals with binocular vision is to integrate and align visual input from the left and right eyes to create a coherent perceptual image (P. O. Bishop & Pettigrew, 1986). This integration occurs swiftly and seamlessly (Blake & Wilson, 2011), enabling us to dynamically perceive the world as a cohesive whole.

Binocular vision offers several benefits over monocular vision (Barton, 2004). First, having two eyes enables improved estimation of distances and positions in three-dimensional space, known as stereopsis (J. Read, 2005), vital for tasks like judging the distance to prey, predators, or obstacles (Nityananda & Read, 2017). Second, having two eyes widens the field of view, enhancing peripheral awareness and aiding in the detection of potential threats or opportunities in the environment (Nityananda & Read, 2017). Having an extra eye also offers redundancy and reliability, as if one eye is compromised, the other can still function (Jones & Lee, 1981). Finally, vision is simply better with overlapping retinal stimulation – seeing something with both eyes simultaneously yields higher visual acuity (Blake & Fox, 1973), bolstering contrast sensitivity (Home, 1978), the detection of briefly flashed objects (Cogan et al., 1982), orientation discrimination (Bearse & Freeman, 1994), and subtle environmental cues (Parker et al., 2016). These advantages have evolved in various species to enhance their chances of survival and success in diverse ecological niches (Nityananda & Read, 2017).

The advantages of binocular vision not only enhance our perceptual experiences but also shed light on the intricacies of our visual system, which, in turn, may harbor potential for dysfunction. Indeed, research suggests that flawed binocular integration lies at the core of various visual deficits and diseases (Hess et al., 2014; Hess &

Thompson, 2015). Conditions such as amblyopia, strabismus, and other binocular vision disorders have been associated with abnormal binocular processing along the primary visual pathway (Birch, 2013; Huang et al., 2011; Mao et al., 2020; Sengpiel & Blakemore, 1996; Sincich et al., 2012; J. Zhou et al., 2016). By unraveling the neural mechanisms of binocular integration under healthy conditions, researchers aim to pave the way for targeted therapeutic interventions and improved clinical outcomes (Hess & Thompson, 2015).

Primary visual pathway

How does the brain accomplish binocular vision? Over the last six decades, neurophysiological studies have meticulously characterized the flow of monocular signals and emergence of binocular responses within the primary visual pathway (P. O. Bishop & Pettigrew, 1986; Blake & Wilson, 2011; Burkhalter & Essen, 1986; DeAngelis & Newsome, 1999; Ghose & Ts'O, 1997; Henriksen et al., 2016; J. C. Horton, 2006; Lehky & Maunsell, 1996; M. S. Livingstone & Tsao, 1999; Maunsell & Essen, 1983; Pack et al., 2003; Parker et al., 2016; Parker & Cumming, 2001; G. F. Poggio, 1995; G. F. Poggio & Fischer, 1977; Schroeder et al., 1990; Smith et al., 1997; Yang et al., 2011). Figure 1 provides an overview of the primary visual pathway.

The journey begins in the retina, where photoreceptor cells convert incoming light signals into electrical impulses (Hartline, 1948). These signals are then transmitted via the optic nerve, a bundle of axons from retinal ganglion cells, which exit the eye and travel towards the brain (Kuffler, 1953). At the optic chiasm, located at the base of the brain, some axons from each eye cross over to the opposite hemisphere, while others continue straight back on the same side (Haden, 1936). This crossover ensures that visual information from both eyes is integrated and processed in both hemispheres of the primate brain (Blakemore, 1970). Note that, despite what this crossing implies, there is no direct neural interchange between the signals from each eye at this juncture.

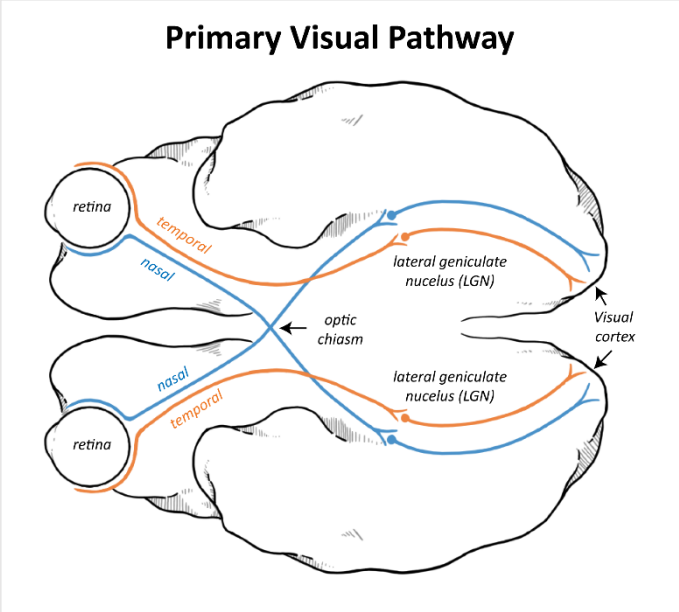

Figure 1. Primary visual pathway. Light signals captured by the retina travel through the optic nerves, optic chiasm, and optic tracts, are relayed by the lateral geniculate nucleus, and projected to the visual cortex for processing of basic image features; the temporal side of each retina (orange) stays in the ipsilateral hemisphere, while the nasal half (blue) crosses at the optic chiasm.

Upon crossing the optic chiasm, the axons carrying visual information from each eye synapse at the dorsal lateral geniculate nucleus (LGN) of the thalamus (G. H. Bishop & O'Leary, 1938). The LGN is a relay center that processes and relays visual information to the primary visual cortex (V1) in the occipital lobe (G. H. Bishop & O'Leary, 1938; Sherman & Guillery, 2002). Importantly, the LGN is organized into distinct layers, with each layer receiving inputs from either the left or right eye (O'Leary, 1940). The eye-specific inputs remain largely separate throughout much of their journey to the cortex

(Casagrande & Kaas, 1994; Kaas et al., 1978), though there do appear to be sparse intersections between adjacent layers of the LGN (Casagrande & Boyd, 1996; Kaas, 2015).

From the LGN, visual signals from each eye are transmitted to the primary visual cortex (V1), also known as the striate cortex, located in the occipital lobe at the posterior pole of the brain (G. H. Bishop & O'Leary, 1938; O'Leary, 1941; Tanaka, 1985). V1 is the primary target destination for LGN neurons and serves as a critical hub for the initial processing of visual information (D. H. Hubel & Wiesel, 1959). Neurons in V1 are organized into distinct functional columns and layers, each responsible for encoding specific features of the visual scene, such as orientation, color, spatial frequency, direction of movement, and retinal disparity (D. H. Hubel & Wiesel, 1962, 1968; D. Hubel & Livingstone, 1987).

Thalamocortical binocular convergence

Having traced the path of monocular signals from the retina to the primary visual cortex (V1), we now turn our attention back to the dorsal lateral geniculate nucleus (LGN) of the thalamus. While the LGN is traditionally viewed as a relay center for transmitting visual information from the retina to V1 (Sherman & Guillery, 2002), recent evidence suggests that it may also play a role in early binocular processing (Dougherty, Schmid, et al., 2019). The alternating eye-specific layers of the LGN have sparse interconnections (Casagrande & Boyd, 1996), and binocular interactions have been observed between them (Dougherty et al., 2021; Howarth et al., 2014; Schroeder et al., 1990; Vastola, 1960). These findings challenge the notion of strict segregation of inputs from each eye within the LGN and raise intriguing questions about the initial site of binocular convergence within the primary visual pathway (Maier et al., 2022).

In carnivores and primates, the primary target for LGN projections is the primary visual cortex (V1) (G. H. Bishop & O'Leary, 1938; O'Leary, 1940). Eye-specific LGN afferents extend via, what is called the optic radiation, to spatially segregated bands within the input-recipient layer of V1 (Layer 4 in carnivores and layer 4C in primates) (Balaram & Kaas, 2014; Kaas et al., 1978). This eye-specific termination pattern gives rise to neurons that are strongly innervated by one eye or the other, or so-called *monocular* neurons (D. H. Hubel & Wiesel, 1972). Figure 2 illustrates these monocular neurons in Layer 4 (using Hassler's (1967) laminar identification scheme) as a darker shade of blue and orange.

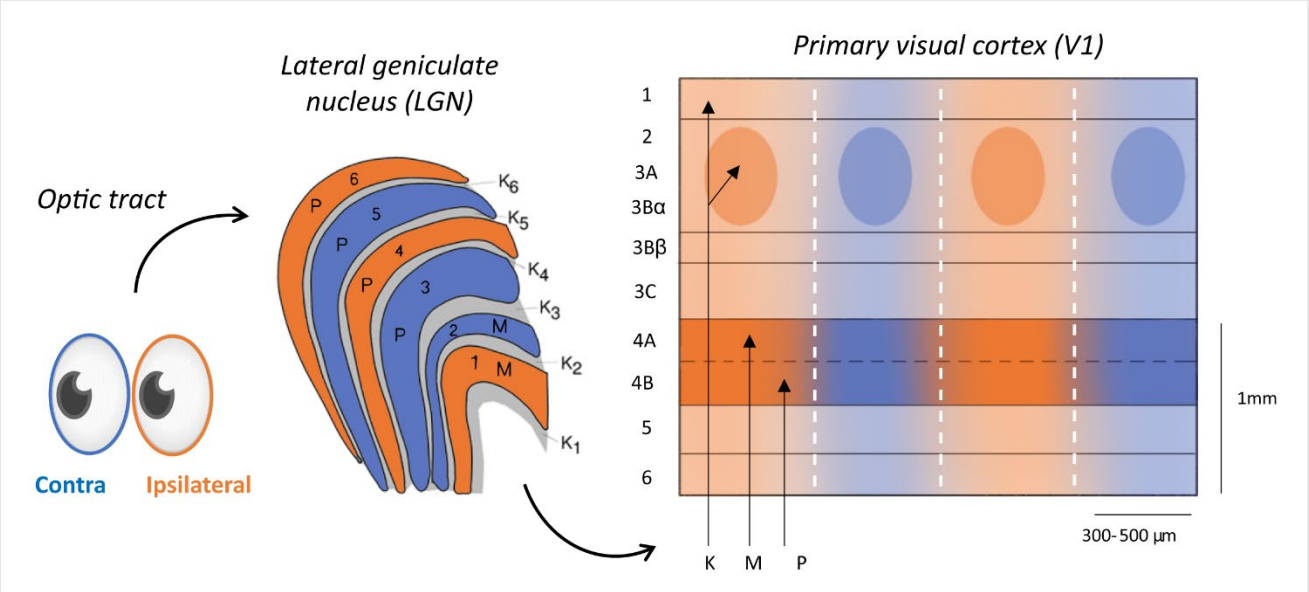

Figure 2. Diagram illustrating binocular convergence along the primary visual pathway. Visual information is received by the retina in each eye and transmitted through the optic nerves to the lateral geniculate nucleus (LGN). From the LGN, eye-specific signals, still largely segregated, are relayed to the primary visual cortex (V1), where binocular convergence occurs. Laminar identification follows Hassler's (1967) scheme.

At the next stage of processing, as information is taxied along the cortical microcircuit, segregation of the two monocular streams is finally lost (D. H. Hubel & Wiesel, 1969; McConnell & LeVay, 1986). Neurons in the input layers of V1 are directly connected to layer 2/3 neurons above (D. H. Hubel et al., 1975, 1976, 1977; M. Livingstone & Hubel, 1984). Importantly, these layer 2/3 neurons also receive inputs from layer 4 cells innervated by the other eye, as well (D. H. Hubel & Wiesel, 1962, 1968, 1972). Finally, layer 2/3 neurons send projections down to layer 5/6 neurons. When recorded using electrophysiology, neurons in layers 2/3 and 5/6 respond more equivalently to both eyes (Wiesel et al., 1974) as compared to neurons in layer 4, while still showing a preference for one eye or the other. This pattern of connectivity is what gives rise to the anatomical presence of ocular dominance columns (D. H. Hubel et al., 1976; D. H. Hubel & Wiesel, 1972; Shatz et al., 1977; Shatz & Stryker, 1978) and the laminar specificity of ocular dominance strength (Wong-Riley, 1979).

Both the anatomy and physiology suggest that superficial layer 2/3 neurons, and their downstream targets in layers 5/6 receive converging inputs from the two eyes (Hendrickson & Wilson, 1979; D. H. Hubel & Wiesel, 1972; Kaas et al., 1978; LeVay et al., 1985; Shatz & Stryker, 1978; Wiesel et al., 1974). These neurons are collectively referred to as *binocular* neurons. It follows then that the representation of both eyes' views can be largely attributed to the function of these V1 binocular neurons (Casagrande & Kaas, 1994). However, not unlike the challenges to the LGN conventions, there is accumulating evidence that binocular convergence in V1 is not as clear-cut as previously thought (Maier et al., 2022). Neurons in layer 4C of primate V1, even the most monocular among them, exhibit physiological binocular interactions when tested under binocular conditions (Dougherty, Cox, et al., 2019). Such interactions are supported by anatomical studies that have detailed collateral axon branches that extend between eye-specific bands in layer 4C (Blasdel & Lund, 1983). There is also evidence that interneurons situated between ocular dominance column borders may facilitate binocular modulation of L4 neurons (Blasdel et

al., 1985; Buzás et al., 2001). This suggests that the traditional model of binocular neurons residing exclusively in layers 2/3 and 5/6 is outdated (see Maier et al., 2022). Nonetheless, it is clear that V1 is the first cortical site along the primary visual pathway where the two monocular streams directly converge onto the same cells. Therefore, it is widely believed that one of the major functions of primary visual cortex is binocular integration.

Binocular gain control in V1

Binocular neurons in V1 face the challenge of integrating redundant yet slightly disparate sensory information from the two eyes, given the considerable overlap in their visual inputs (Ferster, 1981). While a straightforward solution might involve linear operations such as summing the outputs from both eyes, studies employing psychophysics reveal that binocular viewing only yields about a 1.4x improvement over monocular viewing (D. H. Baker et al., 2012, 2018; Blake & Wilson, 2011; Cagenello et al., 1993; Home, 1978). This modest improvement suggests that the visual system employs nonlinear processes to merge monocular information (D. H. Baker et al., 2018; Legge, 1984b). Recent theoretical work based on these findings propose that our visual system merge monocular information nonlinearly by executing processes of gain-control both within and between the eyes' inputs that depend on stimulus contrast (Ding et al., 2013b; Ding & Sperling, 2006). This collective set of processes is often referred to as the gain-control theory of binocular combination (Ding et al., 2013a; Ding & Levi, 2017; Ding & Sperling, 2006). These mechanisms are believed to optimize the integration of sensory information (Schwartz & Simoncelli, 2001), enabling the visual system to adapt to varying levels of contrast across different scenes and lighting conditions (Boynton, 2005) while extracting meaningful differences and similarities between the signals from the two eyes (Ding & Levi, 2021).

Although ample psychophysical evidence supports the gain-control theory of binocular combination (Ding et al., 2013b, 2013a; Ding & Levi, 2017, 2021; M. Georgeson et al., 2007; Liu & Schor, 1995; Meese et al., 2006; Yehezkel et al., 2016), neurophysiological evidence is still forthcoming. Various neurophysiological observations in V1 point to nonlinear processes governing binocular integration, including sublinear binocular responses (Longordo et al., 2013; Zhao et al., 2013) and nonlinear binocular interactions (Anderson & Movshon, 1989; D. H. Baker et al., 2012; Cox et al., 2019; Dougherty, Cox, et al., 2019; Priebe, 2008; Smith et al., 1997). However, the specific mechanisms underlying these binocular observations have not been the primary focus of most studies. Rather, research efforts have predominantly focused on elucidating the foundational gain-control mechanisms of neuronal responses in V1 to single stimuli (Albrecht, 1995; Albrecht & Hamilton, 1982; Bonds, 1991; Carandini et al., 1997; Carandini & Heeger, 2012; Heeger, 1992b). This work provides an excellent foundation to study the neuronal mechanisms of binocular gain-control in V1.

The magnitude of spiking responses in V1 is primarily determined by the strength of input, particularly stimulus contrast, and is typically described by a sigmoidal contrast response function (Albrecht & Hamilton, 1982; Heeger, 1992a, 1992b; Ohzawa et al., 1985; Truchard et al., 2000). Such a relationship underscores a gain-control mechanism in V1 which enhances weaker inputs while attenuating the effect of stronger inputs (Ohzawa et al., 1985; Truchard et al., 2000). An intriguing question arises regarding how the contrast-response relationship in V1 is altered when an additional input from the other eye is introduced, transitioning from monocular to binocular viewing (Fleet et al., 1997; Moradi & Heeger, 2009). Figure 3 illustrates two types of "binocular gain-control" or shifting of V1's contrast-response relationship between monocular (black) and binocular (red) viewing, inspired by investigations of the effects of adding an incompatible stimulus to the other eye on V1 responses (Sengpiel et al., 1998; Sengpiel & Blakemore, 1994). A response gain-control indicates a change in purely a neuron's firing rate under binocular stimulation, a change that is proportional to stimulus contrast (Sengpiel & Blakemore, 1994). Alternatively, a contrast gain-control indicates a change in a neuron's sensitivity to contrast under binocular condition, a change that alters the firing rate of a neuron that depends on stimulus contrast (Sengpiel & Blakemore, 1994). A study that can differentiate between these two kinds of binocular gain-control in V1 would hold promise for distinguishing between contrast-dependent and contrast-independent mechanisms governing V1 excitation under the common condition when the input to V1 is simply doubled.

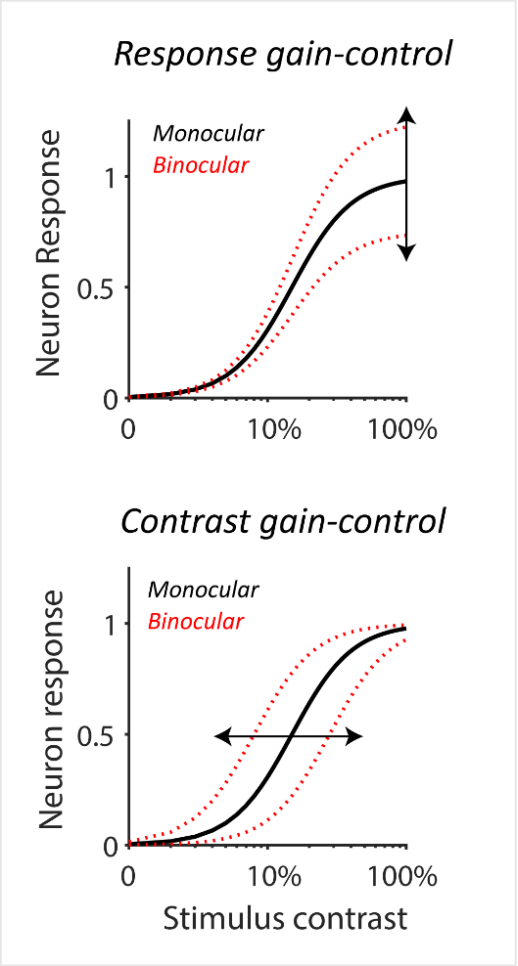

Figure 3. Theoretical types of binocular gain-control in V1. A response-set mechanism shifts the curve vertically along the ordinate (top), whereas a contrast-set mechanism shifts the curve horizontally along the abscissa (bottom).

The enigma of ocular dominance

Despite their discovery over six decades ago, the functional significance of ocular dominance columns remains uncertain (Adams & Horton, 2003; J. C. Horton & Adams, 2005). Early neurophysiological investigations hinted that ocular dominance may influence early visual processing of depth information (Gardner & Raiten, 1986; Gordon & Stryker, 1996; G. F. Poggio & Fischer, 1977). However, subsequent studies spanning six decades has not yielded conclusive evidence supporting this hypothesis (LeVay & Voigt, 1988; G. Poggio et al., 1988; J. C. A. Read & Cumming, 2004). And virtually all alternative hypotheses have been severely hindered by the extensive variability observed in the manifestation of ocular dominance columns among different species without apparent differences in visual faculties (Adams & Horton, 2009; J. Horton & Hocking, 1996a, 1996b). Some species, like certain squirrel monkeys, lack ocular dominance columns altogether or only exhibit them peripherally, yet their

visual abilities (including depth perception) remain intact (Adams & Horton, 2003).This has led to the consensus that ocular dominance columns do not serve a specific purpose for vision (J. C. Horton & Adams, 2005).

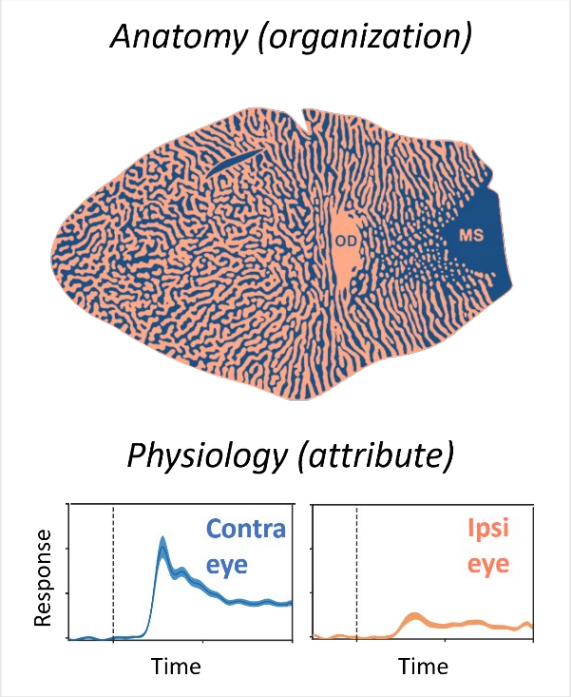

Figure 4. Ocular dominance is a physiological attribute that arises from the anatomy. Flattened V1 image was modified from Horton & Adams, 2003. Distinction between the anatomical organization of ocular dominance columns (top) and the physiological attribute expressed by an individual V1 neuron (bottom) recorded from macaque.

However, there is a distinction to be made between ocular dominance columns and the neurophysiological attribute of ocular dominance (Figure 4). This distinction holds significance as various mammals have demonstrated ocular dominance in their primary visual cortex without exhibiting columnar architecture (J. Horton & Hocking, 1996a; Humphrey et al., 1977) and, in some cases, without any discernible organizing principle at all (Adams & Horton, 2006). This prompts the question: could ocular dominance play a role in binocular vision regardless of its spatial arrangement in V1?

Recently, studies have suggested a relationship between a V1 neuron's ocular dominance (just its ocular preference under monocular stimulation) and properties of its binocular response (Cox et al., 2019; Dougherty, Cox, et al., 2019). Neurons in V1 have been observed to modulate their firing rates under binocular stimulation in a manner than is predictable based on the strength of their ocular dominance (Cox et al., 2019; Dougherty, Cox, et al., 2019). This implies that ocular dominance influences the formation of binocular responses more broadly, but it remains unclear precisely how.

Investigating the relationship between ocular dominance and binocular response formation in V1 is an important endeavor. Quantifying ocular dominance's role during binocular integration could improve pre-existing theoretical models of binocular combination in V1 and potentially put an end to a half-century long debate on the functional significance of ocular dominance. Moreover, disruptions in ocular dominance patterns in V1 have been implicated in various visual disorders, such as amblyopia (lazy eye) and strabismus (crossed eyes) (Birch, 2013; Chapman et al., 1986; D. H. Hubel et al., 1977; Rathjen et al., 2002; Shatz & Stryker, 1978; Tao et al., 2020). Therefore, studying the relationship between ocular dominance and binocular processing not only enhances our understanding of normal visual function but also provides insights into the mechanisms underlying visual disorders and potential therapeutic interventions.

Normalization within and between the eyes: A computational framework

Divisive normalization, initially proposed as a phenomenological model to explain neural responses in the primary visual cortex (V1) (Heeger, 1992b), has garnered considerable attention in the field of visual neuroscience (Hou et al., 2020; Ling & Blake, 2012; Sawada & Petrov, 2017). This model describes a computational mechanism

wherein the response of a neuron is divided by the summed activity of a large pool of neurons, serving to normalize or scale neural responses based on the overall activity level (Heeger, 1992b). At its core, divisive normalization reflects a fundamental principle of cortical computation, representing a mechanism for balancing excitation and inhibition to ensure neural responses remain within an optimal range (Carandini & Heeger, 2012). This process of divisive normalization is thought to enhance the dynamic range of neural responses (Carandini & Heeger, 2012), improve sensitivity to stimuli (Heeger, 1992b), and contribute to the robustness of sensory representations in the brain (Ohshiro et al., 2011; Troyer et al., 1998; Tsang & Shi, 2008).

Beyond its original context in V1, divisive normalization has been implicated in a range of neurophysiological phenomena across various brain regions and sensory modalities. For instance, divisive normalization has been implicated in processes such as spatial integration in the somatosensory cortex (Kohn & Whitsel, 2002), temporal processing in the auditory cortex (Dean et al., 2005), attention regulation (Lee & Maunsell, 2009; Ling & Blake, 2012), and even decision-making in the prefrontal cortex (Louie et al., 2011).

The divisive normalization framework has also been extended to explain V1 responses to binocularly presented stimuli, as well, referred to as binocular or interocular normalization (Fleet et al., 1997). Binocular normalization proposes that a neuron's binocular response results from (contrast) gain-control mechanisms operating within and between monocular channels (Fleet et al., 1997) . This concept closely parallels the psychophysics-derived gain-control theory of binocular combination (Ding & Sperling, 2006). Therefore, a neuronal model of binocular normalization offers a computational framework to explore the gain-control theory of binocular integration at the level of V1 neurons (Figure 5).

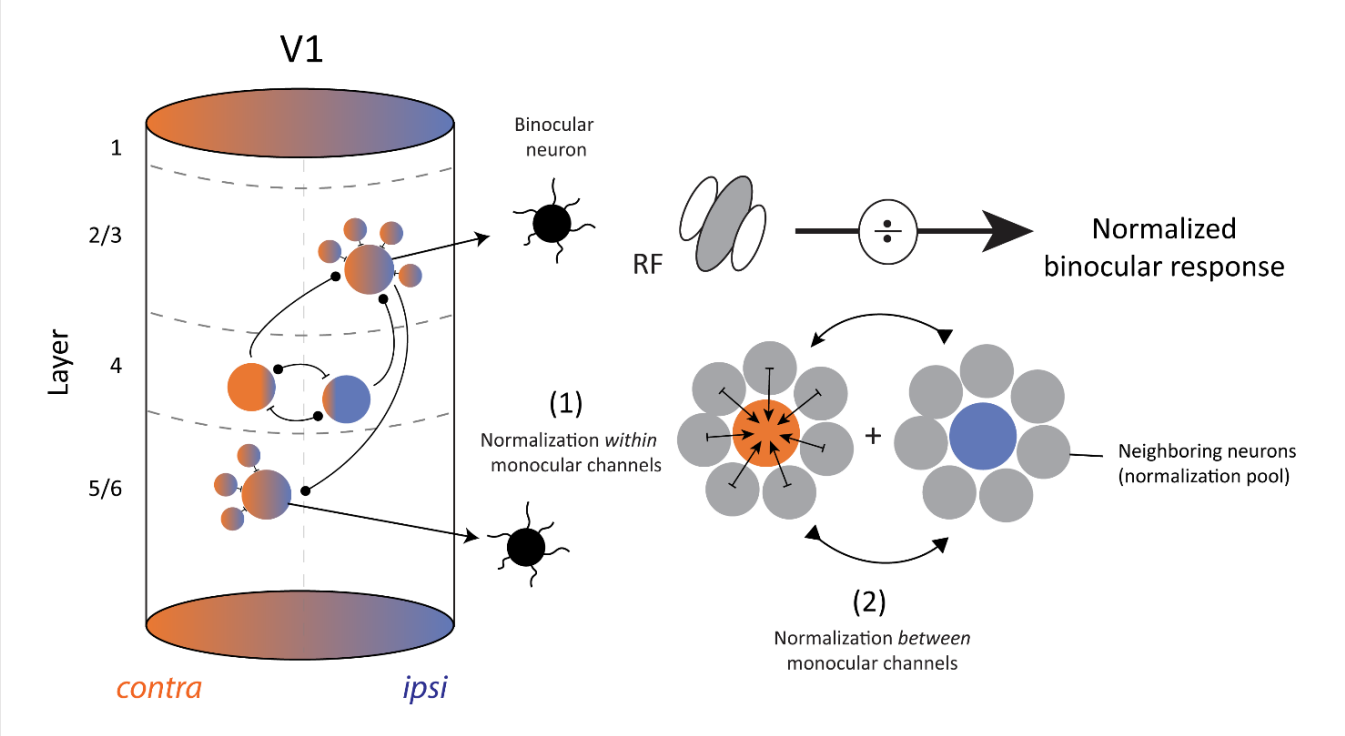

Figure 5. Cartoon schematic of binocular normalization in V1. Divisive normalization is thought to operate both within and between eye-specific geniculate inputs, yielding two stages of contrast gain-control: a monocular stage and a binocular stage.

There is already some electrophysiological evidence supporting binocular normalization in V1. Binocular normalization provides a very good account of interocular gain-control of V1 responses (Hou et al., 2020; Moradi & Heeger, 2009) and contrast normalization in area MT (Heuer & Britten, 2002). However, these studies have primarily utilized fMRI to measure neural activity, which lacks the resolution to discern the activity of individual neurons (Maier et al., 2008). This has left the distribution of binocular normalization processes across the laminar microcircuit of visual cortex largely unexplored. Intracranial electrophysiological studies capable of recording single neurons and populations simultaneously across all cortical layers would therefore enable a more comprehensive investigation of binocular normalization in V1.

Furthermore, the principles of divisive normalization have been incorporated into a broader theory of multi-input integration in the brain. The 'Stabilized Supralinear Network' (SSN) model has been put forth as a unifying circuit-motif for multi-input sensory integration that implements recurrent feedback through divisive normalization (Rubin et al., 2015). Within the SSN model, normalization-based recurrent feedback is pivotal in stabilizing neural activity and enhancing sensitivity to sensory inputs (Holt et al., 2023; Obeid & Miller, 2021) . Therefore, an exploration of binocular normalization adjacently delves into how the SSN model encompasses multi-input stimuli presented to different eyes within the same sensory modality. Investigations into divisive normalization and binocular processing within the V1 laminar microcircuit could clarify how these mechanisms contribute to multi-input integration in the brain more broadly (Wallace et al., 2004) by potentially bridging canonical cortical operations (Carandini & Heeger, 2012) and canonical circuitry (Douglas & Martin, 2004).

Specific Aims

This dissertation describes a series of experiments distributed across three studies designed to evaluate various hypotheses concerning the neural computations underlying binocular integration in V1. Specific unresolved questions to be addressed include:

- **Study 1:** How does V1 excitation alter when input is doubled (i.e., monocular to binocular stimulation)?
- **Study 1:** How does the contrast-response relationship in V1 change when input is doubled?
- **Study 2:** Does cell-to-cell variability in ocular dominance matter for binocular contrast combination?
- **Study 2:** Can ocular dominance be used to improve computational models of binocular combination?
- **Study 3:** Does divisive normalization vary across V1 laminar compartments?
- **Study 3:** How does binocular normalization unfold across the V1 laminar microcircuit?

Chapter 1

V1 responses to binocular versus monocular stimulation[1]

1.1 Summary

Neurons in primate primary visual cortex (V1) play a key role in combining monocular inputs to form a binocular response. While much has been gleaned from studying how V1 responds to discrepant (*dichoptic*) images, equally important is to understand how V1 responds to concordant (*dioptic*) images in the two eyes. Here, we investigated the extent to which concordant, balanced, zero-disparity binocular stimulation modifies V1 responses to varying stimulus contrast using intracranial multielectrode arrays. On average, binocular stimuli evoked stronger V1 activity than their monocular counterparts. This binocular facilitation scaled most proportionately with contrast during the initial transient. As V1 responses evolved, additional contrast-mediated dynamics emerged. Specifically, responses exhibited longer maintenance of facilitation for lower contrast and binocular suppression at high contrast. These results suggest that V1 processes concordant stimulation of both eyes in at least two sequential steps: initial response enhancement followed by contrast-dependent control of excitation.

1.2 Introduction

Neurophysiological studies of binocular combination in V1 have traditionally been geared towards understanding how the visual system responds to images that are different between the two eyes, i.e., *dichoptic* viewing conditions. Less is understood about how V1 responds under *dioptic* viewing conditions, where binocular images are physically identical and fall on corresponding retinal positions. As a matter of subjective experience, the advantages of viewing the same image with both eyes are somewhat elusive (Levelt, 1965). The simple experiment of opening and closing one eye does not elicit a dramatic change in perception. Yet, decades of research have revealed a binocular advantage in numerous psychophysical experiments (For review, see Blake et al., 1981; Blake & Fox, 1973). Psychophysical gains in performance under binocular viewing are commonly referred to as "binocular summation" (e.g., Cagenello et al., 1993). It has now been well established that binocular summation extends beyond than what would be expected from having an additional detector (i.e., probability summation) (For meta-analysis, see D. H. Baker et al., 2018; Matin, 1962; Pirenne, 1943).

The neurophysiological basis for binocular summation is thought to be an enhancement of neural responses along the primary visual pathway (Blake & Fox, 1973). Electrophysiological and neuroimaging techniques provide evidence for this theory in the earliest cortical site for binocular processing, primary visual cortex (V1) (Apkarian et al., 1981; Heravian et al., 1990; Hou et al., 2020; Moradi & Heeger, 2009; Pardhan et al., 1990). While enhanced compared to responses to just one eye, EEG and fMRI binocular signals in V1 are typically much less than the sum of comprising monocular responses (Ates et al., 2006; Giuseppe & Andrea, 1983; Heravian et al., 1990; Moradi & Heeger, 2009), akin to our experience of seeing with two eyes. At the level of spiking activity in V1, the evidence

[1] This chapter is adapted from "Stimulating both eyes with matching stimuli enhances V1 responses" published in iScience and has been reproduced with the permission of the publisher and my coauthors, Kacie Dougherty, Jacob Westerberg, Brock Carlson, Loic Domail, Alex Maier, and Michele Cox. DOI: 10.1016/j.isci.2022.104182

for binocular summation is somewhat mixed. Early investigations of binocular interactions found great diversity in how V1 simple and complex cells modulate under binocular stimulation (D. H. Hubel & Wiesel, 1962). Responses of binocularly activated single cells in striate cortex are shown to be either greater than the sum of monocular responses, greater than the preferred monocular response, or less than monocular responses (Barlow et al., 1967; Burns & Pritchard, 1968; D. H. Hubel & Wiesel, 1962; Pettigrew et al., 1968; G. F. Poggio & Fischer, 1977). The type of binocular interactions in single neurons rely chiefly, among other factors, on the compatibility between retinal disparity of the stimulus and the shape of a given cell's receptive field (Anzai et al., 1999; Barlow et al., 1967; P. O. Bishop & Pettigrew, 1986; Cumming & DeAngelis, 2001; Freeman & Ohzawa, 1990; D. H. Hubel & Wiesel, 1962; Nikara, 1972; G. F. Poggio & Fischer, 1977; Smith et al., 1997). However, it remains unclear to what extent V1 neurons exhibit neural binocular summation on whole, when both eyes are stimulated equally at corresponding retinal position. It is also unclear how the control of excitation during binocular stimulation is affected by the strength of the stimuli (i.e., stimulus contrast).

While the neuronal mechanisms that control V1 binocular responses are not entirely understood, response control in V1 in general has been extensively studied and well characterized (Albrecht & Geisler, 1991; Albrecht & Hamilton, 1982; Carandini et al., 1997; Heeger, 1992a, 1992b; Ohzawa et al., 1985). The magnitude of V1 spiking responses is controlled by the strength of input, i.e., stimulus contrast (Clatworthy et al., 2003). The relationship between stimulus contrast and a V1 neuron's response is typically well-described by a sigmoidal contrast response function (CRF) (Albrecht & Hamilton, 1982; Ohzawa et al., 1985; Sengpiel & Blakemore, 1994). Such a relationship highlights a gain-control feature that exists in V1 that amplifies weaker inputs but reduces the effect of stronger inputs (Ohzawa et al., 1985). Thus, one might ask how the contrast-response relationship changes when an additional input (from the other eye) is added (i.e., monocular to binocular viewing). Doing so would be useful in distinguishing between contrast-dependent and contrast-independent mechanisms that control V1 excitation when input to V1 is simply doubled. Previous investigators have asked a similar question but for dichoptic viewing (Heuer & Britten, 2002; Sengpiel et al., 1998). For example, the addition of an orthogonal grating in the opposite eye suppressed V1 neurons in a manner that shifted the CRF down along the response-axis, rather than the contrast-axis (Sengpiel et al., 1998; Sengpiel & Blakemore, 1994). To the best of our knowledge, shifts in V1's CRF under the much more common visual experience of dioptic stimulation have not been characterized using multi-unit electrophysiological methods.

Here, we studied the time-varying relationship between V1 binocular (dioptic) response modulation and stimulus contrast. We found that V1 population spiking activity was overall greater for binocular stimulation than for monocular stimulation, but binocular responses were considerably less than the left and right eye responses summed. The relationship between binocular modulation and stimulus contrast was dynamic. V1 binocular responses exhibited at least two sequential steps of gain modulation over monocular viewing: initial, rapid (50-100ms) summation that was more contrast-invariant followed by slower, contrast-dependent processing, all within the timeframe of a typical fixation (250 ms) (Salthouse & Ellis, 1980).

1.3 Results

We were interested in determining how V1 activity differs between stimulating one eye versus stimulating both eyes with the *same image* as a function of contrast. To find out, we presented sinusoidal, achromatic gratings through a mirror stereoscope (Figure 6*A*) either monocularly or binocularly to fixating monkeys (Figure 6*B*). The grating varied in Michelson contrast between trials.

We used microelectrode arrays to simultaneously record extracellular voltages to these stimulus presentations at multiple V1 sites. Sampling in this study varied with monkey and condition (Table 1). As a result, population measures of neuronal activity reported below include varying number of units from each monkey depending on the conditions being considered. Potential consequences of sampling-bias, which is not uncommon for studies of this kind, are considered in *1.4.3. Limitations of the study*.

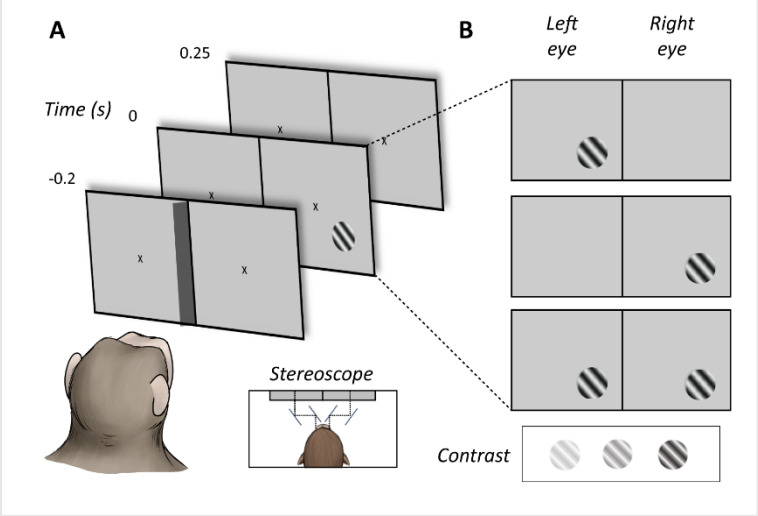

Figure 6. Visual paradigm for Study 1. ***(A)*** *Paradigm. Monkeys fixated while viewing static sinusoidal gratings through a mirror stereoscope. Stimuli covered the previously mapped receptive field location (dashed circle) for 250ms while spiking responses were recorded from V1.* ***(B)*** *Stimulus conditions. Gratings appeared either in the left eye (monocular), the right eye (monocular), or both eyes simultaneously (binocular). Orientation, size, and spatial frequency of gratings were held constant throughout each experiment. Gratings varied in Michelson contrast ([0], [0.20-0.22], [0.40-0.45], [0.80-0.90]) between trials.*

Table 1. Subject and sample information.

Subject	Sessions	Units	Low contrast	Med contrast	High contrast	CRFs
"E"	14	234	234	234	234	234
"I"	5	80	14	74	80	8
Pooled	19	314	248	308	314	242

1.3.1. V1 binocular responses exceed the average of constituent monocular responses

Thresholding the voltage at each site yielded a measure of neuronal activity (multi-unit, see *1.5.6. V1 response categorization and analysis* for details). Figure 7*A* displays spike density functions (SDFs) of a single V1 neuron's response to monocular (blue) and binocular (red) presentations. For each unit, we distinguished the eye that drove V1 activity the most as the dominant eye (DE; Figure 7*A*, dark blue) compared to the non-dominant eye (NDE; Figure 7*A*, light blue).

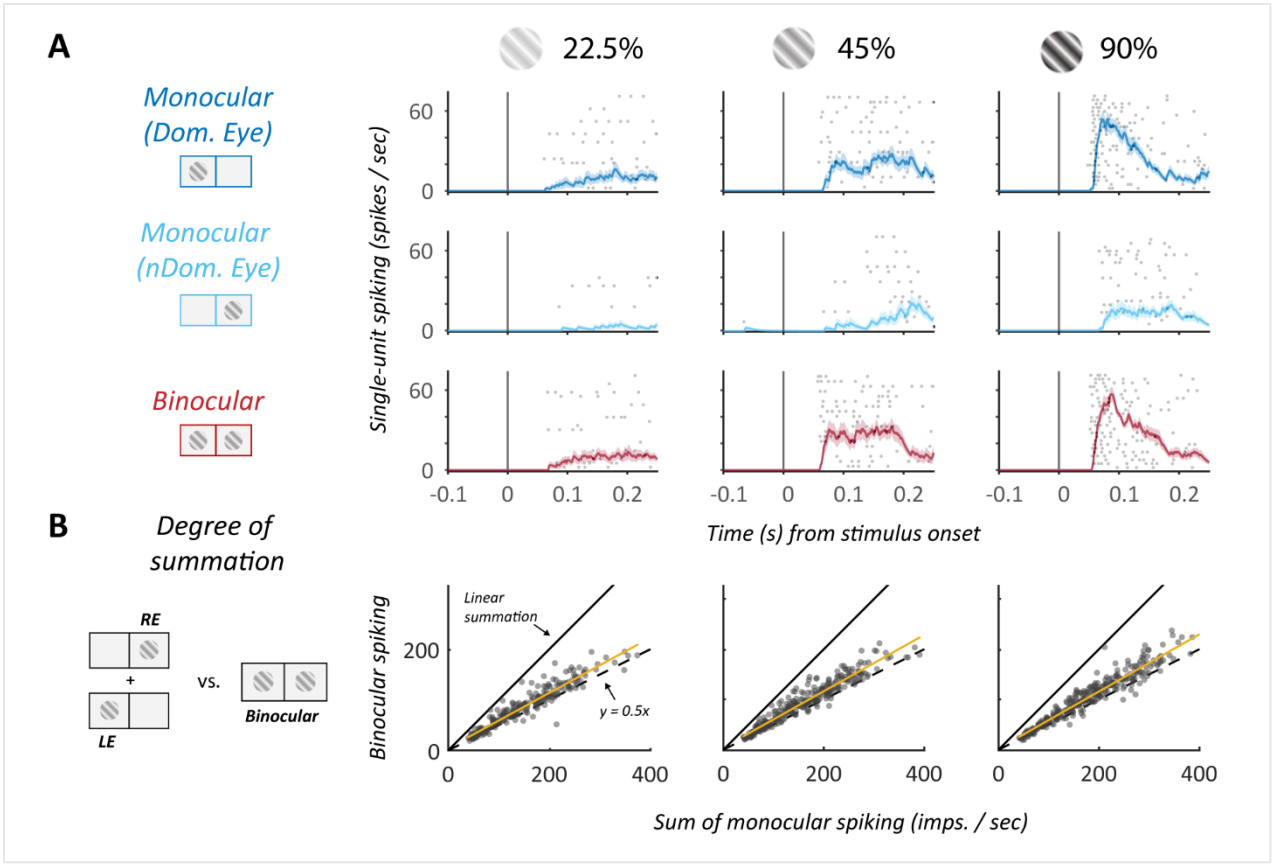

Figure 7. V1 binocular responses are sublinear. ***(A)*** *Example V1 neuron responses to varying stimulus contrast presented either monocularly or binocularly. Spiking activity (spikes. / s) is plotted across time for each type of stimulation (row) at each contrast (column). Shaded region encasing the plot represents +/- SEM. The eye that drove neural activity most vigorously was designated as the dominant eye (darker blue).* ***(B)*** *Sublinear binocular combination. Mean firing rates (N = 314 units, 234 in monkey E) to binocular stimulation are plotted against the sum of monocular firing rates (left + right eye). Solid black line represents linear summation; dashed black line represents y = 0.5x. Binocular responses were generally less than the arithmetic sum of their monocular counterparts at each contrast level and in both monkeys.*

To quantify neuronal binocular summation, we plotted each unit's mean binocular (BIN) responses (0-250ms) against the sum of its respective monocular responses (DE + NDE) (Figure 7*B*). The unity diagonal represents the expected binocular response if binocular summation is linear, and the dashed line represents the average of the two monocular responses (y = 0.5x). Across our sample of multi-units (N = 314), binocular responses were approximately 56% of the summed monocular responses (averaged across contrast) and approximately 82% of the quadratic sum. Thus, at the level of V1 population spiking, binocular responses are greater than the average between the two eyes but less than the linear sum, i.e., exhibit *sublinear summation*.

To control for variance in maximum firing rate between units, we calculated an additivity index at each contrast (Figure 8). The additivity index was derived by dividing the mean binocular response of each unit by the sum of its comprising monocular responses [BIN_{μ} / $\Sigma(LE_{\mu}+RE_{\mu})$]. Values at 0.5 indicate no difference between binocular response and the average between the two monocular responses. An index value of 1 signifies that the binocular response was equivalent to the sum of comprising monocular responses. Therefore, values between 0.5 and 1 indicate a binocular interaction that is greater than the average of the two eyes but less than the linear sum, or *sublinear summation*.

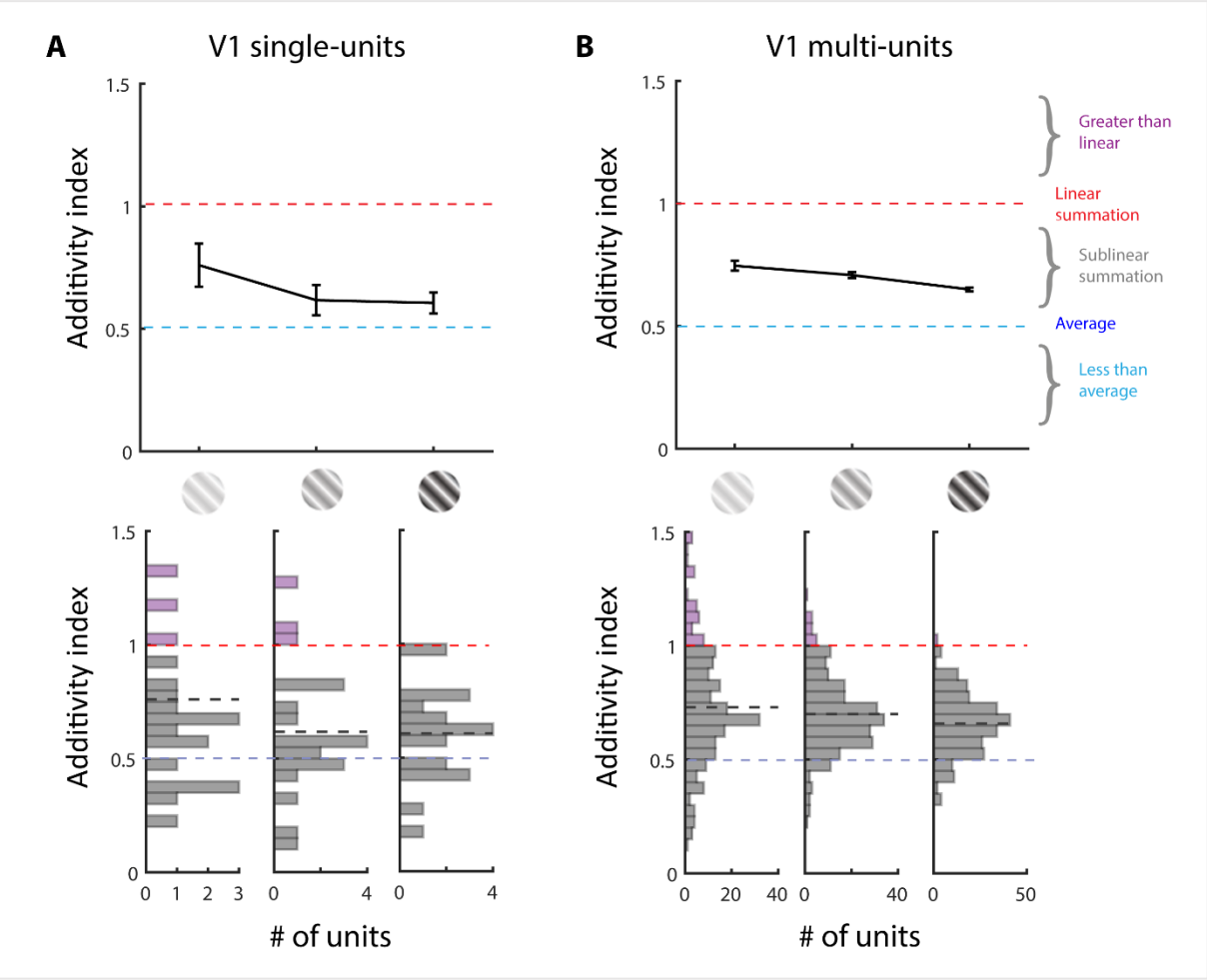

Figure 8. V1 sublinear binocular summation is contrast dependent. (A) Single unit analysis. Values above 1 indicate a cooperative interaction such that binocular responses were greater than the sum of the two monocular responses, which we refer to as super summation here. Values below 0.5 indicate a suppressive interaction, where the binocular response was less than the average of the two monocular responses.

1.3.2. V1 responses are facilitated under balanced binocular stimulation.

The above analysis replicated previous findings, showing that V1 responses are greater than the average of the two separate monocular responses. Another popular measure is to compare binocular stimulation to stimulation of whichever eye evokes the stronger response, or the dominant eye response. We thus quantified this effect as well. To do so, we computed an index of "binocular modulation" as the difference in mean spiking response (0-250ms) when both eyes are stimulated, referenced to the strongest monocular (dominant eye, DE) response (Figure 9*A*).

Binocular modulation index values above zero indicate *binocular facilitation*, whereas values below zero indicate *binocular suppression*. For each unit, we first pooled the data across contrast levels to achieve a grand average of V1 binocular modulation. We derived mean spiking responses over 250 ms (full duration of stimulus presentation). Figure 9*B* displays the grand average binocular modulation index for each unit. Across the population, binocular modulation was significantly greater than zero ($M = 0.057$, $SD = 0.067$, *paired t-test*, $t(313) = 14.95$, $p < 0.001$, *Cohen's d* = 0.843). More than two thirds of V1 units (219 units, 69.7%) were overall facilitated when both eyes viewed the same image relative to monocular viewing.

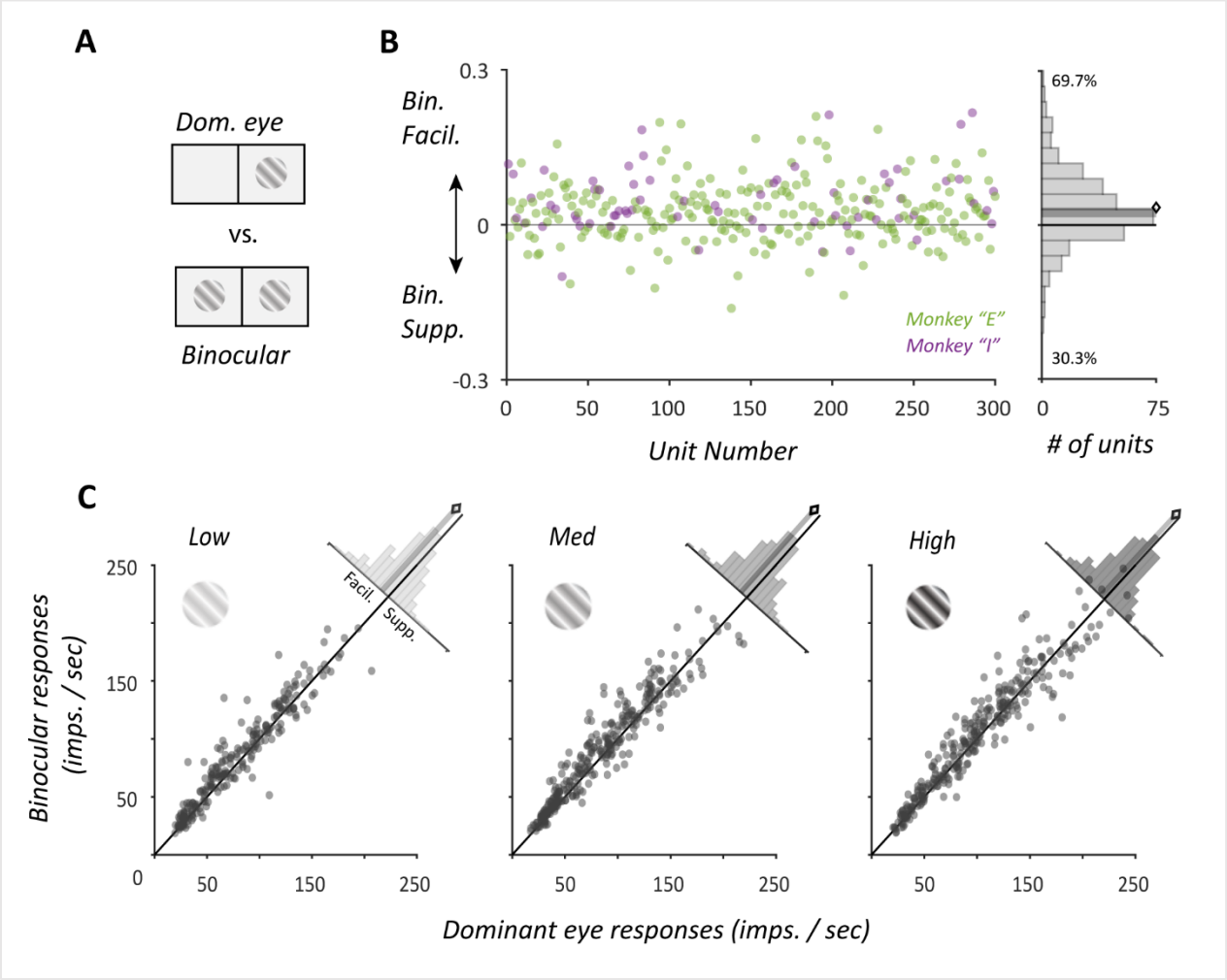

Figure 9. Facilitation of V1 spiking responses to balanced binocular stimulation. ***(A)*** *We computed binocular modulation index to compare a unit's strongest monocular response (its preferred eye) to its binocular response over the full stimulus duration (0-250ms). Values above 0 signify binocular facilitation while values below 0 signify binocular suppression.* ***(B)*** *Within-unit average (across contrast) binocular modulation index (M = 0.057, SD = 0.067, N = 314 [234 from Monkey "E", shown in green]). Distribution to the right shows that most V1 units were facilitated (shaded region encasing 95% CI, diamond marks the mean).* ***(C)*** *Binocular modulation as a function of contrast. In each panel, a unit's binocular response is plotted against its strongest monocular response. Distribution of the binocular modulation index is shown in corner histogram; gray shaded region represents the 95% confidence interval; the black diamond marks the mean of the distribution. Facilitation was observed in most V1 units and at each contrast tested.*

Next, we examined the extent to which contrast modifies binocular modulation. Figure 9*C* shows the binocular response (mean spiking from 0-250ms) of each unit against its dominant eye response as a function of stimulus contrast. Distributions of binocular modulation values are shown in the corner histograms. We found that

binocular modulation varied across stimulus contrast, *Mixed model (N = 314)*, F (1, 869) = 15.55, $p < 0.001$. Binocular modulation was strongest for low contrast ($M = 0.034$, $SD = 0.081$, *paired t test* $H_a\ \mu > 0$, t (247) = 6.62, $p < 0.001$, *Cohen's d* = 0.42) and medium contrast ($M = 0.034$, $SD = 0.072$, *paired t test* $H_a\ \mu > 0$, t (307) = 8.32, $p < 0.001$, *Cohen's d* = 0.47) , and weakest for high contrast ($M = 0.020$, $SD = 0.070$, *paired t test* $H_a\ \mu > 0$, t (313) = 5.10, $p < 0.001$, *Cohen's d* = 0.29). Thus, while V1 spiking was predominantly facilitated over 250ms of binocular stimulation, this boost in activity was attenuated by stimulus contrast.

1.3.3. V1 binocular facilitation is temporally dynamic and contrast-dependent

Informed by previous work (Cox et al., 2019), we suspected that this binocular facilitation in V1 would be transient, i.e., not lasting the entire 250 ms of stimulus viewing. However, the contrast-dependency of the transient facilitation remains unknown. To investigate the temporal rise and decay of facilitation across contrast, we created spike density functions (SDFs) for monocular and binocular V1 responses and compared them across time (Figure 10). For this analysis, we limited our sample to units for which we had balanced observations for pairwise comparisons between contrasts (N = 242 units, 234 from monkey E).

Figure 10*A* displays the population SDFs as a function of stimulus contrast. Below each plot is the mean difference in spiking between monocular and binocular stimulation, normalized within-unit for three levels of contrast. Timepoints where binocular facilitation (above zero) was significant are indicated by a horizontal black line above the delta response (*two-way paired t test*, $p < 0.001$). This time varying SDF analysis revealed that the

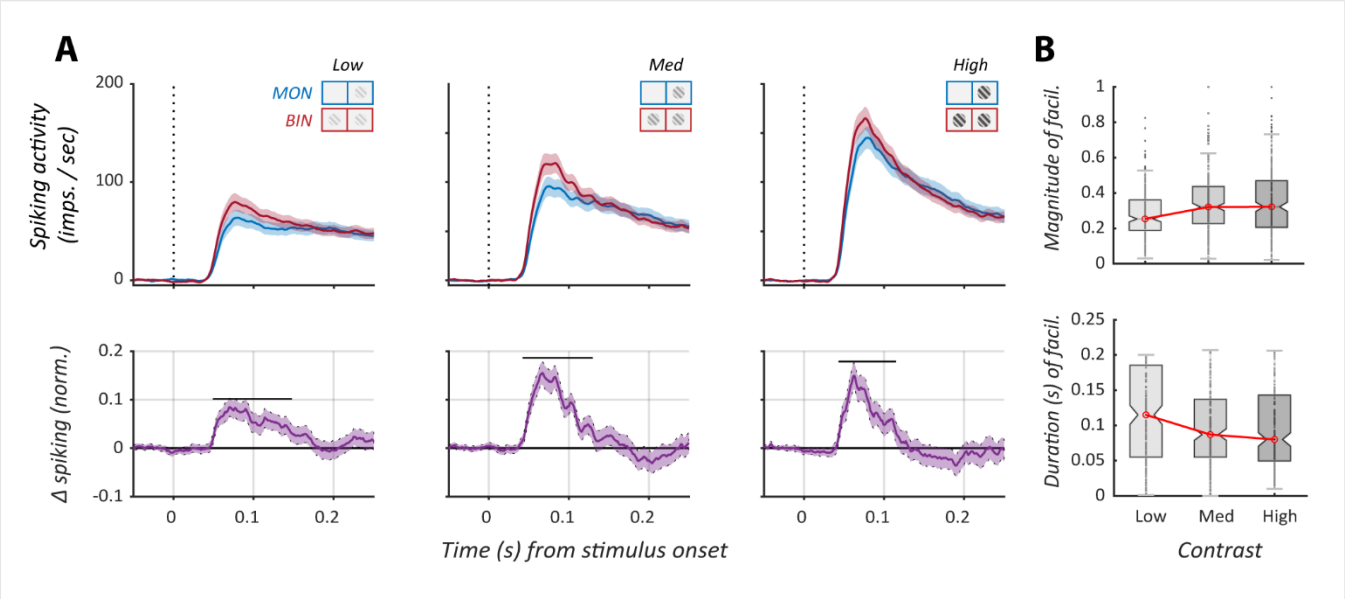

Figure 10. Contrast-dependency of V1 binocular facilitation across time. ***(A)*** *Top - Population spike density functions (SDFs) for monocular (blue) and binocular stimulation (red) are shown for three contrast levels ([0.22, 0.45, 0.90]). Dotted line at zero represents stimulus onset. Shaded region represents 95% CI. Bottom - Difference between the SDFs (BIN – MON) across time, calculated within-unit and normalized to each unit's maximum binocular response. Shaded region represents 95% CI. Note that facilitation was limited to an early phase of the response.* ***(B)*** *Top – Peak magnitude of facilitation increased as a function of contrast. Datapoints are shown in black (dots). Boxplot upper and lower edges indicate the 25th and 75th percentiles, respectively. Red line connects median value (red circle) of each boxplot. Whiskers extend to the most extreme data points that are not considered outliers. Bottom – duration of facilitation systematically decreased as a function of contrast. Same conventions as above.*

magnitude of binocular facilitation varied as a function of time at all three contrast levels. Specifically, binocular

facilitation was largest at an early phase of the response and decreased over time. To further quantify this effect, we calculated the binocular modulation index over sixteen sequential temporal windows. As expected, the binocular modulation index varied significantly with time (medium contrast, *rmANOVA*, F (15, 3525) = 150, $p < 0.001$, n^2_G = 0.190).

We next estimated the magnitude of facilitation at the transient peak of V1 responses as a function of contrast. Peak magnitude varied across stimulus contrast, (*rmANOVA*, F (2, 482) = 24.0, $p < 0.001$, $n^2_G = 0.035$; Figure 10*B – top).* Low contrast facilitation exhibited peak magnitudes ($M = 0.28$, $SD = 0.14$) significantly lower than medium ($M = 0.34$, $SD = 0.16$) and high contrast ($M = 0.35$, $SD = 0.22$) peaks (low vs medium contrast, *post hoc test*, t (241) = -5.74, $p_{Bonferonni} < .001$, *Cohen's d* = -0.37; low vs. high contrast, *post hoc test*, t (247) = -6.15, $p_{Bonferonni} < .001$, *Cohen's d* = -0.39). Peak magnitude of facilitation at medium and high contrast were not statistically different (*post hoc test, t* (241) = -1.53, $p_{Bonferonni} = 0.36$).

Finally, we measured the duration of facilitation across contrasts. Duration of facilitation was defined, for each unit, as the length in samples between the peak magnitude of facilitation (see above) and the point at which the delta response crossed zero (see *1.5.7. Duration of binocular facilitation* for details). We found that duration of facilitation varied across contrast, *rmANOVA*, F (2, 482) = 4.74, $p = 0.009$, $n^2_G = 0.012$; Figure 10*B – bottom*). Facilitation was maintained significantly longer at low contrast (*Median* = 115.0 ms*, SD* = 63.3) compared to medium (*Median = 87.0 ms*, *SD* = 59.7) and high contrast (*Median* = 80.0 ms, *SD* = 62.3) (*post hoc test*, low vs. medium, t (215) = 2.80, $p_{Bonferonni} = .018$, *Cohen's d* = 0.19; low vs. high, t (215) = 2.45, $p_{Bonferonni} = 0.045$, *Cohen's d* = 0.17. Duration of facilitation at medium and high contrast were not statistically different (*post hoc test*, medium vs. high, t (215) = -0.12, $p_{Bonferonni} > 0.9999$).

1.3.4. V1 binocular modulation can be expressed as a form of gain-control.

Results thus far suggest that V1 binocular facilitation is a transient event that evolves over the time course of stimulation in a contrast-dependent manner. To further examine the dynamic relationship between binocular modulation and contrast, we interpolated each units' contrast responses by fitting measured data with the Naka-Rushton function. Trial-averaged spiking responses (over varying time windows) as a function of visual contrast were fit using the Naka-Rushton function:

$$R_{R_{max},C_{50},n,b}(c) = \frac{Rmax * c^n}{c^n + {C_{50}}^n} + b$$

where R is the response of the unit, R_{max} is the projected maximum response of the unit, C_{50} is the semi-saturation constant that represents the contrast at which the output is half of the maximum response, n is the scaling exponent, and c is the contrast of the stimulus (Figure 11*A*). The y-intercept b represents the maintained activity and was fixed for individual neurons to the average activity during blank trials (0 contrast = gray background). The parameters R_{max}, C_{50}, and n collectively determine the shape of the contrast response curve (Carandini & Heeger, 2012). For each unit, the trial-averaged contrast responses under binocular and monocular conditions were fit with all parameters free to vary [R_{max}, C_{50}, n]. V1 units with at least four contrast-level datapoints (234 units in Monkey E, 8 units in Monkey I) were used for fitting contrast response functions (CRFs). Monocular and binocular CRFs were computed over sixteen sequential temporal windows of the V1 spiking response. Windows were 100 ms in length, each sliding by 10 ms forward in time from the preceding window.

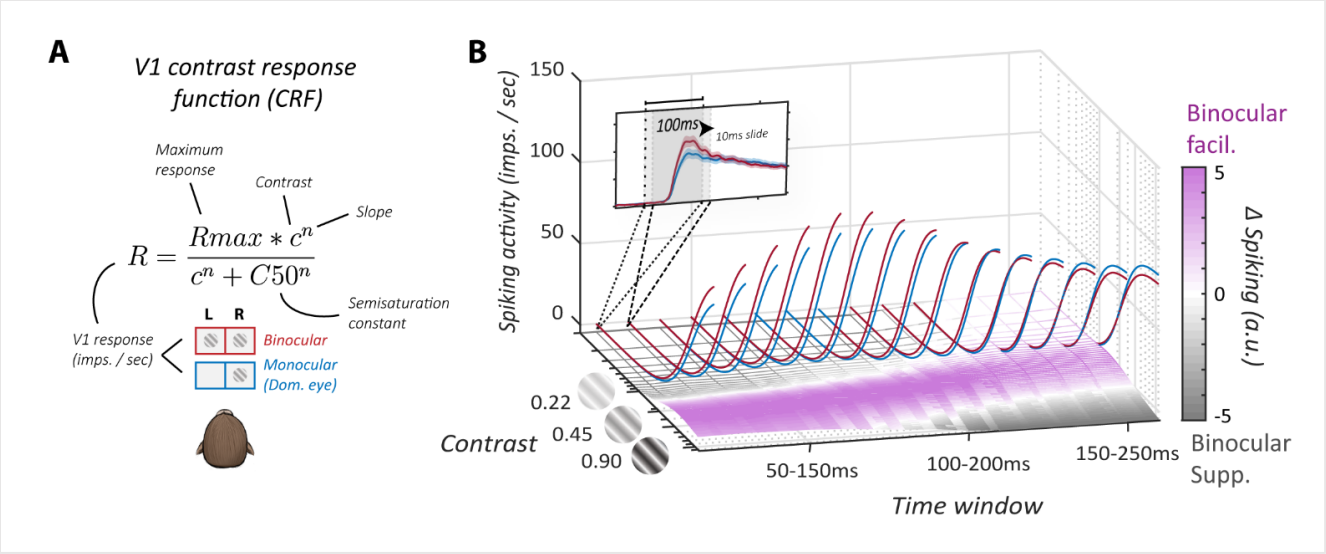

Figure 11. V1 responses at higher contrasts transition from facilitation to suppression. ***(A)*** *Naka-Rushton h-ratio equation used to fit individual contrast response functions (CRFs). Mean parameters were then used to estimate monocular and binocular CRFs of the V1 population.* ***(B)*** *Binocular and monocular CRFs were computed consecutively over 100ms windows of the V1 response, sliding by 10ms forward in time. Sixteen windows in total are shown along the y-axis (x axis is contrast, z axis is spiking response). The floor of the plot reflects the difference between the CRF pairs across time. Color bar translates these differences into strength of facilitation (pink) or suppression (gray)*

To evaluate V1 CRFs at the population level, we generated average curves for each condition using the mean parameters (and their upper and lower bounds). Figure 11*B* plots the mean parameter-generated binocular and monocular CRFs as a function of time. The color and contour of the floor reflects the normalized difference between each CRF pair as it evolves over time (pink = facilitation; white = no difference, gray = suppression. In the early period of the response (50-150ms), binocular facilitation appeared the most proportional to stimulus contrast. In the intermediate period (100-200 ms), binocular facilitation was diminished at high contrast. By the late period (150-250 ms), binocular facilitation had relinquished entirely. Instead, the late period V1 CRF exhibited *binocular suppression* at medium and high contrast.

1.3.5. V1 binocular facilitation predominantly resembles a "response-set" form of gain-control

We next evaluated the contrast-response relationship in the context of simple forms of gain and gain-control. Two hypothetical types of gain can be gleaned from shifts in the CRF (Ling & Carrasco, 2006; Martínez-Trujillo & Treue, 2002; Ohzawa et al., 1985; Sengpiel et al., 1998; Sengpiel & Blakemore, 1994; Thiele et al., 2009). Response-gain is characterized by vertical shifts in V1's CRF, indicating that responses increased with contrast by a constant scaling factor. Contrast-gain, on the other hand, is characterized by horizontal shifts in V1's CRF, indicating a contrast-response relationship that depends on contrast.

To quantitatively evaluate which type of gain (response vs. contrast-gain set) is prevalent at the population level, we directly compared models that isolate the effects of response-gain and contrast-gain (Figure 12). In this procedure, we fixed the parameters of the Naka-Rushton equation to that of the dominant eye. We then introduced a single free parameter (G) to either multiply response (response-gain model, *eq. 1* in Figure 12*A*) or contrast

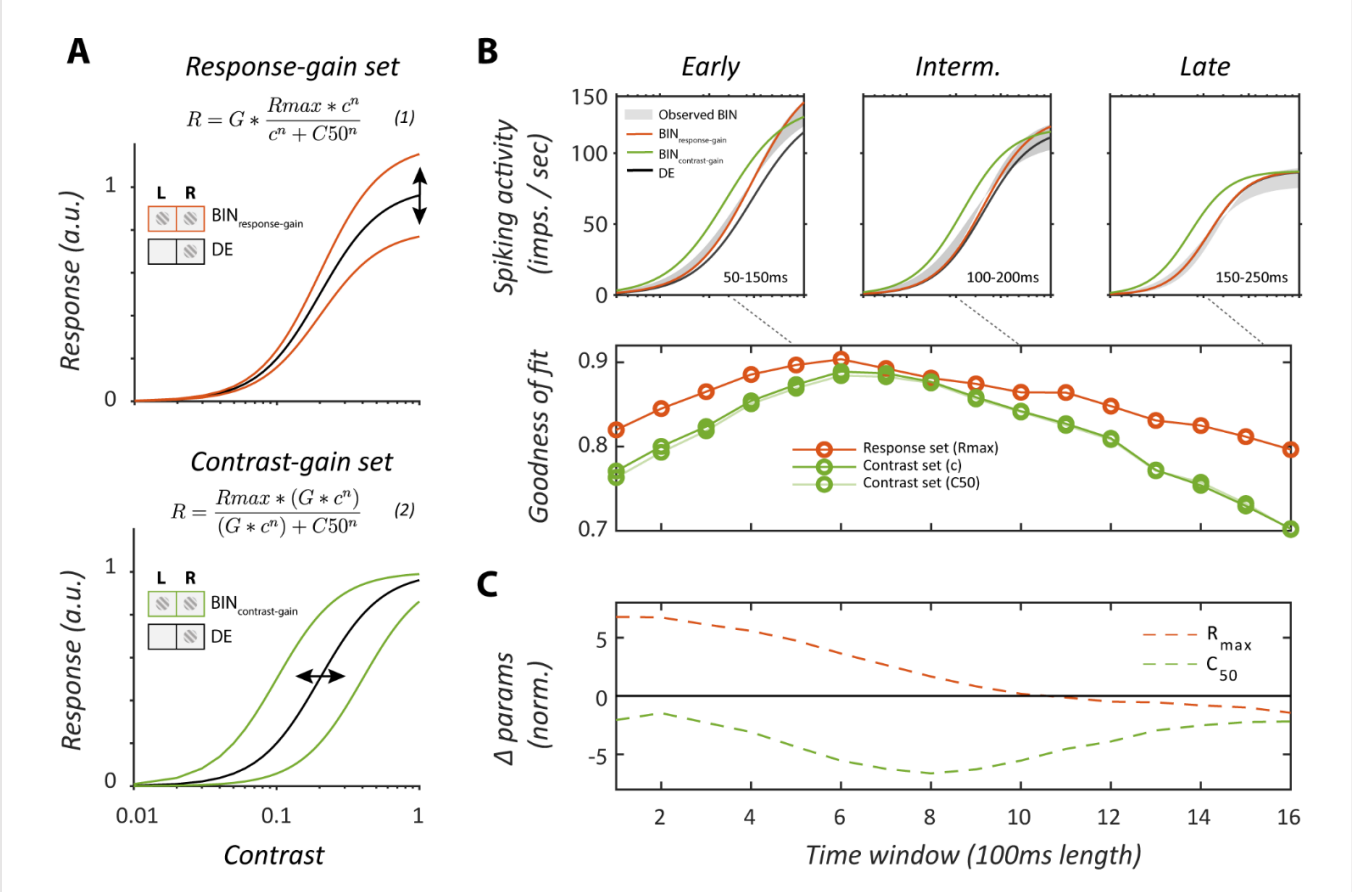

Figure 12. The effect of balanced binocular stimulation in V1 predominantly resembles a response-gain. (A) Models for how binocular stimulation interacts with contrast to modulate V1 responses. A single free parameter G multiplies either response (orange, response-gain) or contrast (green, contrast-gain) to fit binocular responses while all other parameters are fixed to the monocular (dom. eye) condition. (B) Top – model curves overlaid the 95% CI of the binocular CRF fit by the standard function. Bottom – goodness of fit (R2) for both models as a function of time. We additionally tested an alternative model of contrast-gain set (light green) that multiplies the semi-saturation constant (c50). Performance of the two contrast-gain set models were comparable. (C) Difference (normalized) in the parameters Rmax and C50 of the CRFs. Binocular stimulation transiently shifts V1's CRF upward in a manner that resembled response-gain before contrast-dependent dynamics shape the sustained response.

(contrast-gain model, *eq. 2* in Figure 12*A*). Finally, we fit the mean response (over 100ms windows of the response) from the binocular condition with each model and compared their performance.

Figure 12*B* shows the population-level fitted binocular responses for the two models at the early, intermediate, and late phase of the response. Goodness-of-fit for each model across all sixteen windows are plotted below. Both response-gain and contrast-gain set model performance varied significantly across time (response-gain, *rmANOVA*, F (2,482) = 17.8, $p < 0.001$, $n^2_G = 0.030$; contrast-gain, *rmANOVA*, F (2,482) = 40.0, $p < 0.001$, $n^2_G = 0.065$). Response-gain performed best ($R^2 = 0.90$, *95% CI* [0.88, 0.92]) and significantly better than contrast-gain ($R^2 = 0.87$, *95% CI* [0.85, 0.89]) during the early phase (50-150ms, window 5) of the response (*paired t test*, t (241) = 2.84, $p = 0.00491$, *Cohen's d* = 0.18). During the intermediate phase (100-200ms, window 10), response-gain and contrast-gain performances were comparable (response-gain, $R^2 = 0.86$, *95% CI* [0.84, 0.89]; contrast-gain, $R^2 = 0.84$, *95% CI* [0.82, 0.87]). In the late phase (150-250ms, window 15), performance of these simple models of gain decreased overall (response-gain, $R^2 = 0.81$, *95% CI* [0.78, 0.84]; contrast-gain, $R^2 = 0.73$, *95% CI* [0.69, 0.77]). Recall that the late stage of the binocular response exhibited suppression (far right Figure 12*B*). Binocular suppression of V1's CRF was better captured by response-gain set (*paired t test*, t (241) = 6.26, $p < 0.001$, *Cohen's d* = 0.40). We note that binocular suppression unfolded differently across time between the two monkeys. However, in both cases, contrast-dependent suppression was observed following facilitation. Figure 12*C* shows the normalized parameter differences (R_{max} and C_{50}) of the CRF pairs across time. As expected, differences in R_{max} corresponded with response-gain performance, while differences in C_{50} corresponded with contrast-gain performance.

1.4 Discussion

Here, we report V1 binocular interactions at the intermediate level of neural population spiking activity using multi-unit electrophysiology. We found that V1 binocular responses constituted less than the arithmetic sum of left and right eye responses but more than their average (sublinear/partial binocular summation). At the same time, V1 binocular spiking was higher than the that of the population's response to stimulation of the preferred eye alone (binocular facilitation). This increase in neuronal activity for binocular stimulation is in line with results reported from single-neuron experiments in rodents (Longordo et al., 2013; Zhao et al., 2013), cats (M. V. Grünau, 1979; M. W. von Grünau & Singer, 1979; D. H. Hubel & Wiesel, 1962), monkeys (G. F. Poggio & Fischer, 1977), and is consistent with the idea that V1 neurons with near-foveal receptive fields tend to show an excitatory bias towards zero-disparity (G. F. Poggio & Fischer, 1977). Yet, the magnitude of binocular facilitation was less than that reported in single neurons optimally stimulated with images placed at corresponding retinal positions (Burns & Pritchard, 1968). The magnitude of facilitation reported here is quantitatively closer to estimates from fMRI (Moradi & Heeger, 2009) and EEG (Harter et al., 1973). Population measurements contain neurons with different tuning preferences, which might – at least – partially explain this difference.

1.4.1. V1 binocular facilitation and its relation to psychophysical summation

In addition to better spatial sampling of binocular interactions, we were also able to assess the temporal dynamics of neural binocular summation at behaviorally relevant timescales (Salthouse & Ellis, 1980). In a recent

meta-analysis of psychophysical binocular summation, a negative correlation was found between psychophysical binocular summation and stimulus duration (D. H. Baker et al., 2018). That is, the magnitude of binocular summation effects tended to decrease with exposure time. For example, psychophysical binocular summation in orientation discrimination was shown to be greatest for a brief exposure time of 50ms, which approached non-significance (indistinguishable from monocular stimulation) at durations of 100ms or longer (Bearse & Freeman, 1994). We found that V1 spiking responses were transiently facilitated, with peak magnitude of facilitation localized around the initial peak of the response (45-50ms). In the sustained period of the response (100-200ms, binocular responses were comparable to (and even less than) monocular responses. Thus, the timescales of V1 binocular enhancement reported here (45-100ms) appear to match some of the reported timescales of behavioral performance gains under binocular viewing. However, it is worth noting that psychophysical studies have measured binocular summation over periods longer than 100ms (D. H. Baker et al., 2018). This suggests that additional neural structures, likely downstream of V1, contribute to the neural correlate of binocular summation.

1.4.2. Binocular modulation expressed as a form of gain-control.

While simple models of gain control are useful in evaluating contrast-response relationships, it is understood that the rules that govern binocular combination extend beyond a single parameter. Informed by decades of theoretical development and empirical work (Blake, 1989; Campbell & Green, 1965; Legge, 1984a), the predictive power of modern models of binocular combination, such as the DSKL model (Ding & Sperling, 2006), have become progressively robust to a wide range of binocular viewing conditions (Ding et al., 2013b, 2013a; Ding & Levi, 2017, 2021; Huang et al., 2010; Yehezkel et al., 2016). Key to the success of such models has been the incorporation of multiple channels for reciprocal contrast-gain control to occur between the two eyes. Neural models of binocular combination employ similar formalisms and synergize well with the gain-control theory of binocular combination. They must additionally account for known properties of visual neurons, such as the linear spatial summation of V1 simple cells, the nonlinearities of complex cells and spike generation, and the diversity in the interocular balance of inputs to a given cell. Notably, the two-stage model (M. A. Georgeson & Sengpiel, 2021), energy models (Fleet et al., 1996; Haefner & Cumming, 2008; Ohzawa et al., 1997; J. C. A. Read et al., 2002; J. C. A. Read & Cumming, 2003; Tanabe & Cumming, 2008), and binocular/interocular normalization (Chadnova et al., 2018; Hou et al., 2020; Ling & Blake, 2012; Moradi & Heeger, 2009; Tsang & Shi, 2008) have shown promise in accounting for the neural interactions that give rise to V1 binocular responses.

Results discussed in this study are consistent with the contrast-gain control theory of binocular combination. Specifically, in response to matching binocular inputs, facilitation in V1 was attenuated by high stimulus contrast, an explicit prediction of the DSKL model (Ding & Levi, 2021). We also report on the temporal dynamics of binocular modulation as a function of contrast. We found that the contrast-dependency of binocular modulation varied as a function of time. A potential implication of this finding is that binocular integration is comprised of sequential stages that can be operationally defined in terms of the V1 binocular contrast-response relationship. This implication could be further explored by evaluating existing neural models of binocular combination over sequential phases of the V1 response or by comparing model performance across varying levels of stimulus exposure. Based

on the evolving contrast-response relationship we observed here, it is conceivable that the rate at which binocular response-gain decays in V1 could be parameterized.

1.4.3. Temporal dynamics of binocular gain-control

Previous studies have demonstrated that V1 exhibits at least two sequential steps that comprise initial facilitation followed by widespread differentiation between binocular concordance and discordance (Cox et al., 2019). We extend our previous work by revealing a relationship between the temporal dynamics of binocular modulation and stimulus contrast. Specifically, initial facilitation of V1 to dioptic stimulation resembled response-gain, characterized by an upward shift of V1's CRF. As V1 responses evolved, contrast-dependency emerged. Contrast-dependency was evidenced by the finding that contrast inversely correlated with facilitation duration, meaning that facilitation persisted longer for lower contrasts than higher contrasts. Furthermore, contrast positively correlated with suppression, such that V1 responses to high contrast binocular stimulation were lower than responses to monocular stimulation of the preferred eye. Finally, a model that assumes V1's binocular response multiplicatively scales with contrast (contrast invariant) explained the initial transient but varied significantly over the time course of the stimulus presentation. These findings support the notion that binocular contrast combination is a dynamic process that involves at least two distinct stages of processing: an initial, rapid process that is more contrast-invariant and a subsequent, slower process that is more contrast-dependent.

1.4.4. Limitations of the study

Data presented in this manuscript is drawn from multiple subjects but biased towards one. Therefore, populations averages of spiking activity are influenced by one subject more than the other. Subject sampling-bias is not unusual for work of this kind. For transparency, units per subject and condition are detailed in tables and statistical tests throughout the manuscript. Nevertheless, we must consider the implications for the generalizability of the findings reported here. One possibility is that our observations and corresponding conclusions truly only apply to one individual subject and thus do not represent a general processing strategy of primate visual cortex. The observations that rest most firmly on data from a single animal are those pertaining to the shape of the CRFs and the temporal dynamics of contrast-dependent decay of binocular facilitation. In the latter case, there seems to be a slight difference in the timing of transition between contrast-dependent facilitation and suppression in one animal, which can be observed by comparing single-penetration data from each subject. Whether this is a true individual difference, or a result of poor sampling is unclear. Future work that examines these or similar conditions in additional individuals will hopefully add weight to one interpretation or another.

Another caveat relating to the specific finding of contrast-dependent decay of binocular facilitation has to do with an inability to differentiate contrast-dependent effects from magnitude-dependent effects. Specifically, we report a contrast-dependent decay of initial binocular facilitation whereby higher contrasts drive a faster transition between facilitation and suppression of the binocular response compared to the monocular response. However, higher contrast stimuli also evoke more V1 spiking than lower contrasts stimuli when all other stimulus features are kept consistent. Therefore, an alternative explanation is that the magnitude of the initial transient itself determines

the rate of decay of binocular facilitation. Thoughtfully designed future experiments might be necessary to distinguish between these two mechanisms.

1.5. Methods

1.5.1. Subjects

The subjects for these experiments were three healthy, adult macaque monkeys (Monkey I, female; *Macaca radiata*; Monkey J, male, *Macaca mulatta*; Monkey B, male; *Macaca radiata*). Macaque monkeys are essential in visual science research due to their close resemblance to humans in visual system structure and function. These primates serve as valuable models for studying a wide range of visual processes, from basic perception to complex decision-making. Ethical guidelines ensure their humane treatment, but ongoing efforts aim to reduce reliance on animal testing in visual science research through alternative methods and models. All procedures involving these animals followed regulations by the Association for the Assessment and Accreditation of Laboratory Animal Care (AALAC), Vanderbilt University's Institutional Animal Care and Use Committee (IACUC), and National Institutes of Health (NIH) guidelines.

1.5.2. Surgical procedures

Prior to data collection, animals were implanted with a custom-designed plastic head holder and a plastic recording chamber (Crist Instruments) spanning over two separate surgeries. All surgeries were performed under sterile surgical conditions using isoflurane anesthesia (1.5%– 2.0%). Vital signs, including heart rate, blood pressure, SpO_2, CO_2, body temperature, and respiratory rate were monitored continuously. During surgery, the head holder and a recording chamber were attached to the skull using transcranial ceramic screws (Thomas Recording, Gießen, Germany) and self-curing dental acrylic (Lang Dental Manufacturing, Wheeling, IL). A craniotomy was performed over the parafoveal visual field representation of primary visual cortex (V1) concurrent with the position of the recording chamber. Animals received analgesics and antibiotics for postsurgical care and closely monitored by researchers, facility veterinarians, and animal care staff for at least three days following surgery.

1.5.3. Visual apparatus

Stimuli were presented on a linearized CRT monitor running at either 60 Hz (resolution 1,280 x 1,024 pixels) or 85 Hz (resolution 1,024 x 768). Animals viewed all stimuli through a custom-built mirror stereoscope, such that images on the right side of the display were viewed by the right eye and images on the left by the left eye (the monitor was divided by a black, nonreflective septum). The mirrors of the stereoscope were infrared-transparent (Qian & Brascamp, 2017), enabling gaze position to be measured using infrared light-sensitive cameras (EyeLink II). To facilitate binocular fusion, an oval aperture was displayed at the edge of each half of the screen. At the beginning of each experimental session, the stereoscope was calibrated via a behavioral task (Maier et al., 2008), which required the animals to fixate on the same location in visual space while being cued in one eye only. Gaze position was measured for each fixation location and compared across eyes. When the gaze position was comparable for cueing in each eye, the mirrors were considered aligned.

1.5.4. Behavioral task

A trial began once the animal fixated (self-initiated) within 1° of visual angle of a centralized fixation cue appearing in both eyes. A series of sinusoidal grating stimuli were presented to the left eye, right eye, or both eyes at a fixed location in parafoveal visual space, each lasting 250-500ms with a 500ms interval interleaved (details of stimuli are described later). If fixation was held for the duration of the trial, the monkey received a juice reward. Alternatively, the next fixation cue appeared with a brief (1-5 s) delay. The animals were at liberty to end recording sessions at any point by halting the initiation of new trials. No other behavior was required.

1.5.5. Neurophysiological procedure

Experiments were conducted inside a radio frequency-shielded booth. During each recording session, a linear multielectrode array (U-Probe, Plexon Inc., Dallas, TX; Vector Array, NeuroNexus, Ann Arbor, MI) was inserted into V1 orthogonal to the cortical surface. Fluctuating extracellular voltages (referenced to the metallic electrode shaft) were amplified, filtered, and digitized using a 128-channel Cerebus neural signal processing system (Blackrock Microsystems, Salt Lake City, UT). Two neural signals were recorded and stored for subsequent offline analysis: a low-pass filtered signal (0.3–500 Hz) sampled at 1 kHz, corresponding to the local field potential, or LFP, and a broadband (0.3 Hz–7.5 kHz) signal sampled at 30 kHz. The neural signal processing system also recorded non-neurophysiological analog signals related to the monitor refresh (i.e., a photodiode signal; OSI Optoelectronics, Montreal, Quebec) and eye position (i.e., voltage output of eye-tracking system), which were digitized and stored at 30 and 1 kHz, respectively. These time stamps and the photodiode signal were used to align the time-varying intracranial data with the occurrence of visual events.

During recording session, the parameters of the sinusoidal grating stimuli (orientation, phase, spatial frequency, location, etc.) were customized relative to the receptive field and tuning preferences of the population of neurons recorded across the microelectrode array. Details of these procedures, including the reverse correlation-like receptive field mapping procedure and the paradigms used to identify tuning preferences have been described in detail previously (Cox et al., 2019; Westerberg et al., 2019). Note, all receptive fields were mapped binocularly, and receptive fields for a given penetration always overlapped due to the orthogonal angle of the microelectrode array to V1.

1.5.6. Pre-processing of spiking activity

Offline, we computed a discretized measure of multi-unit activity (MUA) by applying a time-varying threshold to the envelope of the broadband signal, with an impulse recorded at every time point where the signal envelope exceeded the threshold on each microelectrode contact. Single-unit activity was extracted using Kilosort, an unsupervised machine-learning spike-sorting algorithm (Pachitariu et al., 2016). Both techniques have been described in detail previously (Cox et al., 2019). Here, all analyses were conducted on the discretized multi-unit activity unless otherwise stated. To be included in this study, the spiking units had to fall within the bounds of V1 and exhibit a significant response to visual stimulation, determined by performing a paired-samples *t* test ($\alpha = 0.05$) on the mean baseline activity on each trial and the mean activity during the epoch of visual stimulation (0-250 ms).

1.5.7. V1 response categorization and analysis

For our purposes here, we analyzed spiking responses to stimulation of one or the other eye (monocular) or stimulation of both eyes simultaneously (binocular). All stimuli of these trials consisted of sinusoidal, monochromatic gratings. Features of the gratings, such as size, spatial frequency, and orientation, were set to values which elicited the strongest spiking response of the V1 population, informed by unit responses collected in the tuning paradigms (see *1.5.4. Neurophysiological procedure*). For binocular presentation of gratings, all parameters (size, orientation, spatial frequency, and contrast) were identical between the two eyes and positional disparity was set to zero (resulting in an actual disparity close to zero given the flat surface of the monitor relative to the curvature of the horopter). Throughout the paper, we use the term *monocular* for all stimuli consisting of a grating of the units' preferred orientation, presented to either the left or right eye in isolation. We use the term *dioptic* (*binocular)* to refer to the condition where the same grating is presented at corresponding retinal points to both eyes.

The stimulus parameter that varied experimentally was the Michelson contrast of the grating(s) between presentations. The exact contrast levels used across recording days varied slightly (e.g., we sampled responses to more, evenly spaced, contrasts on days where the animals' motivation was high). We thus grouped the following contrast ranges: [0, 0.20-0.225, 0.40-0.45, 0.80-0.90].

1.5.8. Duration of binocular facilitation

Duration of binocular facilitation was evaluated in efforts to assess contrast-dependency of binocular modulation across time. For this analysis, we estimated the onset and offset of facilitation from each unit's delta spiking response (250ms). We estimated the onset of facilitation as the timepoint associated with the peak magnitude of facilitation for each unit. We estimated the offset of facilitation for each unit by identifying the timepoint after onset at which the delta response crossed zero. Duration was then computed as offset minus onset of facilitation. This procedure was repeated for each stimulus contrast level. Since we were only interested in the temporal dynamics of facilitation, units that did not show facilitation (positive delta) at any timepoint were excluded from this analysis (n = 32).

1.5.9. Determining the neurons' dominant eye

Our analysis aimed to compare binocular responses of V1 neurons to their monocular counterparts. Neurons in V1 are known to differ in the magnitude they respond to stimuli presented to one eye or the other (D. H. Hubel & Wiesel, 1962). This is the *ocular dominance* of the neuron. We used the neuronal responses to monocular stimulation to compute an ocularity index that quantifies a unit's selectivity for one versus the other eye,

$$ocularity = \frac{mean(LE) - mean(RE)}{mean(LE) + mean(RE)}$$

defined as differences between trial-averaged responses (*mean*, 0-250ms) of each eye divided by their sum. All nonrelevant parameters, such as orientation and contrast, were matched for this process. For each unit, we used this value to distinguish "dominant (DE) eye" and "non-dominant (NDE).

1.5.10. Contrast response functions

Contrast response functions (CRFs) portray a neuron's mean spiking response as a function of stimulus contrast (Albrecht & Hamilton, 1982). To determine how binocular V1 spiking responses vary as a function of contrast, we measured CRFs in units for which there were four datapoints (247 in monkey E, 8 in monkey I) under monocular and binocular stimulation. Trial-averaged spiking responses (over varying time windows) as a function of visual contrast were fit using the Naka-Rushton function:

$$R_{R_{max},C_{50},n,b}(c) = \frac{Rmax * \ c^n}{c^n + {C_{50}}^n} + b$$

where R is the response of the unit, R_{max} is the projected maximum response of the unit, C_{50} is the semi-saturation constant that represents the contrast at which the output is half of the maximum response, n is the scaling exponent, and c is the contrast of the stimulus. The y-intercept b represents the maintained activity and was fixed for individual neurons to the average activity during blank trials (0 contrast = gray background). The parameters R_{max}, C_{50}, and n collectively determine the shape of the contrast response curve (Carandini & Heeger, 2012). For each unit, the trial-averaged contrast responses under binocular and monocular conditions were fit with all parameters free to vary [R_{max}, C_{50}, n].

1.5.11. Statistical analysis

We used custom code written in Matlab (The Mathworks Inc.) for data analysis. All statistical analyses were conducted in Jamovi version 2.0.0, an open-source statistical software. Mean piking responses (N = 314 units, 234 from Monkey E) to stimuli of varying contrast [0, 0.20-0.225, 0.40-0.45, 0.80-0.90] were compared across monocular and binocular stimulation. Mean responses were either taken as time-average spiking across full stimulus presentation (0-250ms) or 100ms windows within this timeframe, as noted. Data from monkey "I" had incomplete observations at low and medium contrast (see Table 1 for sample information), which prevented the use of repeated measures ANOVA on pooled units from both animals. To test effects of stimulus contrast across both animals without discarding data, we employed a mixed-model analysis of variance with contrast as a continuous predictor and the unit as a random factor **(**Figure 7, Figure 8**,** Figure 9, and Figure 10). Subsequent analyses employed repeated measures ANOVA on units with complete observations (Figure 11 and Figure 12). Post hoc tests were performed when appropriate to test for significant ($p < 0.05$) contrasts between samples (two-tailed, paired t tests) with Bonferonni correction. Performance of simple models of gain-control were evaluated by goodness of fit (R^2) to the observed binocular contrast responses (mean spiking over 100ms windows).

Chapter 2

A Role for Ocular Dominance in V1 Binocular Integration[2]

2.1 Summary

Neurons in primate primary visual cortex (V1) combine left and right-eye information to form a binocular output. Controversy surrounds whether ocular dominance, the preference of these neurons for one eye over the other, is functionally relevant. Here, we demonstrate that ocular dominance impacts gain-control during binocular combination, providing the visual system with a way to differentiate dichoptic viewing conditions with the same interocular contrast ratio. We recorded V1 spiking activity while monkeys passively viewed grating stimuli. Gratings were either presented to one eye (monocular), both eyes with the same contrasts (binocular balanced), or both eyes with different contrasts (binocular imbalanced). We found that contrast placed in a neurons' dominant eye was weighted more strongly than contrast placed in a neurons' non-dominant eye. This asymmetry covaried with neurons' ocular dominance. We then tested whether accounting for ocular dominance within divisive normalization improves the fit to neural data. We found that ocular dominance significantly improved model performance, with interocular normalization providing the best fits. These findings suggest that V1 ocular dominance influences normalization of contrast both within and between monocular channels and could potentially serve as a form of eye-specific contrast coding in visual cortex.

2.2 Introduction

In primate V1, most neurons respond to appropriate retinal stimulation of either eye (D. H. Hubel & Wiesel, 1962). That is, most V1 neurons are considered *binocular*. However, V1 neurons tend to express a preference for one eye or the other, or *ocular dominance*. This phenomenon is tied to the segregation of thalamocortical afferents to the recipient layers of V1, forming *ocular dominance (OD) columns* (D. H. Hubel & Wiesel, 1968; Shatz & Stryker, 1978; Tootell et al., 1988). OD columns exist in a wide range of species, typically in those that have front-facing eyes and overlapping monocular visual fields (Adams & Horton, 2009). They have been demonstrated physiologically (D. H. Hubel & Wiesel, 1962; Shatz & Stryker, 1978; Tieman et al., 1983), as well as anatomically after processing striate cortex with a variety of tissue-reactive substances (Fonta et al., 2000; Hitchcock & Hickey, 1980; D. H. Hubel et al., 1977; LeVay et al., 1975; Stryker, 1978).

The existence of ocular dominance in two-eyed mammals has been a puzzle for the past six decades (J. C. Horton & Adams, 2005). Since their discovery, efforts have been made to understand what role, if any, OD plays in visual processing (Adams & Horton, 2003; Gardner & Raiten, 1986; Katz & Crowley, 2002; Ng & Purves, 2019; Swindale, 1981). Anatomical studies have revealed considerable variation in OD column expression across different species with no apparent impact on visual capacity (Adams & Horton, 2009; Casagrande & Boyd, 1996). Certain

[2] This chapter is adapted from "A Role for Ocular Dominance in Binocular Integration" published in Current Biology and has been reproduced with the permission of the publisher and my coauthors, Brock Carlson, Jacob Westerberg, Michele Cox, and Alex Maier. DOI: 10.1016/j.cub.2023.08.019

characteristics of OD columns, such as their size and periodicity, differ even among individuals of the same species(J. Horton & Hocking, 1996b). Notably, some squirrel monkeys lack these columns entirely or only exhibit them in peripheral representations of V1, yet their visual abilities remain comparable to other squirrel monkeys that express them (Adams & Horton, 2003). These observations have led to the proposition that the arrangement of OD into columns and their topographical pattern in V1 may not serve a specific purpose for mammalian vision (J. C. Horton & Adams, 2005). To date, this proposition remains uncontested.

An alternative but not mutually exclusive hypothesis is that the *physiological property* of OD is relevant for early visual processing. That is, OD may play a role in mammalian vision irrespective of its spatial organization in cortex. Indeed, OD has been observed in mammals without any organizing principle, as in rodents (Gordon & Stryker, 1996) and some squirrel monkeys, and in alternate configurations that are non-columnar. However, a cloud continues to hover over interest in the physiological property of OD: sixty years of neurophysiological studies have not delivered replicable evidence for the hypothesis that seemed most promising: OD's involvement in V1's mechanisms for depth detection (Gardner & Raiten, 1986; LeVay & Voigt, 1988; G. Poggio et al., 1988; G. F. Poggio & Fischer, 1977; J. C. A. Read & Cumming, 2004). Consequently, skepticism subsists that OD is involved in any aspect of binocular processing at all.

However, in recent years, evidence has been accumulating in favor of a broader view. Studies have demonstrated a relationship between the physiological property of OD and associated properties of V1 binocular responses (Cox et al., 2019; Dougherty, Cox, et al., 2019). For example, neurons dominated strongly by one eye in the input layers of V1 (i.e., seemingly monocular neurons) have been shown to modulate under binocular stimulation in a manner that is predicted by the strength of their ocular dominance (Cox et al., 2019; Dougherty, Cox, et al., 2019). This suggests that the monocular spiking preferences of V1 neurons, as indexed by their ocular dominance, bears on the formation of binocular responses more generally. No study to date has directly evaluated the relationship between OD of V1 neurons and binocular contrast combination.

Here, we investigate whether ocular dominance is relevant for binocular contrast combination in primate V1. To do so, we recorded from V1 OD columns using linear microelectrode arrays while macaque monkeys viewed grating stimuli either monocularly or binocularly through a mirror stereoscope. We collected spiking responses to these stimuli from V1 units across a wide array of ocular dominance, ranging from purely monocular to fully binocular neurons. We found that placing higher contrast in a neuron's dominant eye was more influential for binocular response formation than the same stimulus placed in the non-dominant eye. This asymmetry scaled with ocular dominance. Using this knowledge, we found that accounting for ocular dominance in computational models of binocular contrast combination significantly improved performance. Together, our results demonstrate that ocular dominance is relevant for binocular contrast combination by contributing to interocular gain-control and suggest that this physiological property embeds an eye-specific contrast code within V1 binocular responses.

2.3 Results

We were interested to determine whether ocular dominance is functionally relevant for binocular contrast combination in primate V1. To do this, we recorded spiking activity from V1 ocular dominance columns while macaque monkeys passively viewed grating stimuli through a custom mirror stereoscope (Figure 13*A*). Gratings were presented to one or the other eye using either the left or the right side of the monitor (*monocular* stimulation) or both eyes in conjunction (*binocular* stimulation) at the mapped receptive field location (Figure 13*B,* see *2.5.4. Receptive field mapping and tuning* for details). The stimuli are presented for 250ms after fixation is acquired (Figure 13*C*). Gratings varied in Michelson contrast (e.g., 0, 0.055, 0.11, 0.225, 0.45, 0.90) across presentations. Binocular presentations additionally varied in contrast between the eyes (e.g., 0.225 in the left eye, 0.45 in the right eye). We analyzed V1 spiking responses (n = 500, 25 sessions, 2 subjects) to 36 combinations of varying contrast across the eyes, comprised of both monocular and binocular conditions (Figure 13*D*).

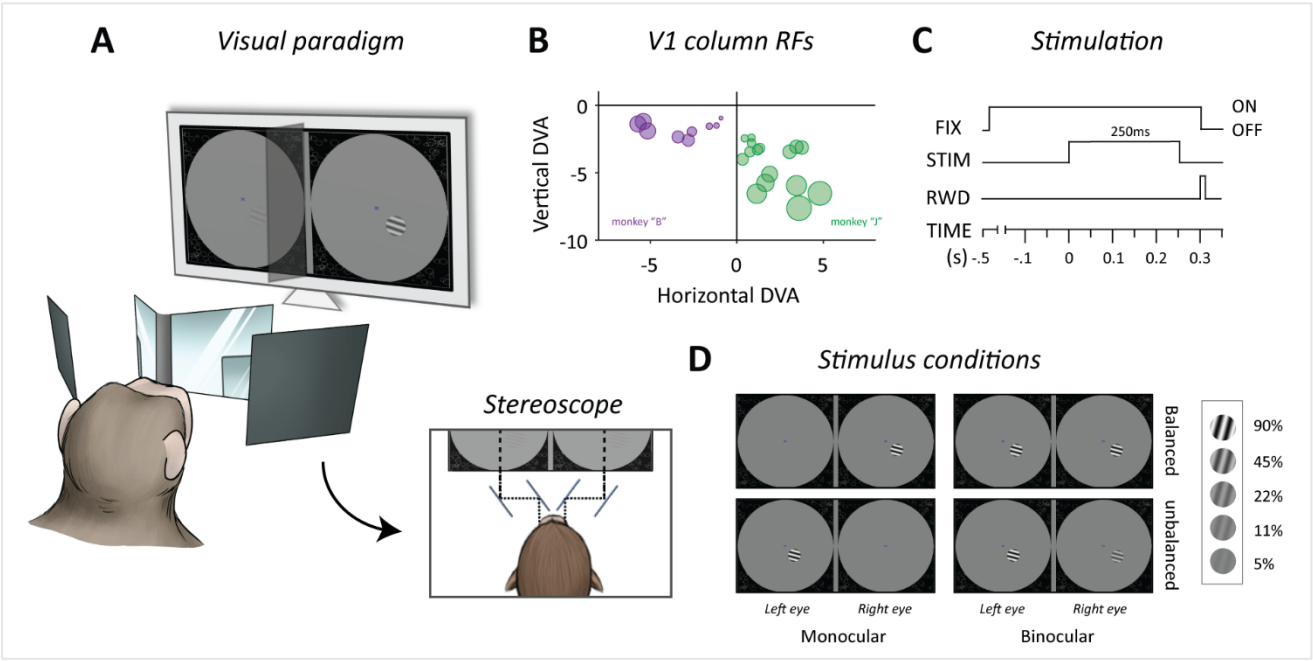

Figure 13. Experimental methodology for Study 2. (A) Visual paradigm. Animals viewed all stimuli through a custom-built mirror stereoscope, such that images on the right side of the display were viewed by the right eye and images on the left by the left eye. Stimuli were presented to one or both eyes parafoveally (while fixating a central cue). (B) V1 columnar population receptive field boundaries and extents. We recorded from 9 V1 columns from monkey B (Right V1, purple) and 16 V1 columns from monkey J (Left V1, green). (C) Gratings appeared on screen for 250ms, up to three times per trial with 300ms interleaved. If fixation was held for the entire trial, monkeys received fluid reward. (D). Stimulus conditions. Gratings were presented two one or the other eye (monocular) or both eyes simultaneously (dioptically or dichoptically binocular). Gratings varied in 6 octave-spaced Michelson contrast levels (0, 0.05, 0.11, 0.225, 0.45, 0.90). Binocular gratings either had the same contrast (balanced) or varied in contrast between the eyes (unbalanced).

Using these data, we tested for a functional relationship between ocular dominance, a property derived from the difference between monocular responses, and the neurons' binocular responses. We took two approaches to answering this question. First, we quantified the extent to which the neurons' dominant eye impacts binocular response formation and combination of contrast. Then, we tested whether neural models of binocular contrast combination can be improved by including information about the neurons' ocular dominance.

2.3.1. Measuring ocular dominance in V1

To facilitate our analysis of ocular dominance's role for binocular combination, we first determined which eye was most effective at driving spiking responses for each unit (n = 502). Specifically, we compared responses across contrast levels between stimulation of the contra- and ipsilateral eye. Using these data, we calculated an ocular dominance index at each contrast level as the difference between the mean response *u* for unit *i* to contralateral presentations and ipsilateral presentations, divided by their sum:

$$(ODI_i) = \frac{Contra(u_i) - Ipsi(u_i)}{Contra(u_i) + Ipsi(u_i)}$$

The output of this formula is a value between -1 and 1, with -1 representing units driven more vigorously by the ipsilateral eye and 1 describing units driven entirely by the contralateral eye We averaged the obtained values across stimulus contrast to derive a single OD index for each unit (Figure 14*A*). Approximately half of the neurons preferred the contralateral eye (49.2%). Because neurons varied in which eye they preferred from column to column, we organized responses to the 36 conditions by contrast shown to the "dominant" versus "non-dominant" eye (Figure 14*B*).

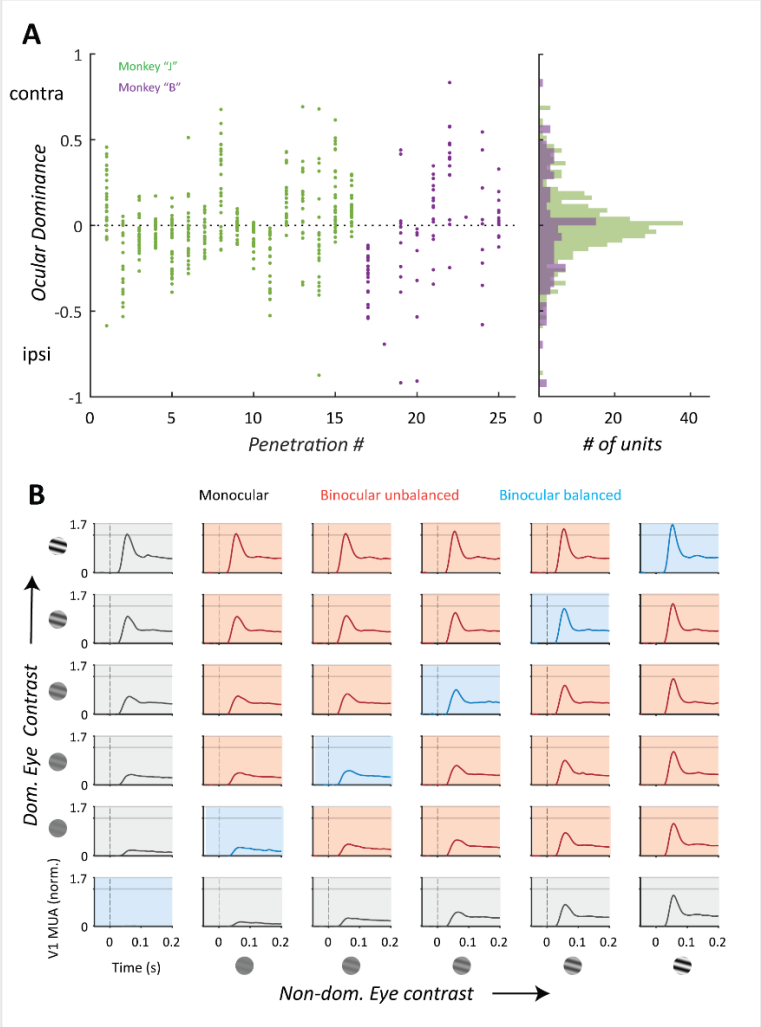

Figure 14. Characterizing ocular dominance in V1. (A) Ocular dominance across penetrations (N = 25). Each datapoint represents a unit (n = 502; 404 from monkey J). Units with ocular dominance values greater than zero exhibited a response preference for the contralateral eye. Histogram shows the distribution of ocular dominance for each subject. (B) Mean V1 responses (n = 502) to all 36 stimulus conditions, organized by contrast shown to the dominant and non-dominant eye.

2.3.2. Contrast placed in the neurons' dominant eye has a greater impact on V1 binocular responses

We started by investigating the relative role of each eye for binocular contrast combination. Analyzing pairs of binocular conditions with swapped contrast in the two eyes provides clues to answer this question. If ocular dominance were irrelevant for binocular contrast combination, a binocular response should be identical when one or the other eye receives higher contrast. If, on the other hand, swapping contrasts between the eyes does not lead to equivalent binocular outputs, ocular dominance needs to be taken into account to understand binocular contrast combination.

To adjudicate between these two possibilities, we compared binocular responses (trial-averaged, 50-200ms) that received the same total contrast energy but differed in which eye (dominant vs. non-dominant) received the higher contrast (e.g., 11% / 45% versus 45% / 11%). Figure 15*A* plots a summary of binocular response magnitudes (averaged across 502 units) organized by contrast in the dominant eye (upper left of the matrix) and contrast in the non-dominant eye (lower right of the matrix). Note that the magnitude of the binocular response increased as a function of total contrast energy. To assess whether contrast in the dominant eye contributed more to binocular responses than contrast in the non-dominant eye, we flipped the matrix about the diagonal and performed a subtraction between the upper and lower off-diagonal responses (i.e., paired contrast conditions). The bottom panel of Figure 15*A* plots the results of this calculation, which we refer to as *response asymmetry*. Finally, we computed an index of response asymmetry for each unit by taking the average delta between paired contrast conditions. Values above zero indicate a binocular response asymmetry that favors contrast placed in the dominant eye (Figure 15*C*)**.** We found that paired binocular conditions with the same contrast energy but flipped contrast in the two eyes were statistically different (*Wilcoxon W* = 107185, $p < 0.0001$, Rank biserial correlation = 0.698). When the higher contrast was in the non-dominant eye, the binocular response tended to be less than when the same stimulus was placed in the dominant eye.

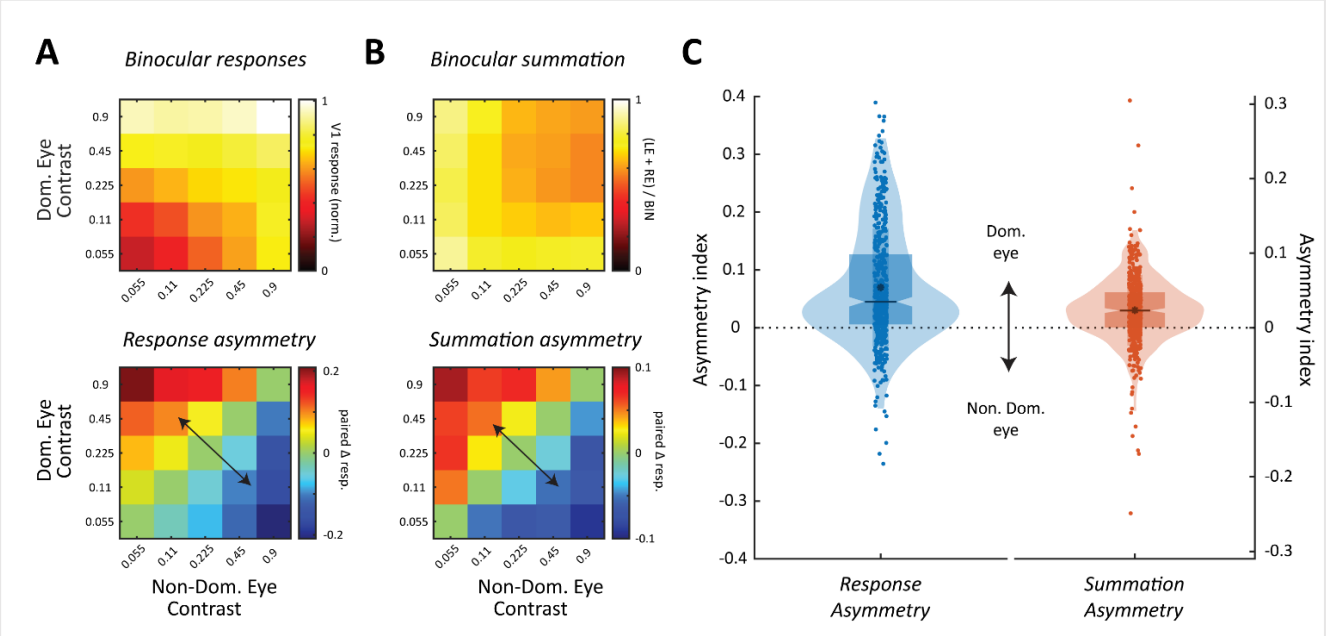

Figure 15. Asymmetries in V1 dichoptic responses and summation. (A). Mean V1 binocular response matrix (average across 502 units) to balanced (diagonal) and unbalanced contrast in the two eyes (off-diagonal). The matrix is organized such that the upper left cells represent responses to binocular conditions where the contrast was always higher in the dominant eye. Below is a pair-wise subtraction between upper left cells and lower right cells to assess whether contrast in the dominant eye carries more weight into the binocular responses. The resulting calculation revealed that V1 responses to unbalanced contrasts in the two eyes are greater when the higher contrast is placed in the dominant eye. (B) Mean V1 binocular summation matrix (average across units) to balanced (diagonal) and unbalanced contrast in the two eyes (off-diagonal). Summation asymmetry is plotted below, using the same procedure as described for A. Binocular summation was greater for unbalanced contrast when the higher contrast is placed in the dominant eye. (C) Unit-by-unit distribution of binocular response asymmetry and binocular summation asymmetry simplified to a single scalar (502 units). Values above and below zero indicate asymmetry favoring higher contrast in the dominant or non-dominant eye, respectively. Individual points represent raw data; Mean indicated with an asterisk; Median indicated with a horizontal black line that defines the notch in the box; bottom and top of the box indicate 1st and 3rd quartiles, respectively; bottom and top of the shaded "violin" region indicate 1st and 99th percentile, respectively.

In a similar vein, we asked whether *binocular summation*, or the extent to which a binocular response can be explained as a linear combination of its monocular subcomponents, is impacted by which eye (dominant or non-dominant eye) receives the higher contrast. Figure 15*B* demonstrates the magnitude of binocular summation (1 = linear summation) across contrast conditions. We found that binocular summation was generally the greatest when the total contrast energy was low in the two eyes and systematically decreased with summed contrast energy. Like the procedure described above, we calculated summation asymmetry by flipping the matrix about its diagonal and subtracting lower and upper off-diagonal responses, and then converting these delta values into an average index for each unit. Values above zero indicate a binocular summation asymmetry that favors contrast placed in the dominant eye (Figure 15*C*)**.** We found that paired binocular conditions with the same contrast energy but flipped contrast in the two eyes summed contrast differently (*Wilcoxon W* = 101420, $p < 0.0001$, Rank biserial correlation = 0.607). When the higher contrast was in the non-dominant eye, binocular summation tended to be less than when the same stimulus was placed in the dominant eye.

2.3.3. Ocular dominance index predicts each eye's contribution to the binocular response

So far, we have shown that contrast placed in the neurons' dominant eye carries more weight into the resulting binocular response than contrast placed in the non-dominant eye. Our organization of dominant and non-dominant eye was based on which eye drove monocular responses more vigorously, which is the common definition of ocular dominance. If ocular dominance impacts the formation of the binocular response, then the magnitude of ocular dominance should predict the magnitude of response and summation asymmetry (shown in Figure 16). To test this, we took the absolute value of each unit's ocular dominance to produce a value between 0 and 1, with 0 representing the most binocular units and 1 representing the most monocular units. We then plotted the strength of absolute ocular dominance as a function of response and summation asymmetry indices. We found a relationship between both asymmetry indices and absolute ocular dominance (Figure 16). Specifically, as absolute ocular dominance increased, mean asymmetry in binocular responses (Figure 16*A*) and binocular summation (Figure 16*B*) systematically increased, respectively (adjusted $R^2 = 0.46$, $t = 20.53$, $p = 2.0798e^{-68}$; adjusted $R^2 = 0.16$, $t = 9.90$, $p = 3.2962e^{-21}$). These findings show that a neuron's absolute ocular

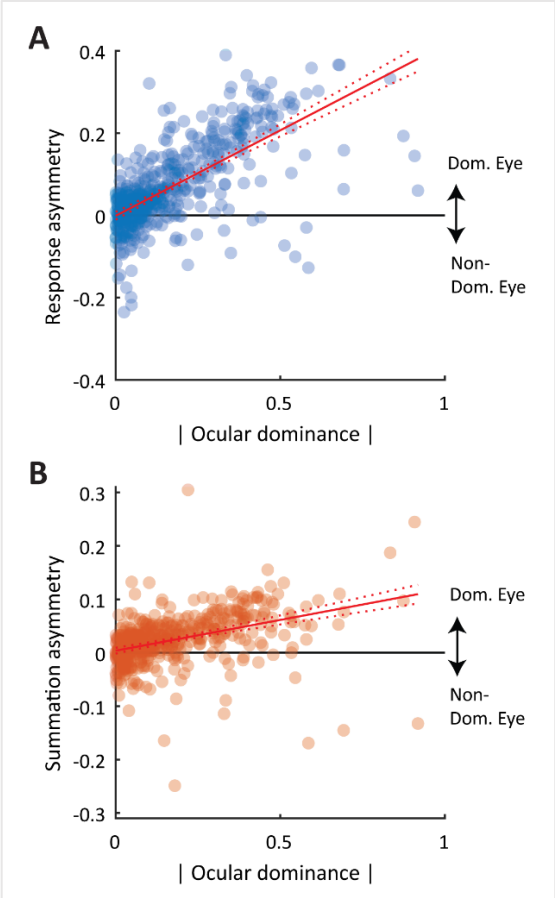

Figure 16. Ocular dominance correlates with asymmetries in binocular responses and summation (A). Absolute ocular dominance index as a function of binocular response asymmetry index. (B) Absolute ocular dominance index as a function of binocular summation asymmetry index.

dominance predicts how strongly that neuron weighs contrast in the dominant eye during binocular response formation.

2.3.4. Modeling ocular dominance within a divisive normalization framework

Results so far suggest that ocular dominance plays a role in binocular contrast combination by modulating the effectiveness of contrast, depending on whether it is shown to the dominant or non-dominant eye. These results are in line with a recent demonstration that ocular dominance modulates stimulus *gain* in cat striate cortex (M. A. Georgeson & Sengpiel, 2021). To find out whether this type of modulation also explains our observations, we wanted to test whether computational models of binocular contrast combination can be improved by including information about a neurons' ocular dominance. We started by modeling monocular responses to stimulus contrast within a divisive normalization framework. Divisive normalization (Heeger, 1992b) has been successful at explaining V1 responses to contrast and a range of other V1 phenomena (Sawada & Petrov, 2017). Accordingly, normalization has been proposed to represent a canonical cortical computation (Carandini & Heeger, 2012).

For each unit, we measured monocular contrast response functions (CRFs) by fitting trial-averaged spiking responses to each contrast level with the Naka-Rushton equation (Naka & Rushton, 1966), allowing all parameters (R_{max}, C_{50}, n) to vary freely. As expected, the parameters of the dominant and non-dominant eye CRFs differed. We hypothesized that, by parameterizing the difference between *monocular* curves, we could effectively parameterize ocular dominance as a kind of gain-control on contrast placed in the neurons' non-dominant eye. This enabled us to then test whether inclusion of ocular dominance improves the ability of *binocular* models to fit V1 binocular responses.

Our first objective was to determine which parameter (R_{max}, C_{50}, n), or which kind of gain-control, explains the most variance between the dominant and non-dominant eye CRFs (Figure 17*A*). To achieve this, we first fitted a curve to the neurons' dominant eye responses to contrast. We then fitted a curve to the neurons' non-dominant eye responses, but this time we fixed two parameters to the dominant eye and allowed just one to vary freely. Figure 17*B* demonstrates the effect of allowing each parameter to vary while holding the other two constant. We found that allowing the parameter R_{max} to vary freely between the fitting dominant and non-dominant eye responses yielded the best fits (Mean adjusted $R^2 = 0.92$, $SD = 0.09$) for the non-dominant eye responses (Figure 17*C*). This finding suggests that the predominant expression of ocular dominance within a divisive normalization framework can be described as response-gain control, or a vertical shift of the CRF along the ordinate. The same effect can be achieved by adding a weight to the contrast in the numerator of the Naka-Rushton equation (Figure 17*D*). Re-fitting the non-dominant again with all parameters fixed to the dominant eye but an additional term (w) matched the effects of R_{max} and produced a distribution of weights (Figure 17*E*) that correlated (Adjusted $R^2 = 0.56$, $t = 25.2$, $p = 2.6770e^{-91}$) with the neuron's ocular dominance index (Figure 17*F*).

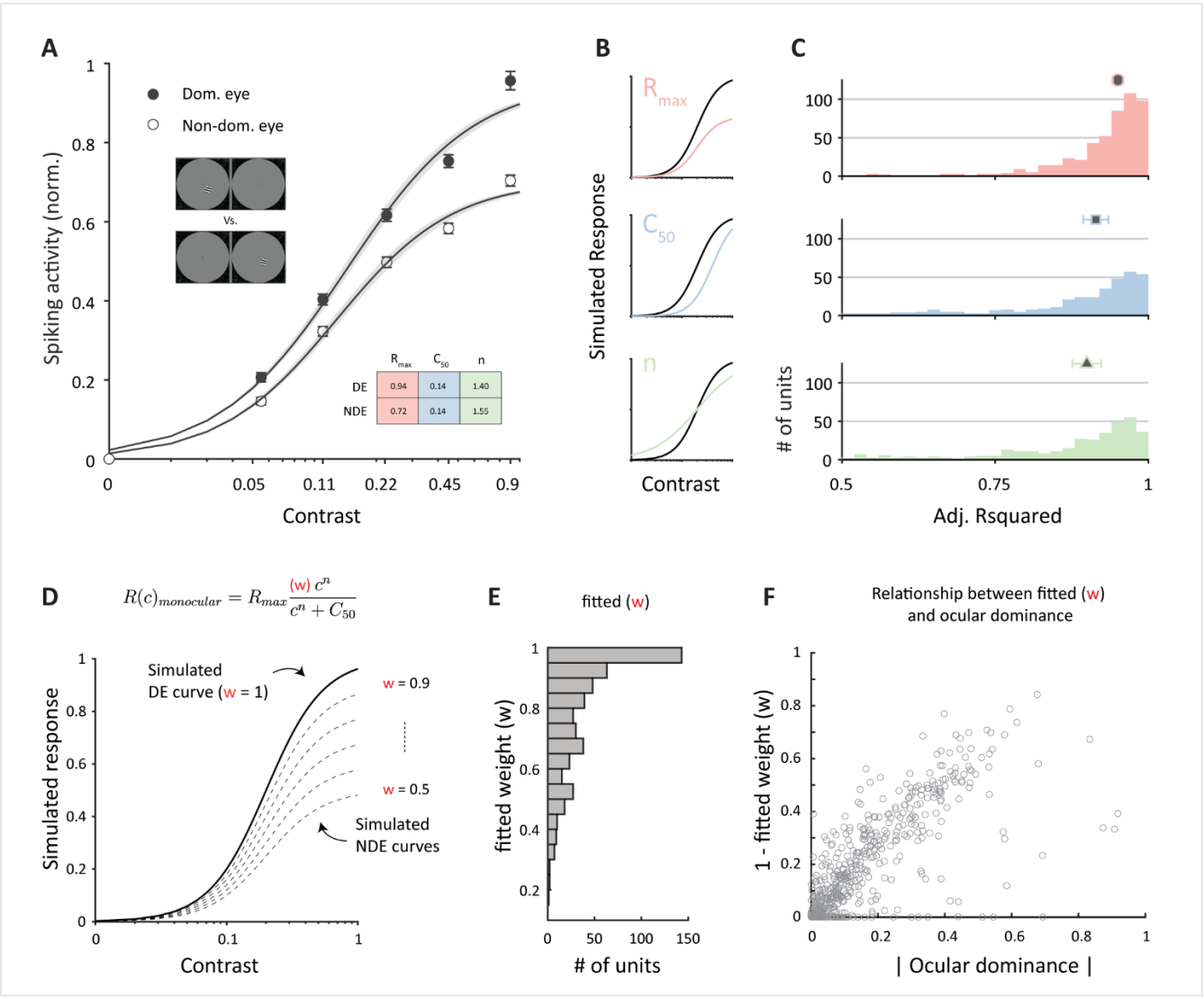

Figure 17. Modeling ocular dominance within the divisive normalization framework. (A). Mean V1 responses as a function of stimulus contrast placed in the dominant and non-dominant eye fitted with the Naka-Rushton equation. Mean parameters for each curve are displayed in the inset box. (B) Effect of each parameter on the contrast response curve. (C) Distribution of goodness of curve fit to the non-dominant eye responses, allowing just one parameter to vary at a time while fixing the other two to the dominant eye curve (Rmax, M = 0.92, SD = 0.09; C50, 0.82, SD = 0.21; n, M = 0.79, SD = 0.24). (D) Placing a weight (w) on contrast in the numerator matches a response-gain control. (E) Distribution of weights (w) after allowing the weight to vary while fixing all other parameters to the dominant eye curve. (F) Relationship between neurons' fitted weight and absolute ocular dominance index

2.3.5. Accounting for ocular dominance improved computational models of binocular combination

Weighting the contrast in the non-dominant eye (w) captured the effect of ocular dominance as a response-gain control within a divisive normalization framework. We next tested whether the inclusion of this weight, derived from monocular responses of each unit, can improve the ability of various binocular models to fit the neurons' binocular responses. Several models have been proposed for how V1 binocular contrast combination is achieved in V1. These models typically vary in the number and position of gain-control mechanisms. We tested various binocular models built on a shared normalization framework which represent different ways for combining the two monocular contrast response functions:

One possibility is that gain-control on binocular signals is applied at a binocular stage after the two eyes are summed:

$$R(c_L, c_R) = 0.5 * (\frac{c_L^n}{c_L^n + c_{50}} + \frac{c_R^n}{c_R^n + c_{50}})$$

Here, the binocular response is modeled as the average of the two monocular contrast response functions, akin to our visual experience when opening and closing one eye.

On the other hand, the two eyes may give rise to independent divisive normalization channels, without possibility for interocular interactions or any form of binocular gain-control. While this linear model has proven to be an unlikely candidate given inherent nonlinearities of spike generation (Burns & Pritchard, 1968; Longordo et al., 2013; Moradi & Heeger, 2009; Zhao et al., 2013), it is still a useful tool to assess the degree of summation of contrast in the two eyes:

$$R(c_L, c_R) = \frac{c_L^n}{c_L^n + c_{50}} + \frac{c_R^n}{c_R^n + c_{50}}$$

Yet another possibility is that the two eyes are normalized monocularly and then summed quadratically:

$$R(c_L, c_R) = \sqrt{\left(\frac{c_L^n}{c_L^n + c_{50}}\right)^2 + \left(\frac{c_R^n}{c_R^n + c_{50}}\right)^2}$$

This historical model employs gain-control at a binocular stage (Legge, 1984b). Unlike the previous model, here magnitude of gain-control scales nonlinearly with contrast.

Alternatively, the two eyes may interact before being summed, such that each eye's input exerts control over the strength of the other eyes' normalization (Moradi & Heeger, 2009). Unlike the other models, this model incorporates interocular interactions at a monocular stage:

$$R(c_L, c_R) = \frac{c_L^n + c_R^n}{c_L^n + c_R^n + c_{50}}$$

We used MATLAB (2021a)'s fit() function to fit each model to the binocular response matrix (5x5 trial-averaged (single contact) or mean (n = 502) responses) using the nonlinear least squares method with two independent variables (C_L, C_R). We additionally weighed each datapoint (i.e., condition) by the number of trials on a unit-by-unit basis. The fit procedure for the binocular response functions allowed each parameter ($R_{max,}$ C_{50}, n) to freely vary to achieve the best fit to the data. We tested whether ocular dominance information improves each fit

by adding a weight (w) as a 'problem' parameter/fixed variable to multiply the contrast in the numerator of the non-dominant eye's function. The placement of this weight was informed by the analysis featured in *Figure 16*. This weight took on a value of 1 (no effect) or that of each unit's fitted ocular dominance weight.

Recall that V1 binocular responses exhibited a response asymmetry, which can be visualized as a bias in response magnitude towards contrast placed in the dominant eye (Figure 18*A*). We showed that this asymmetry varies systematically with the ocular dominance of V1 neurons. By accounting for ocular dominance in each model (Figure 18*C*) via a weight to contrast in the non-dominant eye, we expected model performance to improve over its baseline performance (without OD). Figure 18*B* conveys a visual summary of model performance at the mean (averaging responses across all units) level. Notably, models that do not incorporate ocular dominance produce symmetrical response matrices and therefore cannot account for binocular asymmetry that we observe. Figure 18*D* shows distributions of model performance (adjusted R^2) without (left distribution) and with (right distribution) the fitted ocular dominance weight unique to each unit. As expected, the addition of ocular dominance information generally improved the performance of each model. A Friedman test revealed there were significant differences

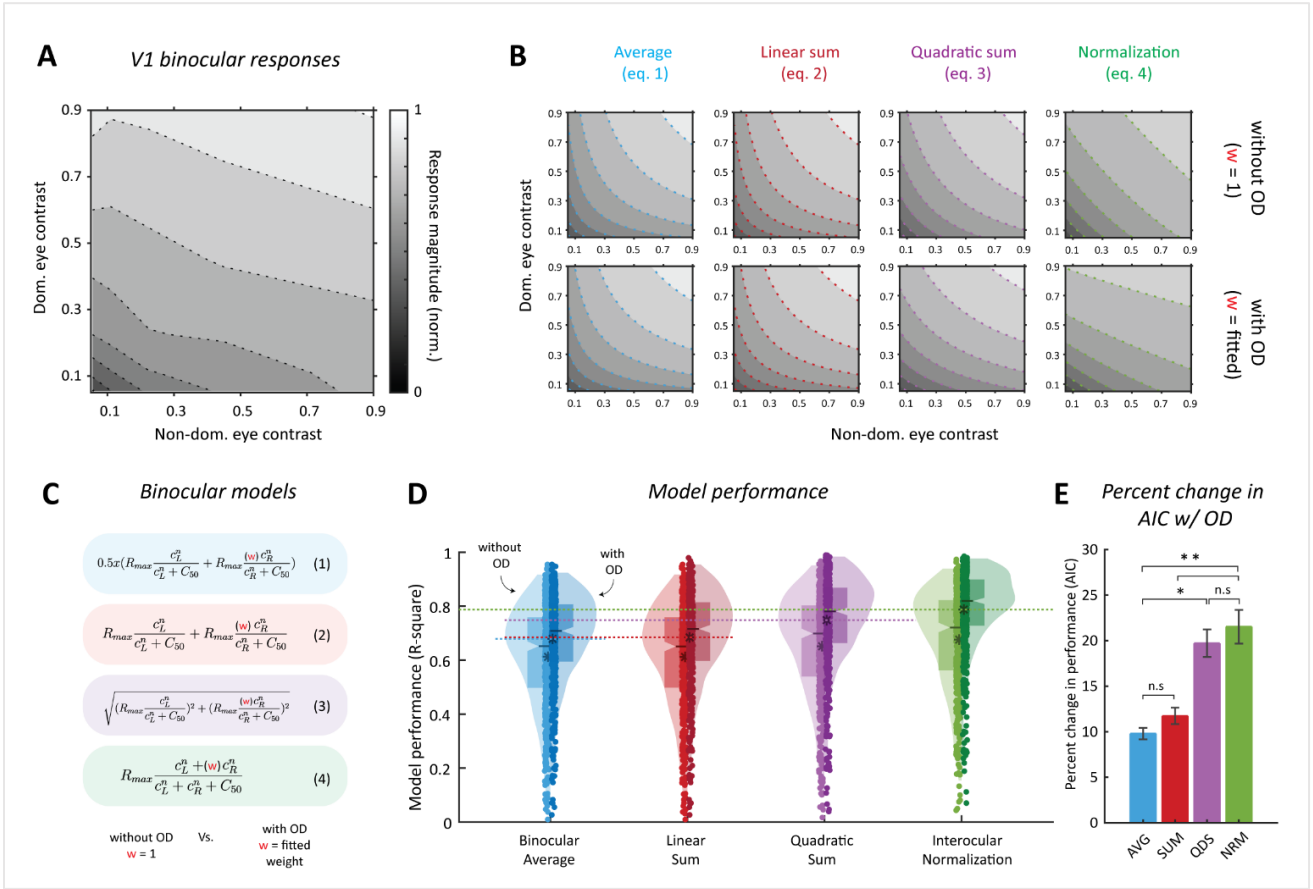

Figure 18. Ocular dominance improves computational models of binocular combination. (A) Contour map of V1 binocular responses highlighting binocular response asymmetry. (B). Mean model performance (fitted to mean data) demonstrates the effect that the fitted ocular dominance weight (w) has on binocular models fits. (C). Computational models of binocular contrast combination. The weight (w) term takes on a value of 1 when testing the models without OD and takes on the individual units' fitted w (derived solely from monocular data) when testing the models with OD. (D) Model performance with and without OD for each unit. A horizontal line is plotted through each model's mean performance with OD to aid visual comparison. (E) The effect of adding OD information calculated as a percent change in estimated Akaike's information criteria (AIC). Generally, the inclusion of the fitted weight derived from monocular data improved the ability of binocular models to fit the binocular response data.

between models equipped with OD ($X^2(3) = 779$, $p < .001$). Post hoc comparisons using the Durbin-Conover test indicated that interocular normalization ($M = 0.79$, $Mdn = 0.82$) performed slightly better than quadratic summation ($M = 0.75$, $Mdn = 0.78$; $p < .001$), and much better than averaging ($M = 0.68$, $Mdn = 0.71$; $p < 0.001$) or summing the contrast in the two eyes ($M = 0.68$, $Mdn = 0.72$; $p < .001$).

To quantify the gain in performance due to OD, we approximated Akaike's information criteria (AIC) for each model fit (Table 2). The formula used for this approximated AIC can be found in *2.5.9. Statistical analysis*. We then calculated the percent change in AIC within each model for each individual unit (Figure 18*E*). Interocular normalization received the biggest boost in performance ($M = +21.5\%$, $SD = 41.6$) followed closely by quadratic summation ($M = +19.7\%$, $SD = 34.1$). Averaging or summing contrast between the two eyes (with one eye weighted) received the smallest boosts in performance ($M = +9.79\%$, $SD = 14.3$; $M = +11.7\%$, $SD = 20.2$, respectively).

Table 2. Effect of ocular dominance weight on model performance

	Akaike's information criteria (AIC)			Statistic		
	Without OD	With OD	Mean Difference	Wilcoxon W	*p*	Rank biserial correlation
Average (eq 1)	52.7	47.7	5.00	13552	< .00001	0.79
Summation (eq 2)	52.6	46.6	6.00	12939	< .00001	0.80
Quadratic (eq 3)	48.8	38.2	10.6	16603	< .00001	0.74
Normalization (eq 4)	46.7	34.0	12.7	19114	< .00001	0.70

2.4 Discussion

We report that binocular combination of contrast in macaque V1 is modulated by the neurons' preference for eye. The contrast placed in the neurons' dominant eye contributed more to binocular response formation than the same contrast placed in the neurons' non-dominant eye. This asymmetry positively correlated with the ocular dominance index of neurons. These findings provide an explanation for the established relationship between OD and binocular modulation in V1(Anderson & Movshon, 1989; Smith et al., 1997). Furthermore, our data are also consistent with previously reported cell-to-cell variations in the slopes of their binocular interaction contours (Anderson & Movshon, 1989), which were originally hypothesized to reflect variation in the strength of inputs from each eye (i.e., ocular dominance) (Smith et al., 1997). Our results, therefore, contribute evidence in favor of the alternative hypothesis that the neurophysiological property of OD is relevant for our study of binocular integration. However, it is important to note that our data do not directly address the question of why ocular dominance exists in the first place, which pertains to its potential ultimate causes. To shed light on this question, one would anticipate

evidence demonstrating that binocular combination, in some aspect, functions more effectively in a system where ocular dominance is present compared to a system where it is absent.

2.4.1. Ocular dominance shapes the formation of binocular responses in V1

A lingering question in the field has been to what extent the ocular dominance index, measured purely from monocular tests, can serve as a useful parameter for our understanding of early visual processing. Using traditional monocular tests, a neuron's ocular dominance index is based on the relative difference in spiking response to left and right eye stimuli (D. H. Hubel & Wiesel, 1962). However, a neurons' discharge magnitude does not adequately capture its synaptic inputs (Priebe & Ferster, 2008). Neurons must depolarize to a critical threshold to fire an action potential. So, in the case of using monocular tests for ocular dominance, synaptic inputs from one eye may not reach this threshold and thus are not represented in the firing rate of the neuron (Priebe, 2008). In such a case, we might mistakenly label these neurons "monocular". Indeed, emerging evidence suggests that most (if not all) monocular neurons in V1, including those in layer 4c, receive inputs from the other eye (Dougherty, Cox, et al., 2019; Dougherty et al., 2021; G. Poggio et al., 1988; G. F. Poggio & Fischer, 1977; Priebe, 2008). Sub-threshold excitation from one of the eyes likely explains how phase-specific binocular interactions can be observed in exclusively monocular cells after monocular deprivation (G. Poggio et al., 1988). But neurons can also receive inhibitory inputs (Krnjević et al., 1966). In a simplified circuit, a monocular neuron that receives excitatory inputs from one eye and inhibitory inputs from the other (silent eye) is theoretically excited by one but suppressed by both (Blake, 1989). Although suppressive phenomena in V1 do not necessarily imply a cortical source of inhibition (Barbera et al., 2022; Priebe & Ferster, 2008), the relative strength of input from the two eyes is at least partially concealed with respect to what the electrode measures (Priebe, 2008).

Hence, whether from sub-threshold excitation or inhibitory influence that "silences" inputs from one of the eyes, an ocular dominance index derived from spiking does not completely capture the strength or number of connections to a given cell from each eye. It then follows that the typical ocular dominance histogram, including our own here, is only a partial index of the strength of connections from each eye for a given V1 cell. Nevertheless, we demonstrate here that ocular dominance, built from spike rates to monocular stimuli, is predictive of a response bias during binocular combination favoring contrast placed in the neurons' dominant eye. Thus, the traditional ocular dominance index is still a useful parameter for our understanding of binocular contrast combination in V1 and may still be relevant for the neurophysiological study of binocular vision.

2.4.2. Implications for computational modeling

The standard neural model of a binocular cell employs a linear system that sums signals from each eye before being subjected to nonlinear spike thresholding (Albrecht & Geisler, 1991; Heeger, 1992b). This model has been informed by numerous quantitative studies in cats and monkeys that demonstrate linear phase-specific binocular interactions in V1 neurons (Ohzawa & Freeman, 1986; Sclar et al., 1986). However, strong modulation of responses as a function of interocular phase-disparity also occurs for unequal contrasts in the two eyes (Freeman & Ohzawa, 1990; Ohzawa & Freeman, 1986; Smith et al., 1997). For example, even when contrast is low in the eye

in which the phase-shift occurs, binocular interaction is stronger than predicted by a linear system (Ohzawa & Freeman, 1986). Rather, modulatory patterns are consistent with a nonlinear contrast gain-control mechanism that enhances gain when contrast is low and reduces gain when contrast is high (Ohzawa et al., 1985). This kind of gain-control between the eyes, or interocular gain-control, is an explicit prediction of the gain-control theory of binocular combination. Our finding that binocular summation of contrast is systematically reduced as a function of total contrast energy provides direct support for the gain-control theory of binocular combination.

The divisive normalization framework explains contrast gain-control in V1 remarkably well (Heeger, 1992a). A 'binocular' version of divisive normalization has been proposed (Fleet et al., 1997) and was recently used to explain interocular contrast gain-control at the level of fMRI BOLD responses in V1 (Moradi & Heeger, 2009). We extend this finding to V1 neurons and demonstrate the need to incorporate ocular dominance in the model at this spatial scale to account for the asymmetry in binocular summation that favors contrast in the neurons' dominant eye. Specifically, our results indicate that V1 neurons lower the gain of contrast placed in its non-dominant eye proportionate to its ocular dominance during interocular normalization. We were able to characterize this effect as response-gain control on the excitatory drive of the non-dominant eye, rather than the normalizing suppressive pool. Thus, binocular responses in primate V1 appear to abide by the same rules of spatial summation and gain-control that underlie many other distinctive response features of cortical neurons (Sawada & Petrov, 2017).

2.4.3. A potential role for ocular dominance in visual processing

V1 neurons encode contrast within each eye by adjusting their spike rates, with their contrast response function (CRF) differing between the two eyes. Our analysis indicates that this ocular dominance-induced difference in contrast coding between the eyes persists during binocular integration and is systematically related to the neuron's ocular dominance. Here, we show that, given the varying preference of V1 neurons for one eye, differences in contrast levels between the eyes lead to distinct patterns of neuronal activation. For instance, when contrast is high in the left eye and low in the right eye, neurons preferring the left eye show stronger responses compared to those preferring the right eye, and vice versa. This distinctive activation pattern suggests that V1 neurons can distinguish between these conditions and retain information about which eye receives higher contrast. However, it is still not clear if this ability to differentiate contrast levels between the eyes leads to enhanced perception. A potential way to explore this question is to study individuals with utrocular discrimination—those who can identify signals specific to each eye (Schwarzkopf et al., 2010). Specifically, research could examine whether variations in ocular dominance among individuals correspond to differences in their ability to discriminate these eye-specific signals.

2.4.4. Implications for the study of amblyopia

Our finding that ocular dominance impacts binocular contrast combination also has implications for the study of amblyopia. Amblyopia is a condition that typically appears in early childhood when there is a disruption in the normal visual input from one eye, leading to reduced vision in that eye (Birch, 2013). Hubel and Wiesel replicated this condition in animals by suturing one eyelid. They found that in the striate cortex, markedly less neurons could effectively respond to visual input from the amblyopic eye (Wiesel & Hubel, 1963). Through the use

of a transneuronal tracer, [3H]proline, it was discovered that the ocular dominance columns in layer 4C of the deprived eye were reduced in size, while those of the normal eye were expanded (D. H. Hubel et al., 1977; LeVay et al., 1980; Shatz & Stryker, 1978). Consequently, it was proposed that early visual deprivation during a critical period leads to the loss of geniculate synapses onto V1 neurons dedicated to the impaired eye, thus causing amblyopia (Wiesel, 1982). It has been noted, however, that shrinkage of ocular dominance columns does not fully account for the severe amblyopia observed following early monocular form deprivation (Sincich et al., 2012). Even after eyelid suturing from two weeks of age, which reduces visual acuity to the level of perceiving only hand motions, the ocular dominance columns of the deprived eye still occupy approximately a third of layer 4C (Sparks et al., 1986). One possibility is that additional anatomical changes downstream of V1 processing contribute to amblyopia (Sincich et al., 2012). Alternatively, the remainder of V1 neurons receiving input from the amblyopic eye may be suboptimally integrating information between the two eyes. Our data demonstrate the relationship between V1 neurons' preference for eye and interocular combination of contrast under normal development conditions. Further exploration of ocular dominance in amblyopic subjects holds promise in elucidating the precise mechanisms by which imbalanced binocular processing in V1 manifests as reduced visual acuity and compromised depth perception in those with amblyopia.

2.5. Methods

2.5.1. Surgical Procedures

Prior to data collection, animals were implanted with a custom-designed plastic head holder and a plastic recording chamber (Crist Instruments) spanning over two separate surgeries. All surgeries were performed under sterile surgical conditions using isoflurane anesthesia (1.5– 2.0). Signs, including heart rate, blood pressure, SpO2, CO2, body temperature, and respiratory rate were monitored continuously. During surgery, the head holder and a recording chamber were attached to the skull using transcranial ceramic screws (Thomas Recording, Gießen, Germany) and self-curing dental acrylic (Lang Dental Manufacturing, Wheeling, IL). A craniotomy was performed over the parafoveal visual field representation of primary visual cortex (V1) concurrent with the position of the recording chamber. Animals received analgesics and antibiotics for postsurgical care and closely monitored by researchers, facility veterinarians, and animal care staff for at least three days following surgery.

2.5.2. Visual apparatus and passive fixation

Visual stimuli were presented on a VIEWPix monitor (VPixx Technologies) running at 120 Hz (22.5-inch display, resolution 1920 x 1200 pixels) with 95% display luminance and color uniformity over 95% of the display area. Animals viewed all stimuli through a custom-built mirror stereoscope, such that images on the right side of the display were viewed by the right eye and images on the left side by the left eye (the monitor was divided by a black, non-reflective septum). The mirrors of the stereoscope were infrared-transparent (Qian & Brascamp, 2017), enabling gaze position to be measured using infrared light-sensitive cameras (EyeLink II). To facilitate binocular fusion, matching oval apertures were displayed at the edge of each half of the screen. At the beginning of each experimental session, the stereoscope was calibrated via a behavioral task (Maier et al., 2008), which required the

animals to fixate on the same location in visual space while being cued in one eye only. Gaze position was measured for each fixation location and compared across eyes. The mirrors were considered aligned once gaze position was comparable for cuing in each eye.

Animals were trained to fixate (self-initiated) within 0.5° of visual angle of a centralized cue (blue x) appearing in both eyes. The task of the animal was to maintain this fixation while a series of sinusoidal grating stimuli were presented at a fixed location in parafoveal visual space. A variety of paradigms were employed to map receptive fields, determine receptive field tuning properties, and probe binocular combination of contrast. Each paradigm is described in detail later. Generally, trials began with fixation for 500ms before the first presentation appeared. If fixation was broken during this period, the trial was aborted. Each presentation lasted 250ms, roughly matching the average time of a typical fixation (Wilming et al., 2017), with a 300ms interval interleaved. If fixation was held for the duration of the trial (3 presentations, 1.35 seconds), the monkey received a juice reward. Alternatively, the next fixation cue appeared with a brief (1-5 s) delay. The animals were at liberty to end recording sessions at any point by halting the initiation of new trials.

2.5.3. Neurophysiological procedure

Experiments were conducted inside a radio frequency-shielded booth. During each recording session, a linear multielectrode array (U-/S-/V-Probe, Plexon Inc., Dallas, TX; Vector Array, NeuroNexus, Ann Arbor, MI) was inserted into V1 orthogonal to the cortical surface. The laminar probes consisted of either 24 or 32 active microelectrodes, linearly spaced 0.1 mm apart, with impedances ranging 0.2– 0.8 M at 1 kHz. The probes were connected to an amplifier using an analog head stage (Blackrock Microsystems), with the shank of the probe used as the reference. Each recording session, one laminar probe was inserted into dorsal V1 through the intact dura mater using a chamber-mounted microdrive (a custom-designed modification of a Narishige International micromanipulator). Probes were adjusted in the z-plane until the majority of microelectrode contacts spanned the entire cortical thickness, from the subdural space to the white matter. Placement of the electrode relative to the cortical laminae was verified using previously established neurophysiological criteria (e.g., CSD profile and power spectral density), as described below. Fluctuating extracellular voltages (referenced to the metallic electrode shaft) were amplified, filtered, and digitized using a 128-channel neural signal processing system (Blackrock Microsystems, Salt Lake City, UT). Two neural signals were recorded and stored for subsequent offline analysis: a low-pass filtered signal (0.3–500 Hz) sampled at 1 kHz, corresponding to the local field potential, or LFP, and a broadband (0.3 Hz–7.5 kHz) signal sampled at 30 kHz. The neural signal processing system also recorded non-neurophysiological analog signals related to the monitor refresh (i.e., a photodiode signal; OSI Optoelectronics, Montreal, Quebec) and eye position (i.e., voltage output of eye-tracking system), which were digitized and stored at 30 and 1 kHz, respectively. These time stamps and the photodiode signals were used to align the time-varying intracranial data with the onset of visual events. Trials where the animal's gaze left the central 1° radius around the fixation spot were excluded from analysis.

The relative depth of each microelectrode contact in cortex was determined from current source density and power spectral density analysis. Current source density (CSD) analysis was performed on the LFP signal using an

estimate of the second spatial derivative appropriate for multiple contact points(Nicholson & Freeman, 1975):

$$CSD(t,c) = -\frac{x(t,c-z) + x(t,c+z) - 2x(t,c)}{z^2},$$

where x is the extracellular voltage recorded in Volts at time t from an electrode contact at position c, and z is the electrode intercontact distance (0.1 mm). To yield CSD in units of current per unit volume, the resulting CSD from the formula was multiplied by 0.4 S/mm as an estimate of cortical conductivity (Logothetis et al., 2007).

2.5.4. Receptive field mapping and tuning

Once satisfactory electrode placement was achieved, we used a reverse correlation-like technique to map the receptive fields of the single units under study. We first estimated the receptive field location from the audible MUA response to bar and grating stimuli that were moved across the screen while the animals fixated for juice reward. These stimuli were presented to each eye separately. We then had the animals fixate while a series of circular static random noise patches were presented monocularly and binocularly at pseudorandomized locations within a predetermined virtual grid that covered the estimated receptive field. Up to five stimuli were shown per trial, for 200 ms each with 200-ms blank periods interleaved. Stimulus size and grid spread varied depending on receptive field estimates, with each recording session typically including an initial "coarse" followed by a "fine" mapping phase of decreasing grid size. We used the resulting neurophysiological data to compute retinotopic three-dimensional receptive field matrices (RFMs) (Cox et al., 2013) to derive spatial maps of neuronal responses as a function of visual space. This procedure allowed us to identify the optimal position and size of grating stimuli for each V1 column. Receptive fields for a given column overlapped due to the orthogonal angle of the microelectrode array to V1.

Parameters of the sinusoidal grating stimuli (i.e., orientation, phase, spatial frequency) were customized to the average tuning preferences along the V1 column each day. To do so, three 250ms monocular stimuli were interleaved with 300ms blank periods. Sinusoidal gratings pseudorandomly varied in phase, spatial frequency, and orientation(Cox et al., 2019; Mitchell et al., 2022; Westerberg et al., 2019) and eye-of-origin (monocular and binocular presentations). All binocular presentations were presented with zero disparity (or close to zero disparity given that the monitor was flat rather than curved in the shape of the horopter) between the eyes. Upon completion of this procedure, we determined the column's mean preferred orientation, spatial frequency, and phase by statistically comparing spiking responses to each parameter ANOVA, $p < 0.05$.

2.5.5. Monocular and binocular stimuli

Sinusoidal gratings were presented on the monitor corresponding to the mapped population receptive field location of each electrode penetration (see Figure 13 for RF boundaries and extents). A trial consisted of three presentations, each lasting 250ms with 300ms interleaved. Gratings were presented to one or the other eye using either the left or the right side of the monitor (monocular stimulation) or both eyes in conjunction (binocular stimulation). Gratings varied in Michelson contrast (e.g., 0, 0.055, 0.11, 0.225, 0.45, 0.90) across presentations.

Binocular presentations additionally varied in contrast between the eyes (e.g., 0.225 in the left eye, 0.45 in the right eye). In total, there were 36 stimulus conditions comprising of monocular, binocular balanced, and binocular unbalanced presentations.

2.5.6. Signal post-processing.

Except for LFPs, all neurophysiological signals were extracted off-line from the recorded broadband signal using custom-written code in MATLAB (version 2021a). We computed an analog signal of multi-unit activity (MUA) by high-pass filtering the broadband signal at 750 Hz with a fourth-order Butterworth filter and rectifying(Supèr & Roelfsema, 2005). For this study, a multi-unit describes the neuronal signal extracted using the techniques described here from a single micro-electrode contact from a single penetration. In addition to the MUA signal, single-unit activity was extracted using Kilosort 2.0, an unsupervised machine-learning spike-sorting algorithm (Pachitariu et al., 2023). We used the default parameters for sorting and clustering. After kilosort extracted clusters, we manually curated the clusters using Phy 2.0, following the general guidelines for 'good' / well-isolated unit selection based on amplitude-to-noise comparisons, inter-spike-interval violations, and stability over the recording session.

2.5.7. Channel selection and data formatting.

We restricted our data to measurements within the cortical gray matter by eliminating channels at the top and the bottom of the electrode array that were void of MUA significantly above baseline firing. We also excluded units in V1 that did not show significant tuning to visual contrast (via a repeated measures ANOVA applies to monocular responses across 6 contrast levels, $p < 0.05$) or did not have at least 5 trials of data in all 36 stimulus conditions. Upon aligning MUA to the stimulus onset, we subtracted the baseline firing rate on a trial-by-trial basis. To enable comparisons between units, we normalized each units' visual responses to the maximum response across all the trials.

2.5.8. Computational modeling

Monocular contrast response functions. Most cortical visual neurons respond nonlinearly to stimulus contrasts. This nonlinearity has been well-described by a divisive normalization function derived from the H-ratio sigmoidal function of Naka and Rushton (Naka & Rushton, 1966). We applied the nonlinear least squares approach to fit monocular responses to contrast, using the divisive normalization function:

$$R_{R_{max},C_{50},n,b}(c) = R_{max}\frac{c^n}{c^n + {C_{50}}^n} + b \ ,$$

where R is the monocular response of the unit, R_{max} represents the projected maximum attainable response of the unit, C_{50} is the semi-saturation constant that represents the contrast at which the output is half of the maximum attainable output, n is the scaling exponent, and c is the contrast of the stimulus. The y-intercept b represents maintained activity and was fixed for individual neurons to the average activity during blank presentations (0%

contrast in each eye). Each parameter was allowed to freely vary within customized limits to achieve the best fit to the data (R_{max}, [0 max response of the unit], C_{50}, [0.01 1], n, [0.5 7]).

Binocular contrast response functions. Several models have been proposed for how V1 binocular contrast combination is achieved in V1. These models typically vary in the number and position of gain-control mechanisms. We tested various binocular models built on a shared normalization framework which represent different ways for combining the two monocular contrast response functions:

One possibility is that gain-control on binocular signals is applied at a binocular stage after the two eyes are summed:

$$R(c_L, c_R) = 0.5 * (\frac{c_L^n}{c_L^n + c_{50}} + \frac{c_R^n}{c_R^n + c_{50}})$$

Here, the binocular response is modeled as the average of the two monocular contrast response functions, akin to our visual experience when opening and closing one eye.

On the other hand, the two eyes may give rise to independent divisive normalization channels, without possibility for interocular interactions or any form of binocular gain-control. While this linear model has proven to be an unlikely candidate given inherent nonlinearities of spike generation (Burns & Pritchard, 1968; Longordo et al., 2013; Moradi & Heeger, 2009; Zhao et al., 2013), it is still a useful tool to assess the degree of summation of contrast in the two eyes:

$$R(c_L, c_R) = \frac{c_L^n}{c_L^n + c_{50}} + \frac{c_R^n}{c_R^n + c_{50}}$$

Yet another possibility is that the two eyes are normalized monocularly and then summed quadratically:

$$R(c_L, c_R) = \sqrt{\left(\frac{c_L^n}{c_L^n + c_{50}}\right)^2 + \left(\frac{c_R^n}{c_R^n + c_{50}}\right)^2}$$

This historical model employs gain-control at a binocular stage (Legge, 1984b). Unlike the previous model, here magnitude of gain-control scales nonlinearly with contrast.

Alternatively, the two eyes may interact before being summed, such that each eye's input exerts control over the strength of the other eyes' normalization (Moradi & Heeger, 2009). Unlike the other models, this model incorporates interocular interactions at a monocular stage:

$$R(c_L, c_R) = \frac{c_L^n + c_R^n}{c_L^n + c_R^n + c_{50}}$$

We used MATLAB (2021a)'s fit() function to fit a each model to the binocular response matrix (5x5 trial-averaged (single contact) or mean (n = 502) responses) using the nonlinear least squares method with two independent variables (C_L, C_R). We additionally weighed each datapoint (i.e., condition) by the number of trials on a unit-by-unit basis. The fit procedure for the binocular response functions allowed each parameter (R_{max}, C_{50}, n) to freely vary to achieve the best fit to the data. We tested whether ocular dominance information improves each fit by adding a weight (w) as a 'problem' parameter/fixed variable to multiply the contrast in the numerator of the non-dominant eye's function. This weight took on a value of 1 (no effect) or that of each unit's fitted ocular dominance weight. The procedure for determining each unit's ocular dominance weight (w) is described in detail in the results section "Modeling ocular dominance within a divisive normalization framework". Briefly, an ocular dominance weight (w) was fitted for each unit to minimize the sum of square residuals between datapoints on the non-dominant eye curve and the dominant eye curve.

2.5.9. Statistical analysis

Statistical analyses were performed via MATLAB or using the open-source statistics Jamovi software package (The Jamovi project 2022 (Version 2.3)). Our data analysis primarily comprised of paired samples tests. When assumptions of normality were violated (via Shapiro-Wilk's test), non-parametric tests were used (Wilcoxon sum rank tests and Friedman with Durbin-Conover post hoc tests). Model performance was assessed through comparing goodness of fit statistic obtained from each fit to the data (adjusted R^2). To evaluate the effect of the ocular dominance weight, we approximated Akaike's information criteria corrected for the number of observations and parameters (AICc) using the following formula:

$$AICc = n \ln\left(\frac{SSE}{n}\right) + 2k + \frac{2k\,(k+1)}{n-k-1} + n\ln(2\pi) + n$$

where *n* is the number of observations and *k* is the number of parameters in the model.

Chapter 3

Binocular Normalization across the V1 Laminar Microcircuit

3.1 Summary

Divisive normalization is a fundamental neural operation observed throughout the cortex. Our study utilized laminar neurophysiological techniques to explore the dynamics of divisive normalization within the V1 laminar microcircuit of awake, behaving macaque monkeys, specifically examining its role in binocular processing. By analyzing contrast response functions (CRFs), we uncovered distinct spatiotemporal patterns that illustrate how contrast sensitivity and normalization differ across cortical layers. We found that while granular layers of V1 displayed predominantly linear response characteristics (flatter CRFs), supragranular and infragranular layers exhibited increased nonlinearity. Employing computational modeling, we demonstrated that a divisive normalization model tailored for binocular integration—termed binocular normalization—adequately accounts for V1 spiking responses to both unbalanced and balanced contrasts across the eyes throughout the V1 laminar circuit. Notably, the laminar pattern of normalization strength coincided with the laminar pattern of sublinear binocular summation: normalization was markedly stronger in the supra- and infra-granular layers, where neurons tend to exhibit heightened binocularity. These findings are contextualized within circuit models that apply divisive normalization via recurrent feedback connections, suggesting that both dynamic normalization and the stabilized supralinear network (SSN) model can be extended to the integration of binocular inputs, as well.

3.2 Introduction

Divisive normalization, originally proposed as a computational explanation for nonlinear responses properties in the primary visual cortex (V1) (Heeger, 1992b), has gained significant traction over the past two decades (Burg et al., 2021; Sawada & Petrov, 2017). This computational model posits that the response of a neuron is divided by the summed activity of a large pool of neurons (Heeger, 1992b). Such normalization helps scale neural responses based on overall activity, allowing neurons to maintain operations (such as orientation detection) across a wide range of input intensities (Carandini & Heeger, 2012). Within simulated neural circuits, normalization is pivotal in balancing excitation and inhibition (Heeger & Mackey, 2019; Heeger & Zemlianova, 2020), which is thought to sharpen sensitivity to stimuli and contribute to the robustness of sensory representations (Ohshiro et al., 2011; Troyer et al., 1998; Tsang & Shi, 2008).

Expanding beyond its foundational applications in V1, divisive normalization has been investigated in various other neurophysiological processes across a range of brain regions, sensory modalities, and animal species (Louie & Glimcher, 2019). For example, normalization has been implicated in spatial integration in the somatosensory cortex (Kohn & Whitsel, 2002), concentration invariant-olfactory coding (Olsen et al., 2010), temporal processing in the auditory cortex (Dean et al., 2005), and even plays a prominent role in cognitive functions such attention regulation (Lee & Maunsell, 2009; Ling & Blake, 2012) and decision-making circuits (Louie et al., 2011). The divisive normalization framework has been extended to binocularly presented stimuli, as well, termed

“interocular” or “binocular” normalization (Fleet et al., 1997). This adaptation proposes that a neuron's binocular response is mediated by gain-control mechanisms operating within and between monocular channels (Fleet et al., 1997), paralleling the psychophysics-derived gain-control theory of binocular combination (Ding & Sperling, 2006).

Evidence supporting binocular normalization continues to grow from electrophysiological studies (Louie & Glimcher, 2019). A notable human fMRI study indicated that the best explanation for sublinear binocular responses in the primary visual cortex (V1) is normalization occurring within and between monocular channels (Moradi & Heeger, 2009). However, employing functional magnetic resonance imaging (fMRI) to investigate the normalization model poses technical challenges (C. Baker, 2018). This difficulty arises because fMRI typically measures aggregated neural activity within each voxel rather than discerning the specific inputs and normalization pools of individual neurons or subpopulations (C. Baker, 2018). To overcome these limitations, subsequent research has employed a forward modeling approach. This technique applies voxel-wise biases to translate overall activity into predicted responses for specific channels (Brouwer & Heeger, 2009; Kay et al., 2008, 2013). These studies have validated the binocular normalization model by demonstrating its ability to describe phenomena such as cross-orientation suppression in the human visual cortex (Brouwer & Heeger, 2011). Despite these advances, the methods are still somewhat limited in their ability to delve into binocular normalization at the level of individual neurons and microcircuits.

Recent neurophysiological research has provided more direct evidence supporting the concept of binocular normalization in V1. Our group showed that binocular spiking responses to balanced and unbalanced contrasts in the two eyes are better explained by a model of binocular normalization than by models based on averaging, linearly summing, or quadratically summing contrasts between the two eyes (Mitchell et al., 2023). The study also revealed that ocular dominance—the preference of neurons for one eye over the other—plays a significant role in this normalization process, highlighting the importance of such detailed investigations. In a separate study, Zhang et al. (2024) replicated these findings at a broader neurophysiological level using two-photon imaging techniques. This approach enabled the simultaneous recording of responses from thousands of layer 2/3 neurons in adjacent ocular dominance columns (Zhang et al., 2024). These experiments provided empirical evidence for binocular normalization at the spatial scale of individual neurons and neuronal populations. However, these studies did not explore binocular normalization across all laminar depths of V1, thus leaving the comprehensive mapping of these normalization processes within the laminar microcircuit largely unexplored.

The present study aims to address this gap through a combination of laminar neurophysiology and computational modeling. By examining divisive normalization and binocular processing across the V1 laminar microcircuit, we characterized the spatiotemporal dynamics of V1 binocular integration as a single, dynamical

process of binocular normalization that begins in the granular input layer and strengthens in step with the canonical cortical microcircuit.

3.3 Results

We examined the spatiotemporal profile of divisive normalization processes across the V1 laminar microcircuit. We employed laminar electrophysiology to record spiking activity from V1 columns (Figure 19*A*) of macaques passively viewing grating stimuli through a custom mirror stereoscope (Figure 19*B*). The stereoscope allowed us to stimulate one eye or the other at corresponding retinal locations (Figure 19*C*) and assess how associated responses are normalized *within* monocular channels to contrast and *between* monocular channels to form binocular responses across the V1 laminar microcircuit. The data analyzed in this study were acquired from 27 penetrations with multi-electrode linear arrays across two monkey subjects (9 for monkey B, 18 for monkey J. We aligned these penetrations between sessions using current source density analysis (session-averaged CSD presented in Figure 19*D*) to identify the initial layer 4 sink aided by power-spectral density (session-averaged PSD presented in Figure 19E) estimates of the cross-over between LFP gamma power in the supragranular layers and alpha-beta power in the infragranular layers (Mendoza-Halliday et al., 2024). For more details on the laminar alignment, see *3.5.4. Identification of the layer 4/5 boundary and laminar alignment*. The result of our laminar identification procedure identified 220 units in the supragranular layers, 118 units in the granular layer, and 195 units in the infragranular layers of V1 (total n = 533) (Figure 19*F*).

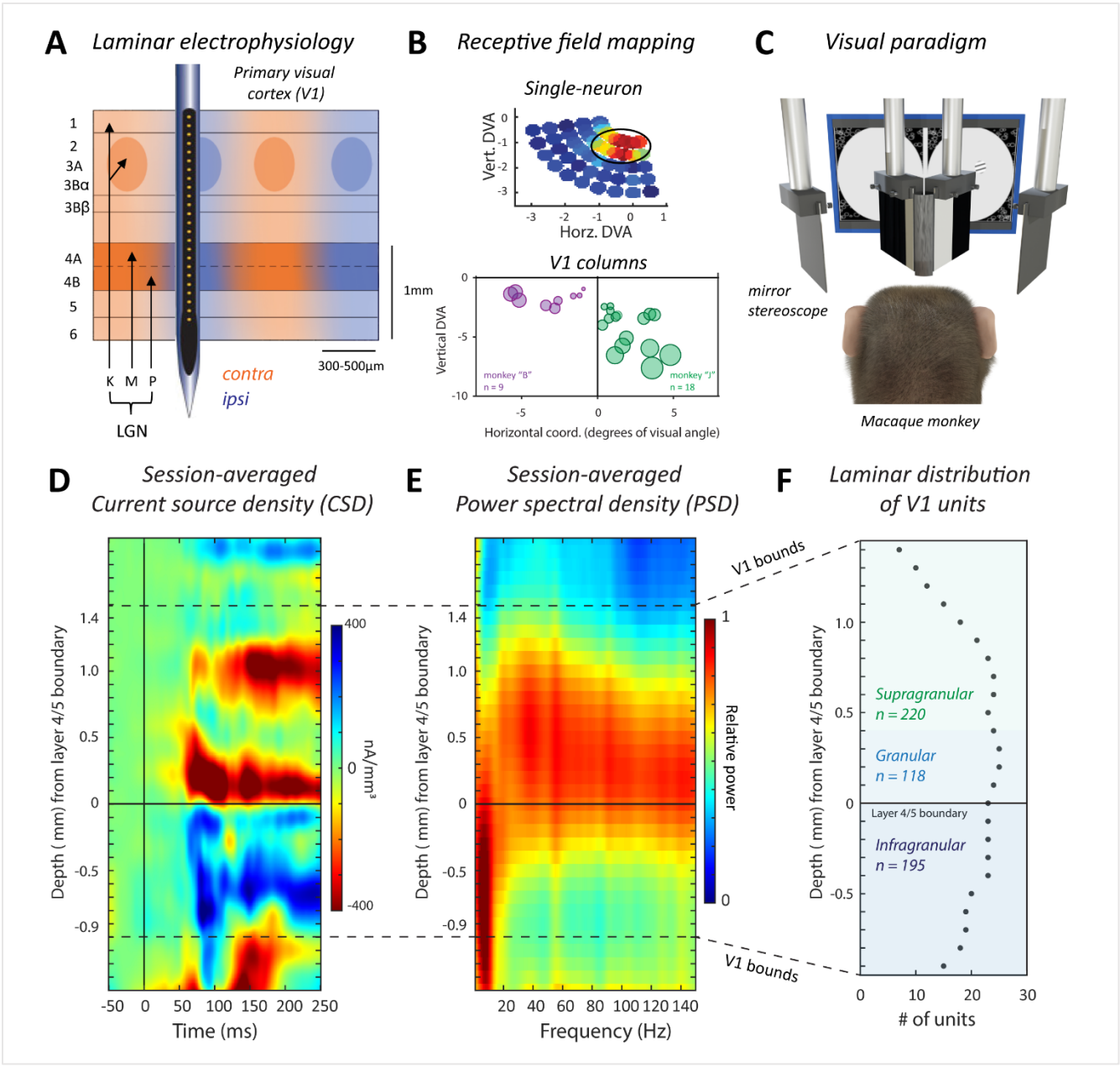

Figure 19. Experimental methodology. (A) Laminar electrophysiology. (B) Mirror stereoscope. (C) Receptive field mapping. A single-unit example receptive field is presented at the top. Summary of putative RFs for all penetrations shown below. (D). Session-averaged current source density (CSD). (E). Session-averaged power spectral density (PSD). (F) Laminar distribution of V1 units.

3.3.1. V1 laminar responses to binocular and monocular stimulation

Our aim was to assess divisive normalization across the V1 laminar microcircuit during binocular combination of contrast. To this aim, we analyzed V1 spiking responses (n = 533, 27 sessions, 2 subjects) to binocular and monocular conditions (Figure 20*A*) across all V1 layers. Figure 20*B* depicts grand average V1 multi-unit activity (MUA) as a function of depth from the cortical surface (layer 1) down to the bottom of layer 6, averaged across all V1 columns regardless of their ocular dominance.

Before initiating our primary analysis, we aimed to replicate laminar patterns of ocular dominance and binocular interactions. We first assessed ocular dominance across V1 layers. Based on anatomy and physiological studies that have mapped out the retinogeniculate projections into V1 (Haseltine et al., 1979; Hendrickson et al., 1978; D. H. Hubel & Wiesel, 1972; Kennedy et al., 1976; Tootell et al., 1988), we expected ocular dominance (defined as a response difference for stimulating one eye versus the other) to be most prominent in granular input layers (L4C in primates) and least prominent in deep, infragranular layers (L5&6). This is what we observed in our data, as well (Figure 20*C*). Ocular dominance varied significantly across three laminar compartments (F (2, 530) = 16.26, p < .001). Post-hoc comparisons revealed that ocular dominance was significantly greater in layers 4 and 2/3, as compared to layers 5/6 (t = 4.67, p_{tukey} < .001; t = 4.83, p_{tukey} < .001).

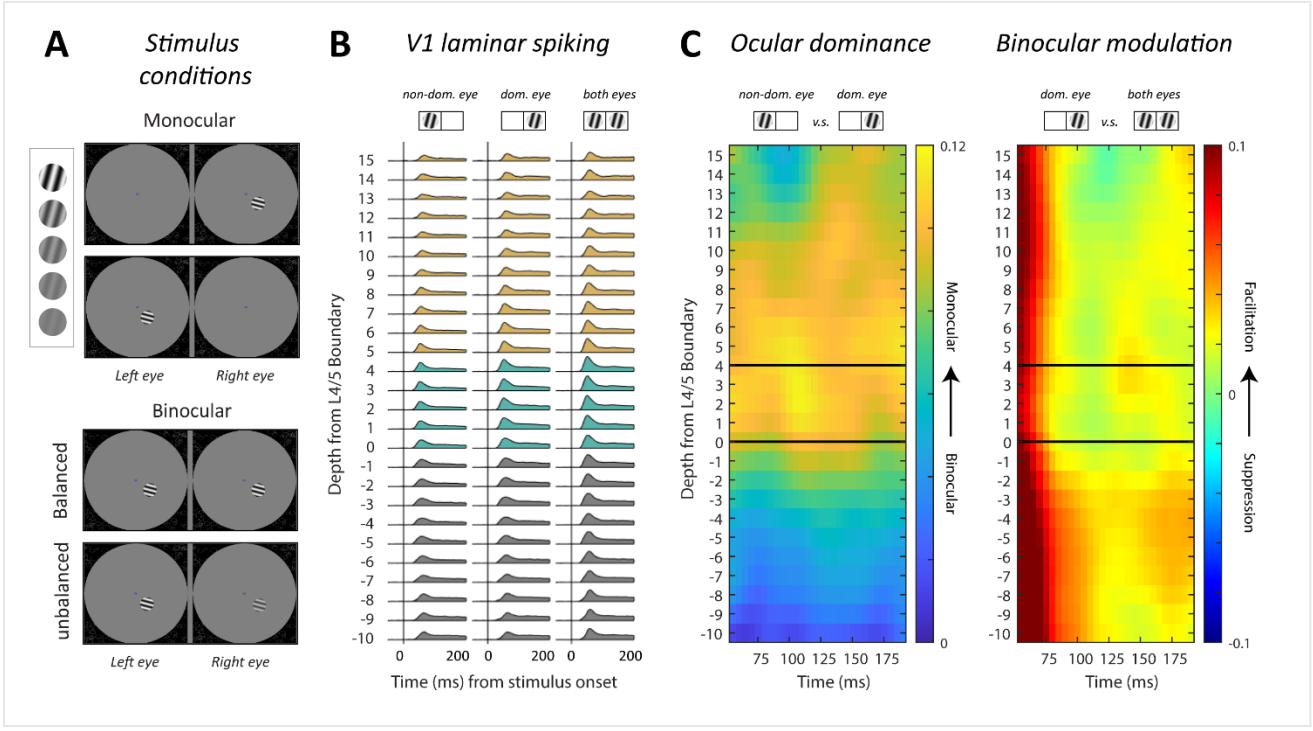

Figure 20. V1 laminar spiking responses to varying types of monocular and binocular stimulation. (A) Stimulus conditions. Stimuli consisted of small (0.5-1.5 degree diameter) gratings presented to the mapped receptive field locations of V1 neurons. Gratings varied in Michelson contrast in six octave steps [0, 0.05, 0.11, 0.225, 0.45, 0.90]. Gratings were presented to one or the other eye (monocularly) or to both eyes simultaneously at corresponding retinal positions (binocularly). Binocular presentations (bottom) comprised of gratings with both balanced and imbalanced contrast in the two eyes. (B) Mean V1 laminar spiking (spike density functions, multi-unit activity) to a stimulus placed in the neurons' non-dominant eye (left), dominant eye (middle), and both eyes (right) as a function of cortical depth from the layer 4/5 boundary. (C) Left. Ocular Dominance, measured as Michelson contrast between the dominant and non-dominant eye responses, as a function of depth. Right. Binocular modulation, measured as Michelson contrast between the binocular response and the dominant eye response as a function of depth.

Binocular modulation, defined as the change in response from monocular to binocular stimulation, has also been previously described across the V1 laminar microcircuit (Cox et al., 2019; Dougherty, Cox, et al., 2019). Based on that work, we expected binocular modulation to be the strongest in the deep layers while still present in upper and even granular input layers. The pattern of binocular modulation we observed is consistent with that precedence (Figure 20*C*).

3.3.2. Contrast normalization differs across the V1 laminar microcircuit

To initiate our investigation into divisive normalization, we examined the characteristics of the classic contrast response function (Albrecht & Hamilton, 1982; Bonds, 1991). Figure 21*A* illustrates the simulated effects of each parameter of the Naka-Rushton equation (Naka & Rushton, 1966). Among the associated parameters, *Rmax* governs the maximum firing rate. Exclusive alterations of *Rmax* induce a distinct vertical shift in the contrast response function (CRF) along the y-axis, commonly termed response gain. *C50*, on the other hand, regulates contrast sensitivity. Exclusive adjustments of *C50* lead to an isolated horizontal shift in the CRF along the x-axis, often referred to as a contrast gain. Finally, *n* determines the dynamic range of the neurons. Exclusive changes of this exponent yield isolated alterations to the slope of the CRF.

We used the original Naka-Rushton equation to fit the binocular responses of each unit to six contrast levels (0, 0.05, 0.10, 0.22, 0.45, 0.90) individually, with all parameters free to vary. V1 binocular contrast response functions (CRFs) have been shown to initially manifest as vertical shift relative to monocular CRFs (Mitchell et al., 2022). In essence, the initial "transient" response (~45-100ms) exhibits response gain, while the sustained or steady-state response (105-200ms) exhibits greater complexity (Mitchell et al., 2022). Here, we examined the parameters of the binocular CRF across both temporal and spatial dimensions. As anticipated, *Rmax* reaches peak during the visual transient (Figure 21*B- left*) and gradually diminishes as the response transitions into a steady state. Across cortical depths, *Rmax* was greatest in the granular input layers ($M = 0.97$, $SD = 0.48$) compared to supra ($M = 0.90$, $SD = 0.41$) and infra-granular layers ($M = 0.82$, $SD = 0.24$) ($F(2,530) = 5.64$, $p < .001$), consistent with response amplitudes across depth (see Figure 20*B*). Contrast sensitivity, as indicated by *C50*, demonstrated laminar differences in both the transient phase ($F(530,2) = 14.95$, $p < .001$) and steady-state phase ($F(2,530) = 5.02$, $p < .001$) (Figure 21*B – middle*). Contrast sensitivity was highest (lowest *C50*) in the infragranular layers ($M = 0.18$, $SD = 0.13$), compared to granular ($M = 0.25$, $SD = 0.18$) and supragranular layers ($M = 0.27$, $SD = 0.17$) above. Lastly, the dynamic range of multi-units, denoted by *n*, did not change significantly over time ($t(532) = 0.15$, $p = 0.88$) (Figure 21*B – right*). However, the exponent's value significantly varied across laminar compartments ($F(2, 530) = 17.8$, $p < .001$). The exponent, n, was lowest in the granular input layers ($M = 1.6$, $SD = 0.93$), indicating a more linear CRF and a broader dynamic range compared to layers above ($M = 2.0$, $SD = 1.0$) and below ($M = 2.3$, $SD = 0.92$).

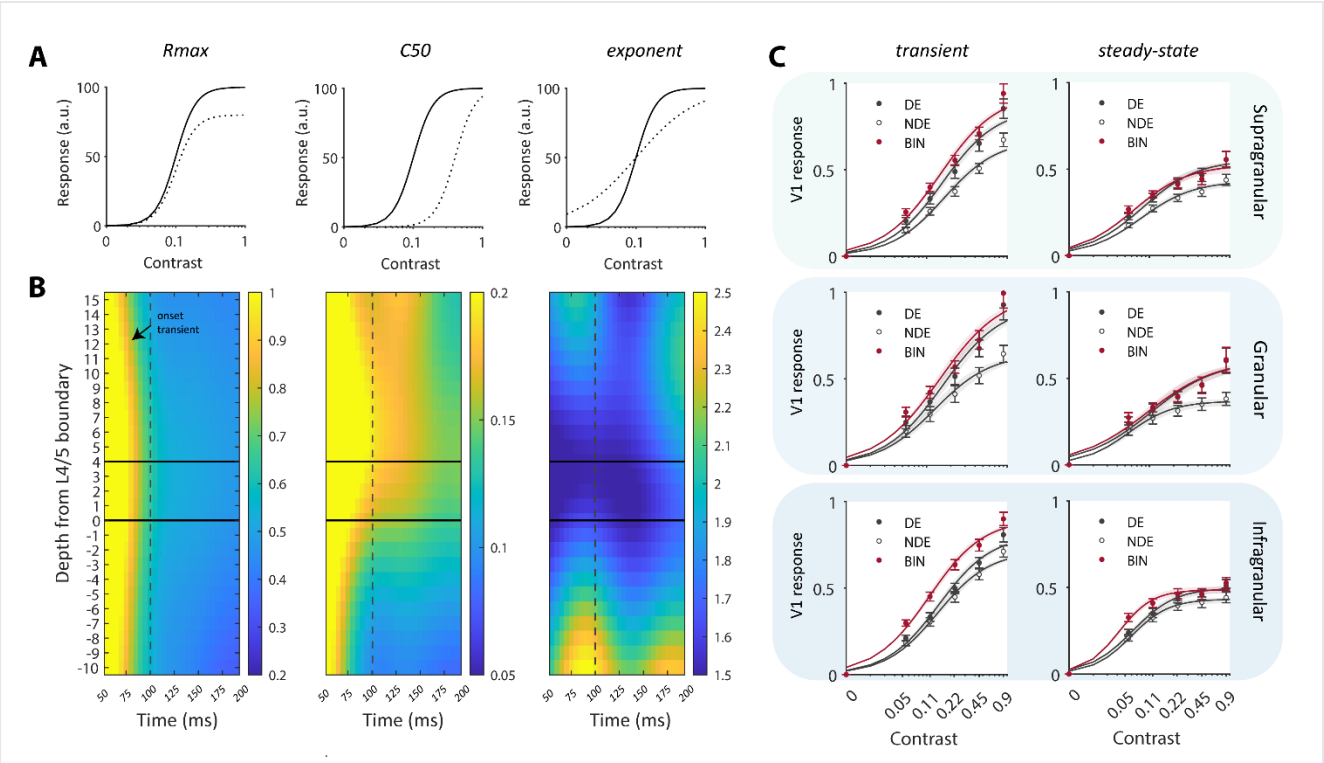

Figure 21. Parameters associated with a divisive normalization model fit vary across the V1 laminar microcircuit. (A). Simulated effects of each parameter of the Naka-Rushton equation for contrast response functions (CRFs). (B). Value of each parameter (Rmax, C50, and n) as a function of cortical depth, indexed relative to the layer 4/5 boundary. Horizontal solid lines encase the estimated V1 granular input layer. Vertical dotted lines denote an arbitrary delineation between two primary periods of V1 responses, the visual onset or transient phase and the steady-state or sustained period. (C). Aggregate contrast response functions (CRFs) for each laminar compartment, and for two windows of the response. Binocular CRFs are shown in red; monocular CRFs are presented in black (filled and unfilled datapoints correspond to dominant and non-dominant eye responses, respectively).

Figure 21*C* provides a synthesis of these observations, depicting aggregated CRFs for each laminar compartment (supragranular, granular, and infragranular), averaged across two primary response phases (transient and steady-state). We also present the CRFs for the dominant and non-dominant eyes (represented by black filled and unfilled datapoints, respectively, Figure 21*C*) to offer a visual comparison with monocular stimulation. Notably, in the infragranular compartment and during the steady-state phase, there is a discernible horizontal "shift" in the binocular CRF relative to the monocular CRFs, indicating an increased sensitivity to stimulus contrast during binocular viewing.

3.3.3. Supersaturation lies outside the retinogeniculate input layer (L4C)

As we have just discussed, V1 neurons exhibit a compressive nonlinearity in response as a function of image contrast, such that, their responses plateau or saturate at higher contrasts (Albrecht, 1995; Anzai et al., 1995; Bonds, 1991; Chao-yi & Creutzfeldt, 1984; Ohzawa et al., 1985). As the backbone of divisive normalization, the classical Naka-Rushton equation (Naka & Rushton, 1966) captures saturation in V1 remarkably well (Albrecht & Hamilton, 1982; Carandini & Heeger, 2012; Heeger, 1992b). However, many V1 neurons also demonstrate a phenomenon referred to as "supersaturation," where their responses do not just stop increasing, but decrease again at the highest levels of stimulus contrast. This behavior has been observed and documented by numerous researchers (Albrecht & Hamilton, 1982; Bonds, 1991; Chao-yi & Creutzfeldt, 1984; Ledgeway et al., 2005; Peirce, 2007; Tyler

& Apkarian, 1985) and has emerged from circuit model simulations of V1 neurons (Somers et al., 1998). Initially, supersaturation was thought to arise from intra-cortical inhibition (Albrecht & Hamilton, 1982). This suggests that supersaturation would likely be found outside of the geniculate input layers. To our knowledge, the laminar specificity of supersaturation has yet to be evaluated. Therefore, we aimed to evaluate this feature of divisive normalization across the V1 laminar microcircuit, as well.

An illustrative example of supersaturation is depicted in Figure 22*A*. Notably, the original Naka-Rushton equation is not capable of representing nonmonotonic data, resulting in an inadequate fit and poor representation of the neuron's actual contrast response function (Peirce, 2007). To quantify this phenomenon, we devised an index based on observed data:

$$\frac{Resp_{max} - Resp_{90}}{Resp_{max} - Resp_{0}}$$

$Resp_{max}$ refers to the multi-unit's maximum response, $Resp_{90}$ is the unit's response at the highest contrast (in our case it was 90%), and R_0 is the unit's response to zero contrast. A supersaturation index exceeding zero indicates the presence of supersaturation. In line with previous reports (Peirce, 2007), approximately 32% of units exhibited supersaturation to some degree (values > 0). The grand-average (over space and time) distribution of supersaturation index values ($M = 0.11$, $SD = 0.21$) are presented in Figure 22*B*. Subsequently, we computed this index across each depth and over time (Figure 22*C*) and found significant variation across depth (F (2, 530) = 13.7, $p < 0.001$). Supersaturation was lowest in the granular layers ($M = 0.03$, $SD = 0.07$), and significantly greater in the supragranular ($M = 0.12$, $SD = 0.007$) and infragranular layers ($M = 0.10$, $SD = 0.01$). This analysis reveals that supersaturation occurred almost exclusively outside of the granular input layer (L4C), suggesting that it is predominantly a cortical phenomenon, commensurate with previous predictions (Albrecht & Hamilton, 1982).

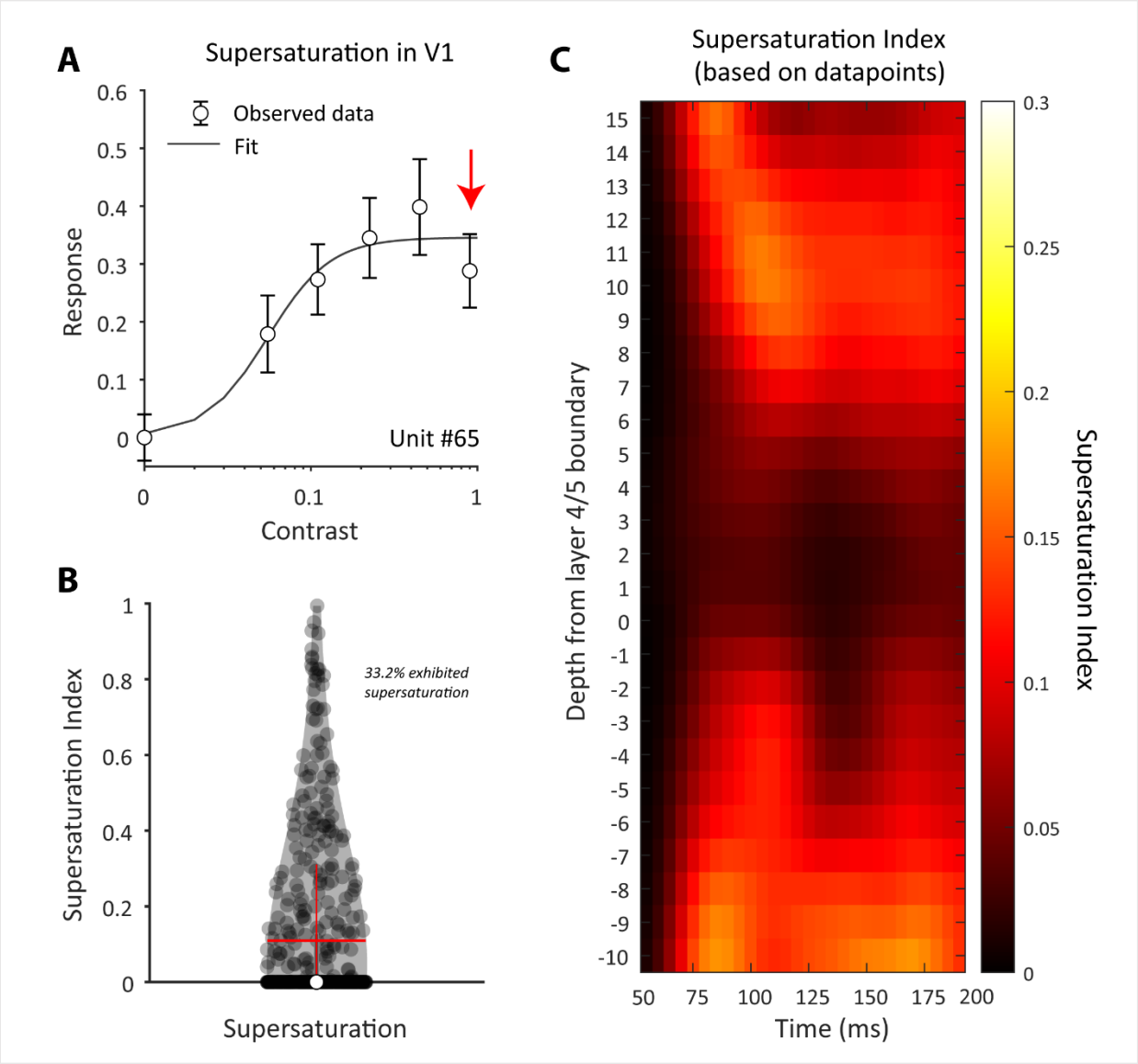

Figure 22. Supersaturation in V1 falls outside of the granular input layer. (A). Example of supersaturation in V1. (B). Distribution (violin) of supersaturation index. Values above zero indicate the presence of supersaturation. (C). Supersaturation as a function of cortical depth.

Recent work has also shown that the Naka-Rushton equation can be modified to account for supersaturation (Peirce, 2007). Figure 23*A* demonstrates the effect of adding an additional parameter "*s*" to the Naka-Rushton equation. This modification amounts to allowing the exponent of the divisive normalization pool to vary separately from the exponent of the excitatory drive (at the expense of the original parameters losing their original interpretations). Re-fitting the V1 binocular responses with the additional "*s*" parameter improved the R-square goodness of fit for the V1 neurons that expressed supersaturation, akin to previous investigations (Peirce, 2007). The "*s*" parameter value ranged from 1 (no supersaturation) to 2, and the distribution of "*s*" resembled the distribution of the supersaturation index calculated from the observed data. Examples of the modified Naka-Rushton fits can be found in Figure 23*C*. Finally, the spatiotemporal profile of "*s*" parameter also corresponds to the spatiotemporal profile of the supersaturation index shown earlier in Figure 22, corroborating the finding that supersaturation is predominantly expressed outside of the granular input layers of V1.

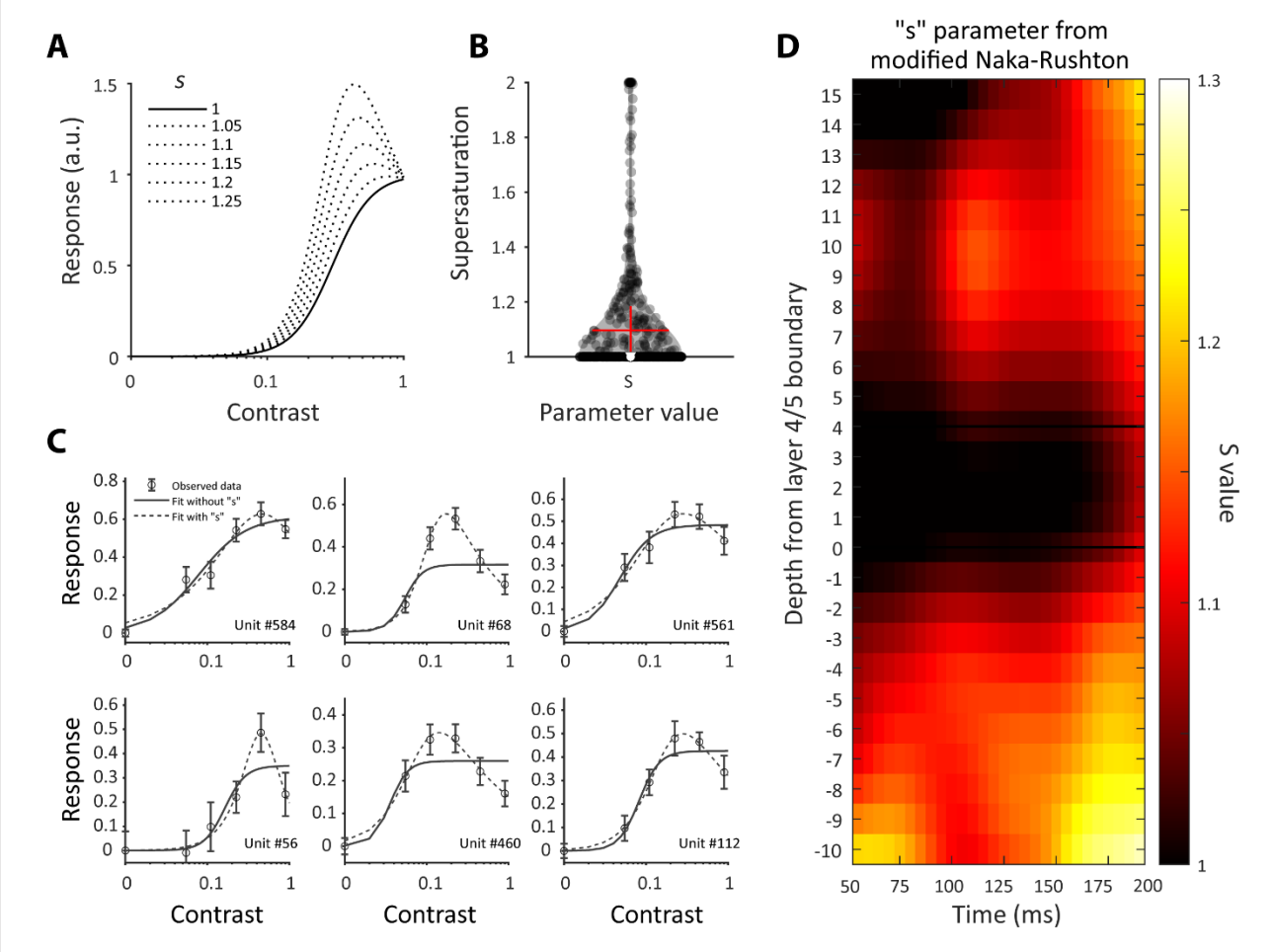

Figure 23. Modified Naka-Rushton equation's parameter for supersaturation across cortical depth. (A). Simulation of the effects of an additional parameter "s" multiplying the exponent in the divisive normalization pool. (B). Distribution of "s" when re-fitting V1 units with all parameters free to vary. (C). Illustrative examples of supersaturation in V1 with the original Naka-Rushton fit (solid line) and modified Naka-Rushton fit with supersaturation (dotted line). (D). Value of "s" parameter in the modified Naka-Rushton equation as a function of cortical depth, indexed relative to the layer 4/5 boundary.

3.3.4. Spatiotemporal profile of V1 binocular summation

Results so far have covered features of divisive normalization (response-gain, contrast-gain, dynamic range, and supersaturation) under binocular stimulation. We now turn our analysis towards the integrative processes that combine left and right eye contrast to produce binocular responses in V1. This integrative process can be conceptualized as a specialized form of divisive normalization occurring not only in response to contrast but also in interactions between the two eyes (Fleet et al., 1997; Moradi & Heeger, 2009; Said & Heeger, 2013). Accordingly, this process has been termed "interocular" or "binocular" normalization (Fleet et al., 1997; Moradi & Heeger, 2009).

To align our findings with existing literature, we opted to first examine binocular summation. Binocular summation refers to the degree to which the left eye response and the right eye response "sum" to the binocular response, measured separately. At the single neuron level, various degrees of summation have been observed, including binocular outputs that exceed the sum of component monocular responses (Barlow et al., 1967; Burns & Pritchard, 1968; D. H. Hubel & Wiesel, 1962; Pettigrew et al., 1968; G. F. Poggio & Fischer, 1977). At the population level and for balanced stimuli presented to corresponding retinal positions, binocular responses typically fall short of the sum of individual monocular components (Giuseppe & Andrea, 1983; M. V. Grünau, 1979; Heravian et al., 1990; Mitchell et al., 2022, 2023; Moradi & Heeger, 2009; White & Bonelli, 1970). This suggests the presence of regulatory mechanisms that control binocular excitation of V1 populations. While this sublinear behavior hints at normalization between the two eyes' signals, it is not a direct measure of binocular normalization. Rather, binocular summation gives insights into the *relative strength* of nonlinear processes underlying binocular integration across the V1 laminar microcircuit.

To assess V1 binocular summation, we took each multiunit's monocular response at each level of stimulus contrast, summed them up, and then divided them by the binocular response to produce an index of summation. Figure 24*A* and Figure 24*B* demonstrate this process on the population-level, as a function of monotonically increasing contrast (left to right). Note that, as contrast increases, V1 responses (monocular and binocular) increase in magnitude while binocular summation (i.e., the index calculated from these responses) decreases. This outcome is expected based on the gain-control theory of binocular combination (Ding & Sperling, 2006), which states that as contrast of input images increases, the interocular gain-control increases, making summation increasingly sublinear (Ohzawa et al., 1985; Truchard et al., 2000). Our V1 multi-units exhibited the same systematic relation between summation and contrast under balanced binocular stimulation (F (4, 2128) = 59.48, $p < 0.001$) (Figure 24*C*). We can also see that summation is dynamic. Binocular summation differed significantly across stimulus processing time (transient onset vs. steady-state, t (532) = 10.9, $p < 0.001$), hitting its maximum at the transient peak before leveling off in the steady-state (Figure 24*D*).

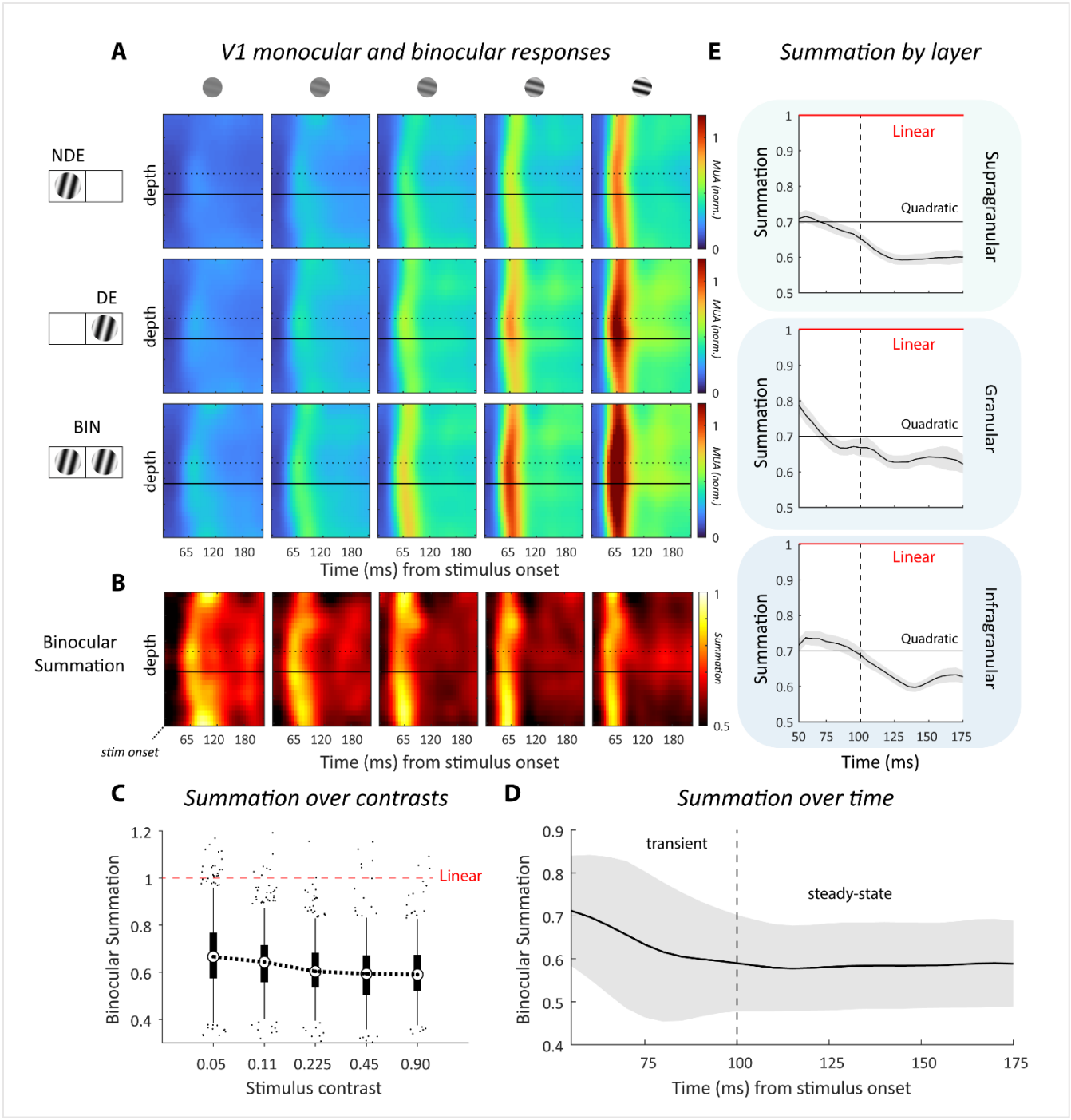

Figure 24. Binocular summation across the V1 laminar microcircuit. (A) V1 laminar spiking responses to monocular (non-dominant eye and dominant eye) and binocular stimulation (balanced) as a function of time (x-axis) and cortical depth (y-axis). Stimulus contrast increases from panel to panel, left to right. (B). Binocular summation as a function of time (x-axis), cortical depth (y-axis), and contrast (panel). (C). Binocular summation as a function of stimulus contrast (averaged over time and depth). (D). Binocular summation as a function of time (averaged over contrast and depth). (E). Binocular summation by V1 layer and time (x-axis) (averaged over contrast).

Finally, binocular summation varied across laminar compartments. Summation was greatest in the granular input layers compared to the supragranular and infragranular layers (Figure 24*D*). This observation, in tandem with the finding that granular layer binocular CRFs are also less sigmoidal (see *3.3.2 Contrast normalization differs*

across the V1 laminar microcircuit), suggests that binocular processing is also relatively more linear in the retinogeniculate input to V1.

In general, binocular vision primarily occurs at or near fixation, where there is significant overlap of the two eyes' views, and vergence aligns objects on the horopter. Under normal conditions, when the images from both eyes are almost identical and fall on corresponding retinal positions, the stimulation is categorized as *dioptic*. However, *dichoptic* stimulation can occur even with retinal correspondence, either when features of the stimuli differ or when the two eyes differ in how they process light information. A prime example of the latter is amblyopia, where the visual input from one eye is consistently weaker or less precise (Birch, 2013). Therefore, we were interested in evaluating binocular summation in V1 under conditions of balanced and imbalanced stimulus contrast between the two eyes.

Figure 25 illustrates binocular summation for balanced (blue) and unbalanced (red) binocular conditions, aggregated over time and laminar compartments. Binocular summation was heightened under conditions where there was an imbalance in contrast between the eyes compared to conditions where the contrast was balanced between them (t (532) = 18.20, p < .001). In both situations, binocular summation was higher in the granular input layer as compared to layers above and below.

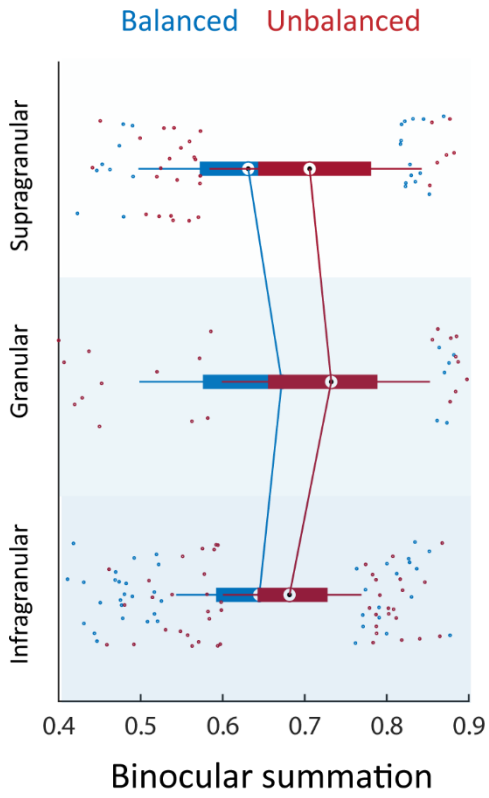

Figure 25. Binocular summation for balanced and unbalanced binocular conditions. Binocular summation was averaged over laminar compartments and time for balanced (blue) and unbalanced (red) binocular conditions.

3.3.5. V1 binocular summation systematically encodes interocular contrast ratio

In our analysis of V1 binocular summation under balanced contrast conditions, we observed an inverse relationship: as contrast increased in both eyes, binocular summation decreased as expected based on known principles of contrast gain-control (Ohzawa et al., 1985). However, scenarios with differing contrasts between the eyes present additional complexity. A recent circuit model of multi-input integration, the "Stabilized Supralinear Network (SSN)", makes a prediction that inputs add sublinearly to superimposed gratings of equal contrast but shifts towards a 'winner-take-all' scenario as contrasts diverge (Rubin et al., 2015). This implies that, for binocularly presented gratings, binocular summation in V1 should intensify systematically with increasing interocular contrast difference, achieving maximum linearity when one eye has significantly higher contrast than the other. We have just demonstrated that binocular summation was greater for unbalanced contrasts in the two eyes compared to balanced contrasts. We were thus curious whether binocular summation in V1 may be more closely aligned with

the degree of 'dichoptic-ness' (i.e., the interocular contrast ratio)—as indicated by the SSN model—rather than the total contrast presented to presented to the system.

To adjudicate between these alternative hypotheses, we sorted our binocular conditions two different ways: by summed contrast in the two eyes (Figure 26*A* – top) and by interocular contrast ratio (Figure 26*A* - bottom). We then plotted binocular summation as a function of these two sorting formats. We found that sorting by interocular contrast difference provided a more systematic relationship with summation compared to sorting by summed contrast (Figure 26*B*).

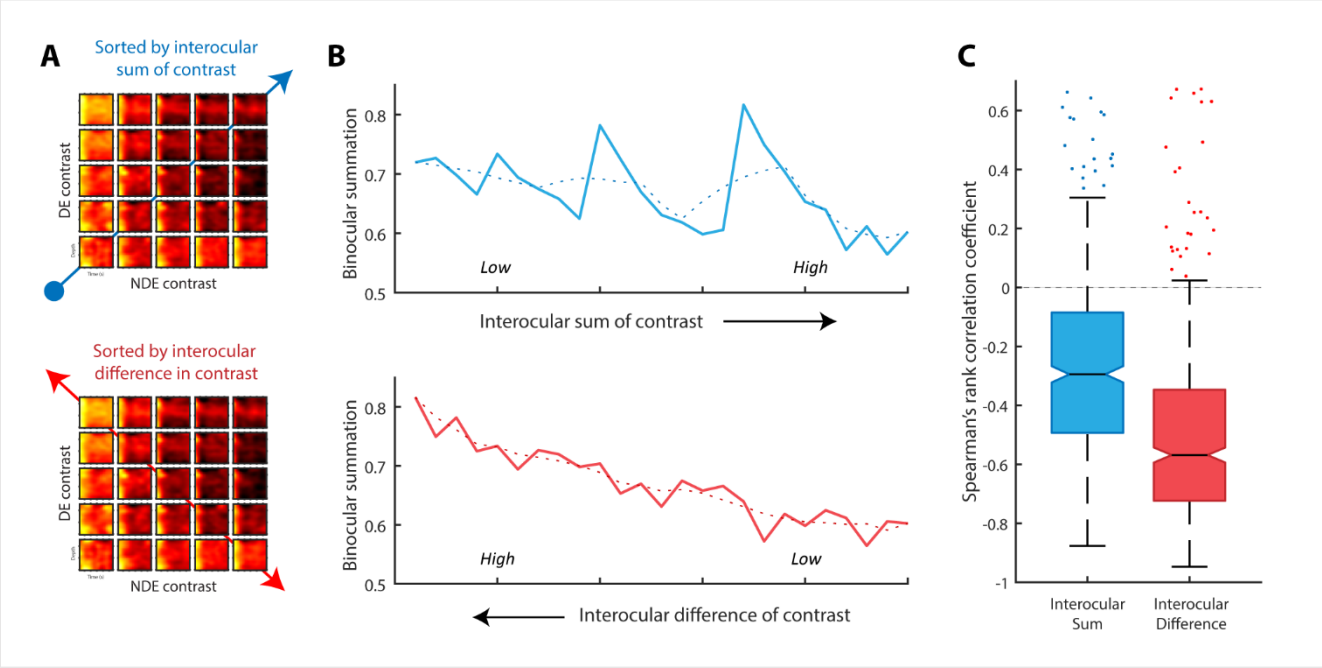

Figure 26. V1 binocular summation systematically encodes interocular contrast ratio. (A). Cartoon representation of sorting binocular conditions by interocular sum of contrast (top) versus sorting by interocular difference in contrast (bottom). (B). Top - Binocular summation as a function of increasing interocular sum of contrast; solid line represents data and dotted line represents smoothed data. Bottom – Binocular summation as a function of decreasing interocular difference of contrast. (C). Spearman's rank correlation coefficient for both sorting formats.

To quantify this, we calculated Spearman's correlation between each unit's summation index and sorted condition. This analysis revealed that binocular summation correlated (negative) much more strongly with interocular difference in contrast (M = -0.51, SD = 0.29) than interocular summed contrast (M = -0.27, SD = 0.30), $t(532) = 20.96$, $p < .001$, *Cohen's d* = 0.91). Thus, similar to how V1 neurons are more affected by stimulus contrast than absolute brightness, they also systematically encode interocular contrast *difference* rather than total contrast presented to the two eyes. Note that this is not the case for the firing rates to these conditions, which increase systematically as a function of total contrast energy. This encoding motif emerges through the integrative process of binocular summation.

We were curious to see whether this correlation between binocular summation and interocular contrast ratio varies over time and/or space. We plotted binocular summation for all 25 binocular conditions over time, organized by either interocular sum or interocular difference of contrast (Figure 27*A*). We then calculated Spearman's correlation coefficient for each temporal window. We found that there is a temporal transition, or "hand-off", between two motifs of encoding for binocular summation. As inputs arrive in V1 (before visually evoked responses have reached their peak), summation magnitude correlated more strongly with summed contrast in the two eyes (Figure 27*B*). However, this relationship is quickly overturned. As summation crescendos, V1 binocular responses begin to differentiate systematically as a function of interocular difference. The temporo-spatial profile of these two forms of summation encoding can be seen in Figure 27*C*.

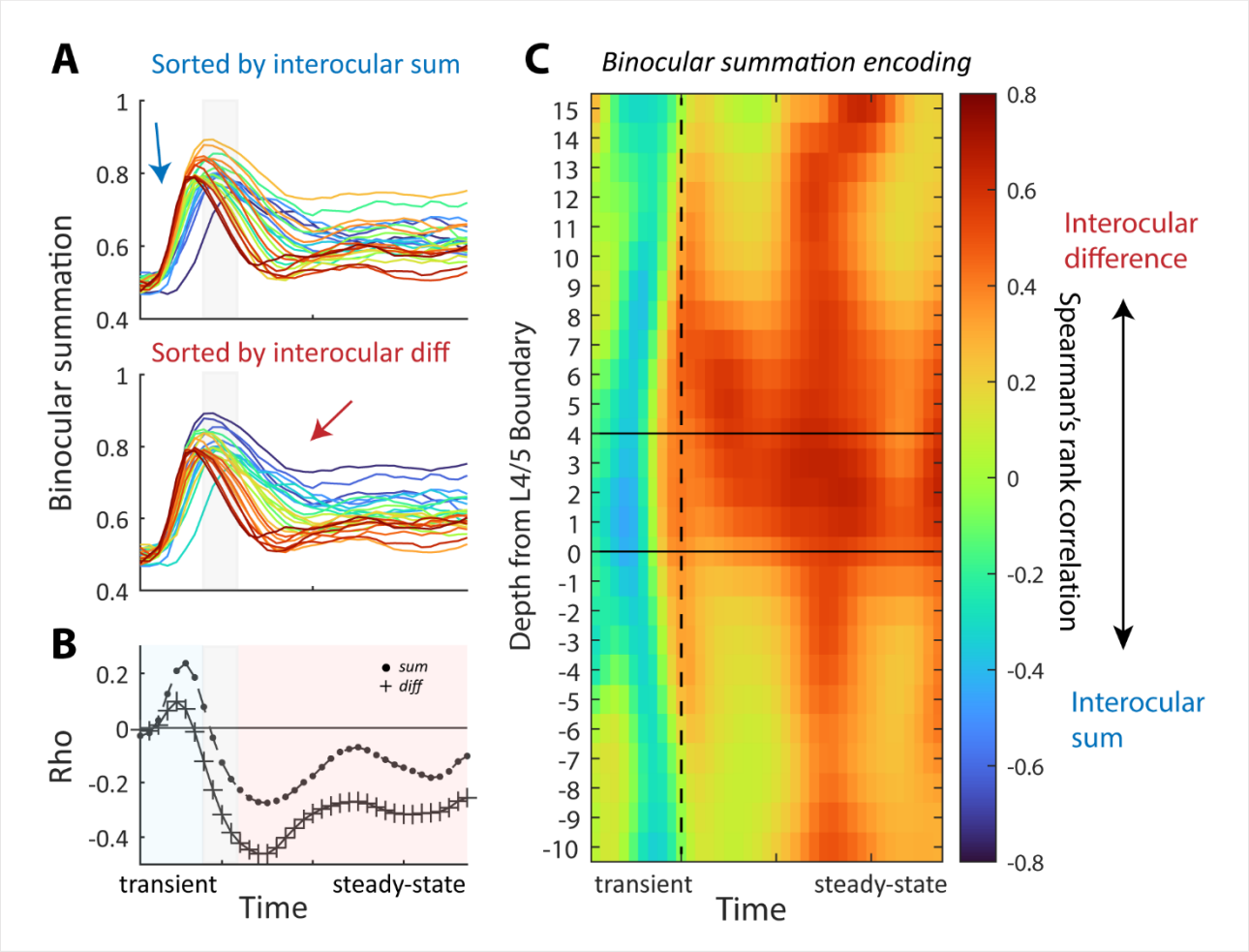

Figure 27. Binocular summation motif temporal dynamics. (A). Binocular summation across time for every binocular condition. Traces are color-coded by either increasing interocular sum (top) or decreasing interocular difference (bottom). Shaded grey bar represents a temporal transition between two motifs. (B). Spearman's rank correlation coefficient over time for the two sorting formats. (C). Binocular summation encoding over time and cortical depth.

3.3.6. Modeling binocular combination within the divisive normalization framework

Our analysis of binocular summation underscores the existence of nonlinear mechanisms within and across monocular channels that modulate excitation in the primary visual cortex (V1). This observation sets the stage for a detailed examination of the computational models that describe these interactions.

We employed a binocular normalization model to assess response variance between different visual conditions across the V1 laminar microcircuit. Prior studies, including our own (Mitchell et al., 2023), have shown that this model provides superior fit to V1 spiking responses compared to other models like linear summation, quadratic summation, and averaging contrasts between the eyes.

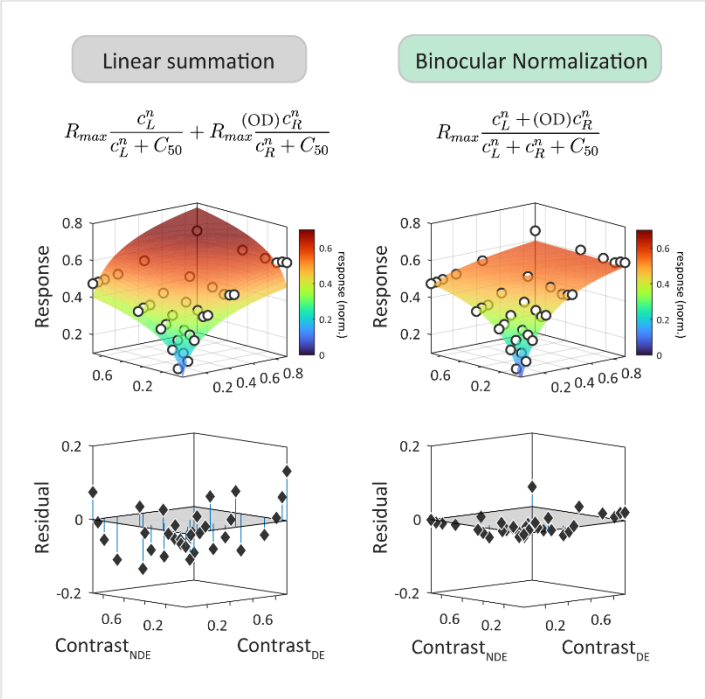

Figure 28. Fitting computational models to V1 spiking data. For demonstration purposes, we fit the entire population of V1 responses (all 36 conditions) with both the linear summation model (left) and binocular normalization model (right). Mean residuals are plotted below each surface fit.

To quantitatively capture the strength of the normalization processes at play, we contrasted the goodness of fit (measured by the adjusted r-square value) of the binocular normalization model against that of the linear summation model. These models account for ocular dominance by weighting the input drive from the non-dominant eye (Mitchell et al., 2023). The population-level model fitting results, which were averaged over both time (50-200ms) and cortical depth, are depicted in Figure 28. The binocular normalization model performed significantly better (M = 0.84, SD = 0.18) than the linear summation model (M = 0.71, SD = 0.18) at fitting all 36 conditions, t (507) = 24.2, p < .001, *Cohen's d* = 1.08). Notably, linear summation showed the lowest residuals under conditions of low contrast in both eyes and conditions with the highest interocular contrast ratio, where linear mechanisms are predominantly observed in previous analyses. By comparison, binocular normalization's residuals were uniformly minimal across all conditions with a notable exception of one condition (binocular balanced, 90% contrast in each eye).

We next assessed the strength of binocular normalization across the V1 laminar microcircuit (Figure 29). Normalization strength was quantified for each multiunit using the following index:

$$\frac{NRM_{fit}-LSM_{fit}}{NRM_{fit}+LSM_{fit}}$$

where NRM_{fit} and LSM_{fit} represent the adjusted r-square values for the binocular normalization and linear summation models, respectively.

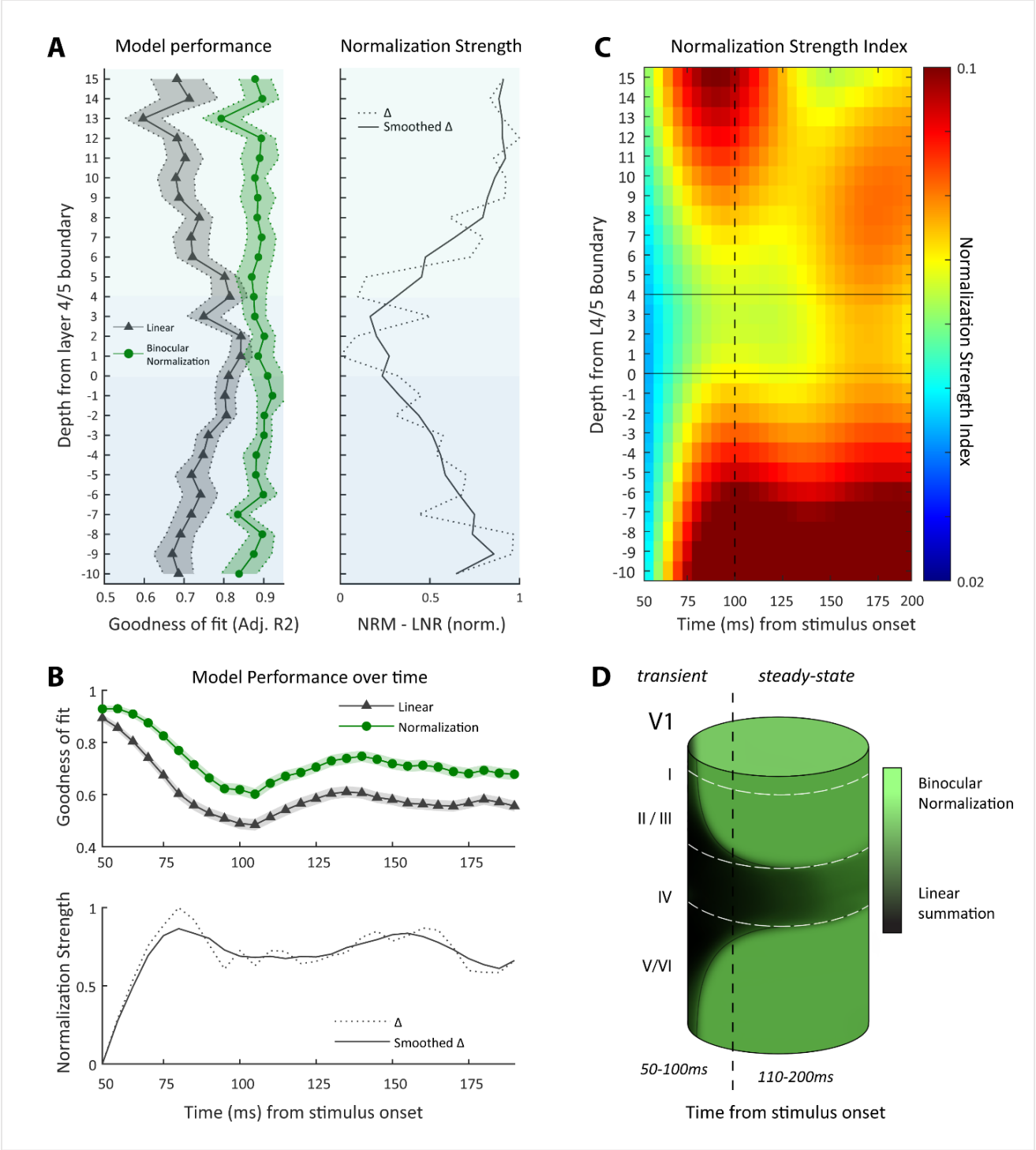

Figure 29. Binocular normalization across the V1 laminar microcircuit. (A). Binocular normalization strength across cortical depth, indexed from the layer 4/5 boundary. Normalization strength was calculated as a Michelson contrast index between the two models' goodness of fit (adj. rsquare). (B). Model performance and binocular normalization strength over time. (C). Normalization strength over time and depth. (D). Cartoon depiction of binocular normalization across the V1 laminar microcircuit.

This analysis revealed that normalization strength was relatively weak in the granular input layers of V1, yet considerably stronger in the supra- and infragranular layers. Temporal analysis revealed an evolution of normalization strength across the stimulus presentation. Normalization strength increased rapidly following the transient onset, indicated by the sustained divergence between the two models after 60ms, exhibiting two significant peaks at 75ms and 150ms. These findings are represented in Figure 29, illustrating the model performance as a function of both cortical depth (Figure 29*A*) and time (Figure 29*B*). A combined spatio-temporal profile of normalization strength (Figure 29C) further elucidated that normalization intensifies in the upper and deep layers following the initial retinogeniculate inputs into the granular layers. A cartoon illustration synthesizing these results is shown in Figure 29*D*.

3.3.7. Dynamics of divisive normalization

The temporal dynamics observed align with the multi-stage theory of binocular integration proposed by Cox et al. (2019), suggesting an initial summative stage followed rapidly by a more complex stage of integration. Notably, the second peak of binocular normalization performance appears to coincide with oscillatory dynamics typically observed following the transient of V1 responses. This phenomenon, sometimes colloquially referred to as the "second peak" of responses, has been linked to recurrent feedback circuits that implement divisive normalization. This observation has motivated further analyses to explore the components of dynamic normalization across the V1 laminar microcircuit.

Dynamic normalization, likely driven by complex intracortical interactions, modulates visual processing in a contrast-dependent manner. We aimed to explore elements of this process across the V1 laminar microcircuit. Initially, we utilized MATLAB code from Heeger & Zemlianova (2020) to simulate V1 neuron dynamics as a function of increasing contrast. This model integrated orientation and spatial frequency preferences through predefined receptive fields, with stimuli encoded via sinusoidal modulations and temporally prefiltered to simulate neural adaptation. Divisive normalization, reflecting competitive interactions among neurons with a range of tuning profiles, was implemented using an interaction matrix that modeled excitatory and inhibitory influences based on proximity and feature similarity. The computed responses of simple and complex cells to a preferred orientation were aggregated over time and plotted to illustrate a subpopulation of neuronal activity, similar to our measure of multi-unit activity.

This simulation identified three principal elements of dynamic normalization that are dependent on contrast: the time-to-peak of V1 responses, the onset transient, and post-peak oscillatory phenomena (Figure 30*A*). We observed these elements in our empirical data as well (Figure 30*B*). We measured the time-to-peak (ms), the magnitude of the transient peak, and response variability (standard deviation) during the sustained period (110ms-200ms) as a function of total contrast energy (up to 100%). Each component was modeled using the curve fitting function that provided the best fit: the time-to-peak and transient magnitude conformed best to an exponential decay function, while the sustained variability was most accurately modeled using a logistic growth function.

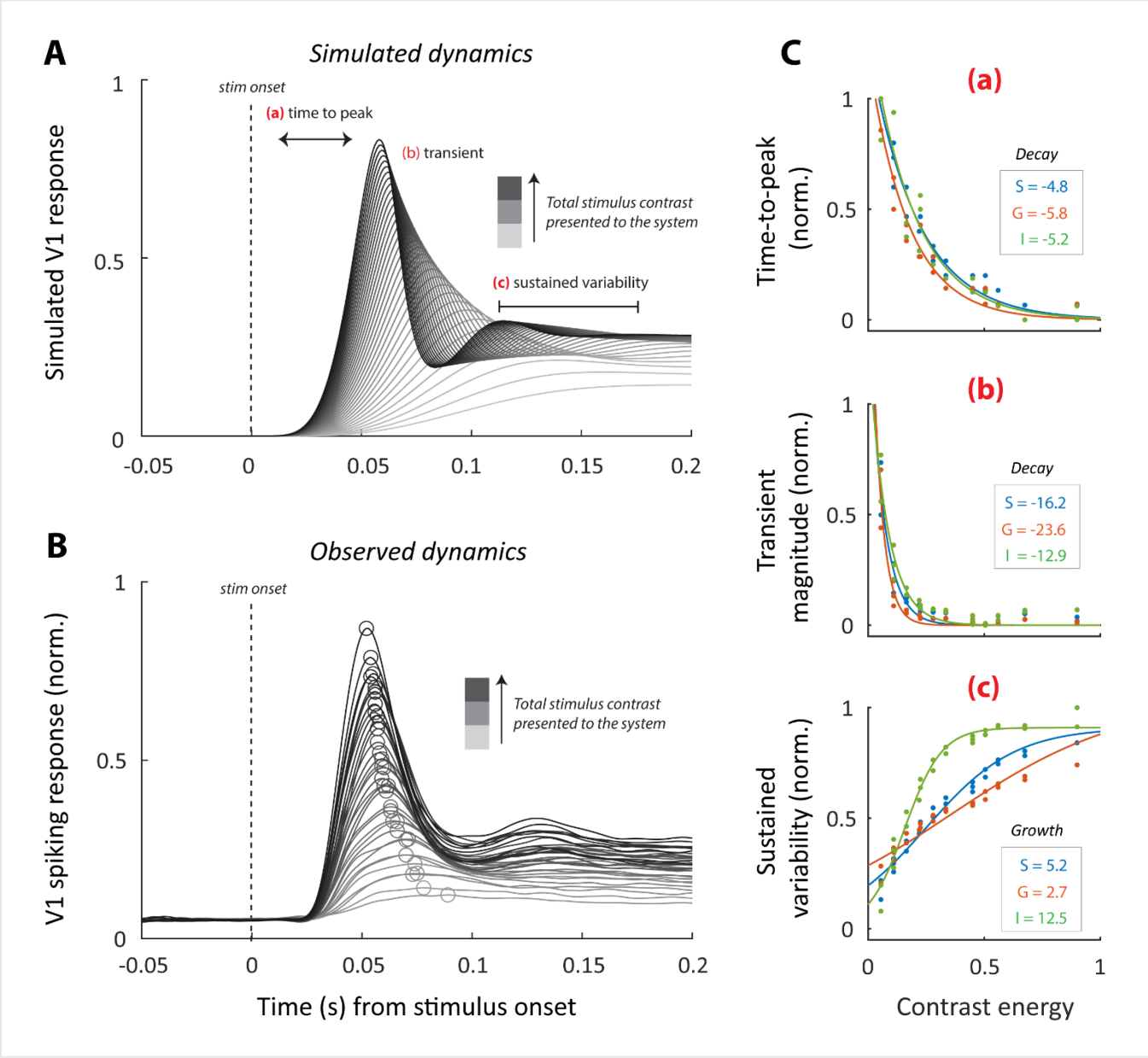

Figure 30. Dynamics of divisive normalization. (A). Simulation of dynamic normalization, using code from Heeger & Zemlianova (2020). Three contrast-dependent aspects emerged: (a) latency to transient peak, (b) transient amplitude, and (c) post-peak dynamics (B) Observed V1 responses, ordered by total contrast energy (increasingly darker shades) presented across the two eyes. (C) Each component of dynamic normalization measured for each laminar compartment (supragranular, green; granular, orange; and infragranular, blue). Time-to-peak (a) and transient magnitude (b) were fit using an exponential decay function. Sustained variability (c) was fit using a logistic growth function.

This analysis generated contrast decay constants for the time-to-peak and transient magnitudes, as well as a contrast growth constant for variability during the sustained period (Figure 30*C*). Notably, the contrast-dependence of each component closely aligned with those observed in simulations of V1 cells (Heeger & Zemlianova, 2020). For example, in the granular input layer, the decay constant for time-to-peak (-5.8) is approximately 1.1x the square root of the decay constant for transient magnitude (-23.6), reflecting a high degree of similarity to the model predictions concerning the relationship between effective time-constant and gain (Heeger & Zemlianova, 2020). However, this relationship progressively deviated from model predictions in the supragranular (1.2x) and infragranular layers (1.4x). The growth constant for variability in the steady state also showed a systematic increase in accordance with the canonical microcircuit hierarchy: it was least pronounced in the granular layer (2.7), more pronounced in the supragranular layers (5.2), and reached its peak in the infragranular layers (12.5).

3.4 Discussion

Our study investigated divisive normalization process within the V1 laminar microcircuit and its implications for binocular processing. We utilized contrast response functions (CRFs) under binocular stimulation to assess normalization across time and depth in V1, revealing distinct spatiotemporal patterns in contrast sensitivity and saturation. Our investigation into binocular summation highlighted the role of nonlinear normalization processes operating between and within monocular channels. Through computational modeling, we demonstrated that these nonlinear processes can be appropriately portrayed as a product of binocular normalization. Finally, we contextualized our findings within models of recurrent feedback, emphasizing the adaptive nature of normalization mechanisms in V1 and their implications for higher-level theories of multi-input integration.

3.4.1. Laminar specificity of divisive normalization

Our investigation into contrast response functions (CRFs) under binocular stimulation unveiled distinct laminar patterns of normalization parameters within V1. We observed laminar variations in the exponent (n) that controls the shape of CRFs and the semi-saturation constant (C50) that controls contrast sensitivity.

In the classic contrast response function (Naka & Rushton, 1966), the exponent (n) controls the sigmoidal shape of the curve (Albrecht & Hamilton, 1982). Higher values lead to greater saturation at high contrast, which manifests as a more sigmoidal curve while lower values lead to a flatter, more linear CRF. We found that exponent values were significantly lower in the granular layer as compared to those in supragranular and infragranular layers. This finding indicates that the granular layer exhibits a wider dynamic range and a more linear contrast-response relationship. Several studies support the notion that the granular input layers of the primary visual cortex (V1) process information in a more linear fashion relative to other layers. Johnson and Burkhalter (1996) demonstrated that layer 4 of V1, which receives direct inputs from the lateral geniculate nucleus (LGN), maintains a more linear response profile to visual stimuli than the supra- and infragranular layers (Johnson & Burkhalter, 1996). Further, computational modeling suggests that the granular layer might function as a linear filter, extracting basic visual features without significant nonlinear transformations (Carandini et al., 1997). Indeed, optical imaging studies have

shown that the functional architecture of orientation selectivity in layer 4 is more isotropic and less orientation-specific compared to other layers (Kondo & Ohki, 2016). These findings are consistent with the notion that the input layers of V1 act as a relatively unaltered conduit for transmitting sensory information from the thalamus to the cortex in a feedforward fashion (Priebe & Ferster, 2012), inheriting nonlinearities they exhibit from their LGN predecessors (Priebe & Ferster, 2008).

Secondly, our study found that the semi-saturation constant of divisive normalization, C50, was significantly lower in neurons located in the infragranular layers. A lower C50 indicates increased sensitivity to stimulus contrast (Albrecht & Hamilton, 1982). This increased sensitivity in the infragranular layers of V1 may be partially attributed to their binocularity. As noted by Hubel and Wiesel (1970), infragranular neurons are typically more binocular, receiving and integrating monocular signals from both eyes. We also found that the infragranular layer neurons were least selective for the eye of origin, and most equivalently driven by each eye. Since they receive more enriched visual input, infragranular binocular neurons may be better suited to detect subtle variations in contrast. If this were the case, then normal integration of monocular inputs in V1 would be crucial for fine-tuning the visual system's sensitivity to contrast (Blakemore & Cooper, 1970). Indeed, studies confirm that the integration of signals from both eyes leads to more robust and reliable neuronal responses, particularly under conditions of low contrast (Blakemore & Cooper, 1970; Priebe & Ferster, 2012). Thus, our findings suggest that the enhanced contrast sensitivity in infragranular layers is not solely a product of intrinsic neuronal properties but also significantly influenced by the integrative aspects of binocular vision.

3.4.2. Cortical origins of supersaturation

In this study, we have further explored the phenomenon of "supersaturation" in the primary visual cortex (V1). Supersaturation refers to the condition where the response of a neuron exceeds the predicted maximal response under high contrast conditions (Albrecht & Hamilton, 1982). Our findings corroborate the existence of supersaturation in V1, with a percentage of units exhibiting this phenomenon (~30%) comparable to previous reports (Peirce, 2007). Our modification of the Naka-Rushton equation to accommodate supersaturation, as outlined by Peirce (2007), allowed the exponent of the divisive normalization pool to vary independently from the exponent of the excitatory drive (Peirce, 2007). We also observed notable improvements in the goodness of fit for V1 neurons expressing supersaturation, and the distribution of the "s" parameter closely resembled the distribution of the supersaturation index calculated from observed data. Both the data-derived and fit-derived measures of supersaturation were assessed across V1 laminar compartments, revealing that supersaturation was predominantly found outside of the retinogeniculate input layer in V1.

Several studies offer insights into why supersaturation tends to be predominantly expressed in layers other than the primary geniculate input layer, Layer 4C. Albrecht and Hamilton (1982) proposed that the emergence of supersaturation in V1 neurons might be influenced by recurrent inhibitory connections within cortical circuits, which are particularly abundant in the supragranular and infragranular layers. These inhibitory interactions are crucial in shaping the nonlinear response properties of V1 neurons, enhancing their sensitivity to high-contrast

stimuli. Furthermore, research by Ledgeway et al. (2005) and Tyler and Apkarian (1985) emphasized the role of cortical feedback mechanisms, which originate from higher visual areas and are likely more influential in layers outside of Layer 4C, thus contributing to the expression of supersaturation in these regions. Indeed, neurons in Layer 4C typically do not receive any feedback inputs (Felleman & Essen, 1991). Additionally, studies by Li and Creutzfeldt (1984) and Maffei and Fiorentini (1973) have suggested that the laminar-specific distribution of different neurotransmitter receptors and neuromodulatory systems may also contribute to the differential expression of supersaturation across V1 layers. Collectively, these findings highlight the complex interplay of local circuitry, recurrent connections, and neuromodulatory mechanisms in shaping the nonlinear response properties of V1 neurons and provide potential explanations for the extragranular expression of supersaturation in the visual cortex that we observe here.

3.4.3. Binocular integration across the laminar microcircuit

Our investigation of V1 binocular processing began by replicating laminar and temporal patterns that have been previously reported. First, binocular modulation was observed across all cortical layers, not just the layers that have been traditionally modeled as binocular convergence layers. This finding aligns with previous reports of binocular neurons residing in all sub laminae (4A, 4B, 4Cα, and 4Cβ) of primate layer 4 (Hawken & Parker, 1984) and recent observations of binocularly modulated monocular neurons in layer 4C (Dougherty, Cox, et al., 2019). While binocular interactions were observed at all cortical depths, binocular facilitation was the greatest in the infragranular layers where neurons typically exhibit the greatest degree of binocularity, matching previous reports (Cox et al., 2019).

Previous work has also indicated that binocular integration is a dynamic process that evolves over the course of visual stimulation. Cox et al., (2019) described an initial pattern of response enhancement to balanced binocular stimuli, followed rapidly by more complex dynamics that potentiate response suppression (Cox et al., 2019). These temporal dynamics were subsequently characterized as a transition from an initial contrast-independent (i.e., multiplicatively scaled by contrast) stage of integration to a more contrast-dependent stage (Mitchell et al., 2022). This suggests that binocular integration comprises multiple, sequential stages of processing of stimulus contrast in the two eyes. However, it remained unclear from earlier studies whether these stages are underpinned by distinct mechanisms or represent the dynamic unfolding of a single mechanism.

Here, we observed binocular summation of contrast was the most linear at the onset transient, followed by a rapid decline in summation and shifts in the binocular contrast-response curve (along the contrast axis) that changed over time. This pattern supports the view that binocular integration unfolds dynamically in a contrast-dependent manner (Cox et al., 2019; Mitchell et al., 2022). Expanding on previous research, our analysis suggests that both the initial "linear" and the subsequent "sublinear" stages are governed by a single mechanism of divisive normalization, operating both within and between the two eyes. This mechanism of binocular normalization was observed to initiate in the granular layers and increase in strength (decrease in linearity) across the V1 laminar microcircuit.

3.4.4. Binocular normalization and models of recurrent feedback

Our analysis delved into the spatiotemporal dynamics of binocular integration across the V1 laminar microcircuit. We employed a binocular normalization model (Fleet et al., 1997; Moradi & Heeger, 2009), which demonstrated superior fit to V1 spiking responses across various visual conditions compared to models like linear summation. Our results suggested that the normalization processes are particularly robust in supra- and infragranular layers and exhibit temporal dynamics, including dual peaks of normalization strength during stimulus presentation. These dynamics we observed notably mirror the neural dynamics that emerge from circuit-models that implement recurrent feedback connections that give rise to recurrent amplification (Heeger & Mackey, 2019).

Dynamic normalization

Dynamic normalization is a circuit-level extension to the divisive normalization model by Heeger and Zemlianova (2020). Their research outlines a recurrent circuit model that achieves normalization through mechanisms of recurrent amplification (Heeger & Mackey, 2019), providing a circuit-level, computational framework for understanding V1's response dynamics to visual stimuli (Heeger & Zemlianova, 2020). Central to their model is the concept that each neuron's response is normalized by a factor that includes a weighted sum of activity from a pool of neurons (Carandini & Heeger, 2012; Heeger & Zemlianova, 2020). These weights adjust dynamically based on the contrast and other visual features, allowing for nonlinear interactions to modulate neuronal firing (Heeger & Zemlianova, 2020). Dynamic normalization reproduces several key phenomena observed in V1, including response saturation under high-contrast conditions (Albrecht & Hamilton, 1982; Bonds, 1991; Ohzawa et al., 1985), response latencies as a function of contrast (Albrecht et al., 2002; Bair et al., 2002; Bonds, 1991), and reverberation effects post-transient that resemble a "2nd peak" (Hermes et al., 2015). Moreover, the model links these phenomena to gamma oscillations observed in neural activity, as previously posited (Ray et al., 2013), describing the gamma rhythm as an emergent property of the normalization process facilitated by the recurrent connections within the cortical circuit (Heeger & Zemlianova, 2020). This comprehensive theoretical framework provides an essential backdrop for our empirical exploration of normalization dynamics within V1.

The neural dynamics in response to varying stimulus contrast that we observed closely matched an in-house simulation of dynamic normalization. We observed contrast-dependence of the time-to-peak latencies, visual transients, and reverberation dynamics post-peak, commensurate with dynamic normalization's core properties (Heeger & Zemlianova, 2020). The recurrent circuit of dynamic normalization further provides an explanation of the contrast-dependence of the post-peak phenomena: The neural dynamics observed following the initial onset response in V1 can be interpreted through the lens of recurrent neural circuits optimized for efficiency and reaching stabilization. In the dynamic normalization model, once the initial feed-forward input (the first peak) is processed, recurrent connections within the cortical network contribute to a re-evaluation or reinforcement of the initial signal. This recurrent processing enhances or suppresses the initial response based on stimulus intensity and internal network dynamics, leading to a reverberation of responses that is contrast dependent (Heeger & Zemlianova, 2020). Inhibitory neurons can modulate the activity to prevent overstimulation and to refine the response pattern,

contributing to the appearance of a second peak or, depending on the strength of the normalization pool, gamma oscillations may emerge (Heeger & Zemlianova, 2020).

Feedback inputs from higher cortical areas, which are involved in more complex processing tasks such as attention and perceptual grouping, can also contribute to steady-state dynamics (Bastos et al., 2015; Johnson & Burkhalter, 1996; Nassi et al., 2014). These inputs can modify or reinforce the information being processed based on broader cognitive contexts (H. Zhou & Desimone, 2011), enhancing certain signals while suppressing others. Thus, the dynamic normalization model provides a unifying framework to explain both the initial more summative phase of binocular integration, as well as the post-peak, more complex dynamics that we and others (Carlson et al., 2023; Cox et al., 2019; Mitchell et al., 2022; Westerberg et al., 2019) observe.

Our findings also indicated that normalization is expressed differently across the V1 laminar microcircuit. We found that supra- and infragranular layers exhibited stronger binocular normalization compared to the granular layers. One interpretation of this differential pattern of normalization across layers is based on distinct excitatory and inhibitory connections prevalent in these layers. The computational model by Heeger and Zemlianova speculates that such differences might arise from the specific roles that various cell types and their interconnections play in cortical circuitry. Specifically, the authors posit a recurrent circuit comprised of 'principal' cells and 'modulator' cells that, through interconnections, control the effect of strong inputs and amplify the effect of weak inputs (Heeger & Zemlianova, 2020). The principal cells are posited to be large pyramidal cells and the modulator cells as inhibitory cells, such as parvalbumin-expressing cells (Heeger & Zemlianova, 2020). The distributions of these cell types in primate V1 are known. Pyramidal cells have a relatively strong presence in layers 2/3 and 5 while PV-expressing cells are relatively abundant in layer 4 and 5 (Fitzpatrick et al., 1987; Vanni et al., 2020). Pyramidal cells are also believed to be crucial for generating gamma oscillations (Cardin et al., 2009) and intra-cortical inhibition (Bartos et al., 2007). Consistent with these laminar distributions, we found that post-peak response variability was heightened in the supragranular (2/3) and infragranular (5/6) layers, as compared to the granular layer. An alternative but not mutually exclusive interpretation of the laminar hiearchy of post-peak phenomena could potentially be attributed to feedback connections from higher cortical areas (Bastos et al., 2015; Johnson & Burkhalter, 1996), as well, as neurons in layer 4C typically do not receive any feedback inputs (Felleman & Essen, 1991). Feedback projections are known to modulate sensory processing (Gilbert & Li, 2013), potentially enhancing or altering the timing of responses (Hupé et al., 1998) and influencing oscillatory activities (Bastos et al., 2015).

Stabilized Supralinear Network (SSN)

The stabilized supralinear network (SSN) model offers a unifying framework for understanding multi-input integration in sensory cortices, including phenomena like surround suppression and response normalization (Rubin et al., 2015). Rubin et al. (2015) describe SSN as emerging from four primary properties: supralinear input-output functions of neurons, strong recurrent excitation, feedback inhibition, and specific spatial properties of intracortical connections. This model provides a unifying motif to explain the dynamic transition from facilitation to suppression with increasing stimulus strength under various visual conditions. To our knowledge, this is the only model that can

explain the temporal dynamics of dichoptic cross orientation suppression (Carlson et al., 2023; Cox et al., 2019) and the facilitation-to-suppression transition observed in V1 under dioptic stimulation, where inputs are feature-matched (Mitchell et al., 2022).

In our experiments, we observed that neuronal responses were more additive at lower stimulus contrasts, with this summation declining as stimulus intensity increased—aligning with the SSN model's predictions. The model further posits that, at lower input levels, weak synaptic coupling allows responses to sum supralinearly. The nature of the multi-unit signal likely impacted the detectability of supralinear phenomena, thus limiting our interpretation here. However, while supralinear summation was not evident at the population level in our data, instances of supralinear summation at the individual-multi-unit level were almost exclusively found for low contrast intensities. Moreover, the observed linear-to-sublinear gradient of binocular integration aligns with the model's foundation of contrast dependence, as discussed in recent studies (Holt et al., 2023) .

A more specific prediction of the SSN model is that V1 responds sublinearly when presented with superimposed gratings of equal contrast, transitioning to a 'winner-take-all' scenario as the contrasts of the two inputs diverge (Rubin et al., 2015) —an effect physiologically observed for plaid stimuli in previous studies (Busse et al., 2009; MacEvoy et al., 2009). This model behavior resonates with the correlation we found between binocular summation and interocular contrast differences, where binocular summation was shown to increase systematically with interocular contrast difference. Our findings suggest that this 'winner-take-all' effect extends to binocular stimuli, indicating a common underlying mechanism where the visual system prioritizes more salient stimuli, effectively modulating integration based on relative contrast.

Given the SSN model's success in explaining the integrative properties observed in our experiments, future studies could further explore its applicability in binocular integration. Investigating the specific roles of different neuron types in this network model could also provide deeper insights into how exactly these cortical circuits give rise to single binocular vision.

3.5 Methods

3.5.1. Subjects

The subjects for these experiments were two healthy, adult macaque monkeys (Monkey J, male, *Macaca mulatta*; Monkey B, male; *Macaca radiata*). Macaque monkeys are essential in visual science research due to their close resemblance to humans in visual system structure and function. These primates serve as valuable models for studying a wide range of visual processes, from basic perception to complex decision-making. Ethical guidelines ensure their humane treatment, but ongoing efforts aim to reduce reliance on animal testing in visual science research through alternative methods and models. All procedures involving these animals followed regulations by the Association for the Assessment and Accreditation of Laboratory Animal Care (AALAC), Vanderbilt University's Institutional Animal Care and Use Committee (IACUC), and National Institutes of Health (NIH) guidelines.

3.5.2. Stereoscopic stimulation

Visual stimuli were displayed using a VIEWPix monitor from VPixx Technologies, which has a refresh rate of 120 Hz and a screen size of 22.5 inches with a resolution of 1920 x 1200 pixels. The monitor ensured high display fidelity, providing 95% luminance and maintaining uniform color distribution across more than 95% of its surface area. All visual stimuli were viewed by the subjects through a custom-built mirror stereoscope. This arrangement allowed the right eye to view stimuli presented on the right side of the screen and vice versa for the left eye, with a non-reflective black divider separating the two halves of the screen. The stereoscope mirrors were made of an infrared-transparent material (Qian & Brascamp, 2017), to facilitate the recording of gaze data using infrared-sensitive cameras (EyeLink II). Oval apertures were used at the boundaries of each screen half to potentiate binocular fusion of the images. Calibration of the stereoscope was conducted at the start of each session via a behavioral task (Maier et al., 2008), that assessed the alignment of the mirrors by comparing gaze positions when cuing was done in one eye at a time.

Subjects were conditioned to initiate fixation within 0.5 degrees of visual angle on a centrally positioned cue (blue x) that appeared to both eyes simultaneously. The objective for the subjects was to maintain this fixation as sinusoidal grating stimuli were intermittently shown in the parafoveal visual space. Various experimental paradigms were used to evaluate the receptive fields, analyze tuning properties of these fields, and examine the integration of binocular contrast. Detailed descriptions of each experimental paradigm are provided in subsequent sections. The protocol for each trial involved maintaining fixation for 500 milliseconds before the initial stimulus presentation. Trials were discontinued if fixation was lost during this interval. Each stimulus was displayed for 250 milliseconds, which aligns closely with the duration of a typical fixation (Wilming et al., 2017). This was followed by a 300-millisecond gap before the subsequent presentation. Successful completion of a trial, encompassing three presentations over 1.35 seconds, resulted in a juice reward for the subject. A new fixation cue was introduced after a brief delay of 1-5 seconds if fixation was maintained throughout a trial. Subjects could terminate the session voluntarily by ceasing to initiate new trials.

3.5.3. Intracranial Electrophysiological Recordings in V1

We used linear multielectrode arrays to record spiking activity across the laminar microcircuit of V1. Prior to performing the experiments, perpendicular trajectories for the probes were established through co-registration of high-resolution CT and MR scans (Godlove et al., 2014). Following successful electrode penetration, several analyses were routinely performed to validate the position of the probe in V1. Notably, we used online multi-unit activity (MUA) in tandem with current source density (CSD) to ensure the probe spans all laminar compartments of V1. Receptive fields and orientation tuning of online-sorted single neurons provide additional information as to the angle of the probe relative to the cortical surface. In our experience, a perpendicular penetration is reliably indicated by overlapping receptive fields and comparable orientation preference (~15°) down the length of the linear array (Cox et al., 2019; Dougherty, Cox, et al., 2019; Mitchell et al., 2022).

Fluctuating extracellular voltages (referenced to the metallic electrode shaft) were amplified, filtered, and digitized using a 128-channel Cerebus neural signal processing system. The neural signal processing system also

records non-neurophysiological analog signals related to the monitor refresh (i.e., a photodiode signal; OSI Optoelectronics, Montreal, Quebec) and eye position (i.e., voltage output of eye-tracking system of EyeLink 1000). The event-locked time stamps and the photodiode signal are used to align the time-varying intracranial data with the occurrence of visual events.

3.5.4. Identification of the layer 4/5 boundary and laminar alignment

We used current source density (CSD), a well-established and histologically verified neurophysiological method (Mitzdorf, 1985; Nicholson & Freeman, 1975; Schroeder et al., 1991), to determine V1's granular input layer. CSD analysis has been shown to reliably indicate the location of primary geniculate input to V1 in the form of a distinct current sink that is thought to reflect combined excitatory postsynaptic potentials of the initial retinogeniculate volley of activation (Mitzdorf, 1985; Schroeder et al., 1991). Current source density (CSD) analysis was performed on the LFP signal using an estimate of the second spatial derivative appropriate for multiple contact points (Nicholson and Freeman, 1975):

$$CSD(t,c) = -\frac{x(t,c-z) + x(t,c+z) - 2x(t,c)}{z^2},$$

where x is the extracellular voltage recorded in Volts at time t from an electrode contact at position c, and z is the electrode intercontact distance (0.1 mm). To yield CSD in units of current per unit volume, the resulting CSD from the formula was multiplied by 0.4 S/mm as an estimate of cortical conductivity (Logothetis, Kayser, and Oeltermann, 2007).

For each penetration with the laminar multielectrode array, CSD analysis was used to resolve this prominent initial current sink immediately following stimulus onset. The bottom of this sink was used as a marker of the transition between granular Layer 4C and the deeper Layer 5 (Maier et al., 2010). In addition to CSD, we also analyzed LFP power at each electrode contact across the array. The cortex generates a canonical laminar pattern of oscillatory activity composed of gamma rhythms (50 – 100 Hz) in superficial layers and alpha-beta (10 – 30 Hz) rhythms in deep layers (Maier et al., 2011; Mendoza-Halliday et al., 2024) . The intersection of gamma and alpha-beta has been localized histologically to the granular input layer (Mendoza-Halliday et al., 2024) . Thus, the spectrolaminar motif of oscillatory power can be used as a complimentary technique (to CSD) for determining laminar position. The supragranular to granular boundary was set to 0.4 mm above the granular-to-infragranular boundary.

3.5.5. Receptive field mapping and feature tuning

Once satisfactory electrode placement was achieved, we used a reverse correlation-like technique to map the receptive fields of the online-sorted single units. We first estimated the receptive field location from the audible MUA response to bar and grating stimuli that were moved across the screen while the animals fixated for juice reward. These stimuli were presented to each eye separately. We then had the animals fixate while a series of circular static random noise patches were presented monocularly and binocularly at pseudorandomized locations

within a predetermined virtual grid that covered the estimated receptive field. Up to five stimuli were shown per trial, for 200 ms each with 200-ms blank periods interleaved. Stimulus size and grid spread varied depending on receptive field estimates, with each recording session typically including an initial “coarse” followed by a “fine” mapping phase of decreasing grid size. We used the resulting neurophysiological data to compute retinotopic three-dimensional receptive field matrices (RFMs) (Cox et al., 2013) to derive spatial maps of neuronal responses as a function of visual space. This procedure allowed us to identify the optimal *position* of grating stimuli for each V1 column.

Parameters of the sinusoidal grating stimuli (i.e., orientation, size, spatial frequency) were customized to the average tuning preferences along the V1 column each day. To do so, three 250ms monocular stimuli were interleaved with 300ms blank periods. Sinusoidal gratings pseudo randomly varied in size, spatial frequency, and orientation (Cox et al., 2019; Mitchell et al., 2022; Westerberg et al., 2019) and eye-of-origin (monocular and binocular presentations). All binocular presentations were presented with zero disparity (or close to zero disparity given that the monitor was flat rather than curved in the shape of the horopter) between the eyes. Upon completion of this procedure, we determined the column’s mean preferred orientation, spatial frequency, and phase by statistically comparing spiking responses to each parameter ANOVA, $p < 0.05$.

3.5.6. Monocular and binocular stimuli

Sinusoidal grating stimuli were displayed on a monitor at locations determined by the population receptive field mapping associated with each electrode penetration (refer to Figure 13 for details on RF boundaries and sizes). Each experimental trial comprised three sequences; each sequence lasted for 250 milliseconds, interspersed with 300 milliseconds of rest. The gratings were shown either to the left or right eye (monocular stimulation) or to both eyes simultaneously (binocular stimulation). The stimuli's Michelson contrast levels varied (examples include 0, 0.055, 0.11, 0.225, 0.45, 0.90) throughout the trials. For binocular trials, contrast levels differed between the eyes (for example, 0.225 in the left eye and 0.45 in the right eye). Altogether, the experimental conditions included 36 different stimulus configurations, which involved monocular views, as well as balanced and unbalanced binocular views.

3.5.7. Signal processing and criteria for exclusion

Neurophysiological signals, except for local field potentials (LFPs), were processed post-recording using MATLAB (version 2021a) through tailored scripts. Multi-unit activity (MUA) was derived by applying a high-pass Butterworth filter (fourth-order, cutoff at 750 Hz) to the broadband signal, followed by signal rectification (Supèr & Roelfsema, 2005). A "multi-unit" refers to signals aggregated at a single micro-electrode contact per penetration. Data analysis was confined to cortical gray matter, excluding electrode array channels lacking significant MUA. Units in V1 showing negligible visual contrast tuning (assessed via repeated measures ANOVA across six contrast levels, $p < 0.05$) or those without adequate trials in each of the 36 conditions were omitted. MUA was aligned to stimulus onset, and baseline firing rates were subtracted for each trial. For comparative purposes, unit responses were normalized to the peak response observed across all conditions.

3.5.8. Analysis of contrast response functions

Contrast response functions were analyzed using a divisive normalization function modeled after the H-ratio sigmoid described by Naka and Rushton (1966). Using nonlinear least squares in MATLAB (version 2021a), we fitted the trial averaged V1 responses with the following:

$$R_{R_{max},C_{50},n,b}(c) = R_{max}\frac{c^n}{c^n + {C_{50}}^n} + b \ ,$$

Here, R_{max} is the maximal response, C_{50} the semi-saturation constant, n the scaling exponent, and c the stimulus contrast. The y-intercept b, representing ongoing activity, was set to the mean activity during no-stimulation trials for each neuron, with all parameters allowed to adjust within predefined bounds.

3.5.9. Computational models of binocular combination

We fit all V1 responses (to 36 different conditions) to binocular models built on a shared normalization framework which represent different ways for combining the two monocular contrast response functions: binocular linear summation and binocular normalization. Linear binocular summation simply adds the monocular contrast response functions linearly, without possibility for interocular interactions or any form of binocular gain-control:

$$R(c_L, c_R) = \frac{c_L^n}{c_L^n + c_{50}} + \frac{(w)c_R^n}{c_R^n + c_{50}}$$

This linear model has proven to be an unlikely candidate since V1 responses have been observed repeatedly as less than the sum of monocular components (Burns & Pritchard, 1968; Longordo et al., 2013; Moradi & Heeger, 2009; Zhao et al., 2013). We use it here as a point of reference and to enable a comparison to the binocular normalization model. The binocular normalization model allows the two eyes to interact before being summed, such that each eye's input exerts control over the strength of the other eyes' normalization (Moradi & Heeger, 2009):

$$R(c_L, c_R) = \frac{c_L^n + (w)c_R^n}{c_L^n + c_R^n + c_{50}}$$

We used MATLAB (2021a)'s fit() function to fit a each model to the binocular response matrix (6x6 trial-averaged (single contact) or mean (n = 584) responses) using the nonlinear least squares method with two independent variables (C_L, C_R). We additionally weighed each datapoint (i.e., condition) by the number of trials on a unit-by-unit basis. The fit procedure for the binocular response functions allowed each parameter ($R_{max,}$ C_{50}, n) to freely vary to achieve the best fit to the data. The additional term w is a weight placed on contrast in the unit's non-dominant eye. This weight took on a value of 1 (no effect) or that of each unit's fitted ocular dominance weight. Ocular dominance weight (w) was fitted for each unit to minimize the sum of square residuals between datapoints on the non-dominant eye curve and the dominant eye curve.

3.5.10. Simulating dynamic normalization

We employed the dynamic normalization model to simulate contrast responses of a subpopulation of simple and complex cells in V1 (Heeger et al., 2020). The model was structured to represent the orientation and spatial frequency preferences of V1 neurons through predefined receptive fields. Visual stimuli were characterized by contrast levels linearly spaced from low to high. We encoded these stimuli into neural signals using sinusoidal modulations that correspond to the receptive field characteristics of the neurons. Prior to normalization, inputs were temporally prefiltered to incorporate effects such as neural adaptation and response dynamics.

The core of this simulation, divisive normalization, was implemented to account for the competitive interactions among neurons. This was achieved by normalizing the neural input using a matrix that represented both excitatory and inhibitory interactions based on proximity and feature similarity. The output responses of the neurons were then calculated over a simulated time course, capturing key dynamics such as adaptation to stimulus intensity and temporal integration. Finally, responses were aggregated across the simulated neuron population to produce a collective output, which was plotted over time to visually represent the neuronal activity in response to each contrast level.

Conclusions

The investigations detailed in this dissertation contribute to our understanding of binocular vision processing within the primary visual cortex (V1) under various visual conditions. Chapter 1 explored the core differences between monocular to binocular stimulation, revealing that binocular responses in V1 are marked by sublinear summation and transient facilitation. These findings further elucidated the temporal dynamics of binocular integration over behaviorally relevant timescales. Additionally, we observed a transition in the contrast-response relationship from a simpler "response-gain" into more sophisticated stages of gain control. This underscores the adaptive processing capabilities of V1 in response to integrated visual inputs.

In Chapter 2, we delved into the significance of ocular dominance in binocular contrast combination. Our investigation revealed that ocular dominance shapes the formation of V1 binocular responses. We used this knowledge to then integrate ocular dominance as a scaling factor into neural models of binocular combination, which significantly enhanced the predictive accuracy of said models. This advancement underscores the importance of considering ocular dominance in the computational mechanisms of binocular integration, offering a more nuanced understanding of the role that ocular dominance plays in visual processing.

Finally, Chapter 3 focused on divisive normalization processes within the V1 laminar microcircuit. Our work identified variations in contrast sensitivity and dynamic range across different cortical layers. We then show how these normalization processes apply to binocular inputs, as well, through a process of binocular normalization. We contextualize binocular normalization within prevailing theories of neural dynamics and multi-input integration, suggesting a broader applicability of these models to encompass binocular processing. The insights gained from this investigation enrich our understanding of sensory processing in general, illustrating the ways in which canonical operations are orchestrated within canonical circuitry.

Collectively, these studies advance our comprehension of the complex mechanisms of binocular processing and establish a groundwork for future research aimed at refining models of sensory signal integration in the brain. This dissertation not only bridges significant gaps in current knowledge but also proposes new avenues for further exploration in the neuroscience community.

Specific aims addressed.

How does V1 excitation alter when input is doubled (i.e., monocular to binocular stimulation)? I showed that V1 binocular responses exhibited sublinear or partial binocular summation, as they constituted less than the arithmetic sum of responses from the left and right eyes. Simultaneously, V1 binocular spiking was notably higher than the response of the population to stimulation of the preferred eye alone, indicating binocular facilitation. This facilitation was transient, occurring at behaviorally relevant timescales, and consistent with previous findings in psychophysical performance when viewing through both eyes.

How does the contrast-response relationship in V1 change when input is doubled? We evaluated the contrast-response relationship in the context of simple forms of gain and gain-control. We found that the contrast-response relationship in V1 varied as a function of time when input is doubled. Binocular integration of matching inputs was

initially more contrast-independent, resembling a "response-gain" followed by a sustained, more complex stage of binocular gain-control.

Does cell-to-cell variability in ocular dominance matter for binocular contrast combination? We demonstrate that binocular combination of contrast in macaque V1 was modulated by ocular dominance, with contrast from the dominant eye contributing more to binocular response formation. Thus, while the traditional ocular dominance index derived from spike rates to monocular stimuli may not capture the complete strength of connections from each eye, it should be considered a useful parameter for understanding binocular processing in V1.

Can ocular dominance be used to improve computational models of binocular combination? We tested a variety of computational models of binocular combination in their ability to account for V1 spiking responses to binocular conditions. The performance (goodness of fit to the data) of all models was improved by adding ocular dominance as a scaling weight attached to contrast in the neurons' non-dominant eye. Overall, binocular normalization, a model that incorporates interocular interactions at a monocular stage, characterized V1 binocular responses better than linear summation, quadratic summation, or averaging contrast in the two eyes.

Does divisive normalization vary across V1 laminar compartments? Parameters of divisive normalization equation that control contrast sensitivity and dynamic range varied across laminar compartments. Contrast sensitivity was highest in the infragranular layers, where binocularity is the highest, whereas dynamic range was found to be the broadest (i.e., the most linear) in the granular input layers. The observed variation in the parameters of the divisive normalization equation across different laminar compartments suggests that divisive normalization processes are not uniformly applied throughout the visual cortex.

How does binocular normalization evolve as signals are fed through the canonical cortical microcircuit? Binocular normalization in the V1 laminar microcircuit evolves through the interplay of distinct response characteristics across cortical layers. Initial signals exhibit more linear summation in the granular layers, where direct sensory inputs are first processed. As these signals propagate to the supragranular and infragranular layers, which exhibit more complex interconnections and increased nonlinearity, binocular normalization becomes more pronounced, reflecting a dynamic modulation of response based on the integration of dual inputs and recurrent feedback.

Overall, our neurophysiology results support the psychophysically derived gain-control theory of binocular combination and its proposed neuronal implementation through mechanisms of divisive normalization which are possibly implemented biophysically through recurrent feedback connections. Continued efforts to understand the interplay between ocular dominance/binocularity, contrast gain-control, and binocular normalization across the V1 laminar microcircuit are likely to lead to more useful models for how the visual system integrates the two visual streams. Each of these refinements brings us closer to a complete understanding of the neural machinery that gives rise to cyclopean vision.

Avenues for future directions

Building upon the findings from this dissertation, several promising avenues for future research can be explored to deepen our understanding of visual processing mechanisms within V1 and potentially extend these insights to broader neural contexts. First is the exploration of the molecular and cellular underpinnings of the observed phenomena, particularly how specific neurotransmitters and neuromodulators influence the dynamics of binocular normalization. By employing optogenetic or chemogenetic tools to selectively activate or inhibit different neuron types or pathways, researchers could directly test the causal relationships between specific cellular activities and the overall binocular integration process. Such studies could provide a clearer picture of the underlying biological mechanisms that carry out canonical computations (i.e., divisive normalization) within circuit motifs (i.e., recurrent feedback) to enable binocular integration in V1.

Moreover, extending the computational models developed in this work to incorporate additional elements of neural circuitry, such as the roles of inhibitory interneurons and the effects of top-down feedback from higher cortical areas, could lead to more comprehensive models of early binocular processing in visual cortex. These enhanced models could be applied not only to basic neuroscience research but also to practical applications in artificial vision systems or in the development of therapeutic strategies for visual disorders.

Lastly, given the foundational role of V1 in visual perception, understanding how binocular normalization interacts with higher cognitive functions such as attention would be prudent, as normalization processes have been intimately tied to attentional states. Investigating the interaction between binocular processing and cognitive states could uncover new dimensions of how sensory information is integrated and utilized in complex behavioral contexts. Such research could pave the way for multi-disciplinary approaches that link perceptual, cognitive, and computational neuroscience, offering richer insights into the brain's ability to interpret and respond to its environment.

References

Adams, D. L., & Horton, J. C. (2003). Capricious expression of cortical columns in the primate brain. *Nature Neuroscience*, *6*(2), 113–114. https://doi.org/10.1038/nn1004

Adams, D. L., & Horton, J. C. (2006). Monocular Cells Without Ocular Dominance Columns. *Journal of Neurophysiology*, *96*(5), 2253–2264. https://doi.org/10.1152/jn.00131.2006

Adams, D. L., & Horton, J. C. (2009). Ocular Dominance Columns: Enigmas and Challenges. *The Neuroscientist*, *15*(1), 62–77. https://doi.org/10.1177/1073858408327806

Albrecht, D. G. (1995). Visual cortex neurons in monkey and cat: Effect of contrast on the spatial and temporal phase transfer functions. *Visual Neuroscience*, *12*(6), 1191–1210. https://doi.org/10.1017/s0952523800006817

Albrecht, D. G., & Geisler, W. S. (1991). Motion selectivity and the contrast-response function of simple cells in the visual cortex. *Visual Neuroscience*, *7*(6), 531–546. https://doi.org/10.1017/s0952523800010336

Albrecht, D. G., Geisler, W. S., Frazor, R. A., & Crane, A. M. (2002). Visual Cortex Neurons of Monkeys and Cats: Temporal Dynamics of the Contrast Response Function. *Journal of Neurophysiology*, *88*(2), 888–913. https://doi.org/10.1152/jn.2002.88.2.888

Albrecht, D. G., & Hamilton, D. B. (1982). Striate cortex of monkey and cat: contrast response function. *Journal of Neurophysiology*, *48*(1), 217–237. https://doi.org/10.1152/jn.1982.48.1.217

Anderson, P. A., & Movshon, J. A. (1989). Binocular combination of contrast signals. *Vision Research*, *29*(9), 1115–1132. https://doi.org/10.1016/0042-6989(89)90060-6

Anzai, A., Bearse, M. A., Freeman, R. D., & Cai, D. (1995). Contrast coding by cells in the cat's striate cortex: Monocular vs. binocular detection. *Visual Neuroscience*, *12*(1), 77–93. https://doi.org/10.1017/s0952523800007331

Anzai, A., Ohzawa, I., & Freeman, R. D. (1999). Neural Mechanisms for Processing Binocular Information I. Simple Cells. *Journal of Neurophysiology*, *82*(2), 891–908. https://doi.org/10.1152/jn.1999.82.2.891

Apkarian, P., Levi, D., & Tyle, C. W. (1981). Binocular Facilitation in the Visual-Evoked Potential of Strabismic Amblyopes. *Optometry and Vision Science*, *58*(10), 820–830. https://doi.org/10.1097/00006324-198110000-00007

Ates, K., Demirtas, S., & Goksoy, C. (2006). Binocular interactions in the guinea pig's visual-evoked potentials. *Brain Research*, *1125*(1), 26–30. https://doi.org/10.1016/j.brainres.2006.10.016

Bair, W., Cavanaugh, J. R., Smith, M. A., & Movshon, J. A. (2002). The Timing of Response Onset and Offset in Macaque Visual Neurons. *The Journal of Neuroscience*, *22*(8), 3189–3205. https://doi.org/10.1523/jneurosci.22-08-03189.2002

Baker, C. (2018). Promises and pitfalls of imaging the brain. *Nature*, *562*(7727), 340–342. https://doi.org/10.1038/d41586-018-07043-3

Baker, D. H., Lygo, F. A., Meese, T. S., & Georgeson, M. A. (2018). Binocular Summation Revisited: Beyond √2. *Psychological Bulletin*, *144*(11), 1186–1199. PubMed. https://doi.org/10.1037/bul0000163

Baker, D. H., Wallis, S. A., Georgeson, M. A., & Meese, T. S. (2012). Nonlinearities in the binocular combination of luminance and contrast. *Vision Research*, *56*, 1–9. https://doi.org/10.1016/j.visres.2012.01.008

Balaram, P., & Kaas, J. H. (2014). Towards a unified scheme of cortical lamination for primary visual cortex across primates: insights from NeuN and VGLUT2 immunoreactivity. *Frontiers in Neuroanatomy*, *8*, 81. https://doi.org/10.3389/fnana.2014.00081

Barbera, D., Priebe, N. J., & Glickfeld, L. L. (2022). Feedforward mechanisms of cross-orientation interactions in mouse V1. *Neuron*, *110*(2), 297-311.e4. https://doi.org/10.1016/j.neuron.2021.10.017

Barlow, H. B., Blakemore, C., & Pettigrew, J. D. (1967). The neural mechanism of binocular depth discrimination. *The Journal of Physiology*, *193*(2), 327–342. https://doi.org/10.1113/jphysiol.1967.sp008360

Barton, R. A. (2004). Binocularity and brain evolution in primates. *Proceedings of the National Academy of Sciences of the United States of America*, *101*(27), 10113–10115. https://doi.org/10.1073/pnas.0401955101

Bartos, M., Vida, I., & Jonas, P. (2007). Synaptic mechanisms of synchronized gamma oscillations in inhibitory interneuron networks. *Nature Reviews Neuroscience*, *8*(1), 45–56. https://doi.org/10.1038/nrn2044

Bastos, A. M., Vezoli, J., Bosman, C. A., Schoffelen, J.-M., Oostenveld, R., Dowdall, J. R., De Weerd, P., Kennedy, H., & Fries, P. (2015). Visual Areas Exert Feedforward and Feedback Influences through Distinct Frequency Channels. *Neuron*, *85*(2), 390–401. https://doi.org/10.1016/j.neuron.2014.12.018

Bearse, M. A., & Freeman, R. D. (1994). Binocular summation in orientation discrimination depends on stimulus contrast and duration. *Vision Research*, *34*(1), 19–29. https://doi.org/10.1016/0042-6989(94)90253-4

Birch, E. E. (2013). Amblyopia and binocular vision. *Progress in Retinal and Eye Research*, *33*, 67–84. https://doi.org/10.1016/j.preteyeres.2012.11.001

Bishop, G. H., & O'Leary, J. (1938). POTENTIAL RECORDS FROM THE OPTIC CORTEX OF THE CAT. *Journal of Neurophysiology*, *1*(5), 391–404. https://doi.org/10.1152/jn.1938.1.5.391

Bishop, P. O., & Pettigrew, J. D. (1986). Neural mechanisms of binocular vision. *Vision Research*, *26*(9), 1587–1600. https://doi.org/10.1016/0042-6989(86)90177-x

Blake, R. (1989). A Neural Theory of Binocular Rivalry. *Psychological Review*, *96*(1), 145–167. https://doi.org/10.1037/0033-295x.96.1.145

Blake, R., & Fox, R. (1973). The psychophysical inquiry into binocular summation. *Perception & Psychophysics*, *14*(1), 161–185. https://doi.org/10.3758/bf03198631

Blake, R., Sloane, M., & Fox, R. (1981). Further developments in binocular summation. *Perception & Psychophysics*, *30*(3), 266–276. https://doi.org/10.3758/bf03214282

Blake, R., & Wilson, H. (2011). Binocular vision. *Vision Research*, *51*(7), 754–770. https://doi.org/10.1016/j.visres.2010.10.009

Blakemore, C. (1970). Binocular depth perception and the optic chiasm. *Vision Research*, *10*(1), 43–47. https://doi.org/10.1016/0042-6989(70)90060-x

Blakemore, C., & Cooper, G. F. (1970). Development of the Brain depends on the Visual Environment. *Nature*, *228*(5270), 477–478. https://doi.org/10.1038/228477a0

Blasdel, G. G., & Lund, J. S. (1983). Termination of afferent axons in macaque striate cortex. *The Journal of Neuroscience : The Official Journal of the Society for Neuroscience*, *3*(7), 1389–1413.

Blasdel, G. G., Lund, J. S., & Fitzpatrick, D. (1985). Intrinsic connections of macaque striate cortex: axonal projections of cells outside lamina 4C. *The Journal of Neuroscience : The Official Journal of the Society for Neuroscience*, *5*(12), 3350–3369.

Bonds, A. B. (1991). Temporal dynamics of contrast gain in single cells of the cat striate cortex. *Visual Neuroscience*, *6*(3), 239–255. https://doi.org/10.1017/s0952523800006258

Boynton, G. M. (2005). Contrast Gain in the Brain. *Neuron*, *47*(4), 476–477. https://doi.org/10.1016/j.neuron.2005.08.003

Brouwer, G. J., & Heeger, D. J. (2009). Decoding and Reconstructing Color from Responses in Human Visual Cortex. *The Journal of Neuroscience*, *29*(44), 13992–14003. https://doi.org/10.1523/jneurosci.3577-09.2009

Brouwer, G. J., & Heeger, D. J. (2011). Cross-orientation suppression in human visual cortex. *Journal of Neurophysiology*, *106*(5), 2108–2119. https://doi.org/10.1152/jn.00540.2011

Burg, M. F., Cadena, S. A., Denfield, G. H., Walker, E. Y., Tolias, A. S., Bethge, M., & Ecker, A. S. (2021). Learning Divisive Normalization in Primary Visual Cortex. *BioRxiv*, 767285. https://doi.org/10.1101/767285

Burkhalter, A., & Essen, D. V. (1986). Processing of color, form and disparity information in visual areas VP and V2 of ventral extrastriate cortex in the macaque monkey. *The Journal of Neuroscience*, *6*(8), 2327–2351. https://doi.org/10.1523/jneurosci.06-08-02327.1986

Burns, B. D., & Pritchard, R. (1968). Cortical conditions for fused binocular vision. *The Journal of Physiology*, *197*(1), 149–171. https://doi.org/10.1113/jphysiol.1968.sp008552

Busse, L., Wade, A. R., & Carandini, M. (2009). Representation of Concurrent Stimuli by Population Activity in Visual Cortex. *Neuron*, *64*(6), 931–942. https://doi.org/10.1016/j.neuron.2009.11.004

Buzás, P., Eysel, U. T., Adorján, P., & Kisvárday, Z. F. (2001). Axonal topography of cortical basket cells in relation to orientation, direction, and ocular dominance maps. *Journal of Comparative Neurology*, *437*(3), 259–285. https://doi.org/10.1002/cne.1282

Cagenello, R., Halpern, D. L., & Arditi, A. (1993). Binocular enhancement of visual acuity. *Journal of the Optical Society of America A*, *10*(8), 1841. https://doi.org/10.1364/josaa.10.001841

Campbell, F. W., & Green, D. G. (1965). Monocular versus Binocular Visual Acuity. *Nature*, *208*(5006), 191–192. https://doi.org/10.1038/208191a0

Carandini, M., & Heeger, D. J. (2012). Normalization as a canonical neural computation. *Nature Reviews Neuroscience*, *13*(1), 51–62. https://doi.org/10.1038/nrn3136

Carandini, M., Heeger, D. J., & Movshon, J. A. (1997). Linearity and Normalization in Simple Cells of the Macaque Primary Visual Cortex. *The Journal of Neuroscience*, *17*(21), 8621–8644. https://doi.org/10.1523/jneurosci.17-21-08621.1997

Cardin, J. A., Carlén, M., Meletis, K., Knoblich, U., Zhang, F., Deisseroth, K., Tsai, L.-H., & Moore, C. I. (2009). Driving fast-spiking cells induces gamma rhythm and controls sensory responses. *Nature*, *459*(7247), 663–667. https://doi.org/10.1038/nature08002

Carlson, B. M., Mitchell, B. A., Dougherty, K., Westerberg, J. A., Cox, M. A., & Maier, A. (2023). Does V1 response suppression initiate binocular rivalry? *IScience*, *26*(8), 107359. https://doi.org/10.1016/j.isci.2023.107359

Casagrande, V. A., & Boyd, J. D. (1996). The neural architecture of binocular vision. *Eye*, *10*(2), 153–160. https://doi.org/10.1038/eye.1996.40

Casagrande, V. A., & Kaas, J. H. (1994). *Primary Visual Cortex in Primates*. 201–259. https://doi.org/10.1007/978-1-4757-9628-5_5

Chadnova, E., Reynaud, A., Clavagnier, S., Baker, D. H., Baillet, S., & Hess, R. F. (2018). Interocular interaction of contrast and luminance signals in human primary visual cortex. *NeuroImage*, *167*, 23–30. https://doi.org/10.1016/j.neuroimage.2017.10.035

Chao-yi, L., & Creutzfeldt, O. (1984). The representation of contrast and other stimulus parameters by single neurons in area 17 of the cat. *Pflügers Archiv*, *401*(3), 304–314. https://doi.org/10.1007/bf00582601

Chapman, B., Jacobson, M. D., Reiter, H. O., & Stryker, M. P. (1986). Ocular dominance shift in kitten visual cortex caused by imbalance in retinal electrical activity. *Nature*, *324*(6093), 154–156. https://doi.org/10.1038/324154a0

Clatworthy, P. L., Chirimuuta, M., Lauritzen, J. S., & Tolhurst, D. J. (2003). Coding of the contrasts in natural images by populations of neurons in primary visual cortex (V1). *Vision Research*, *43*(18), 1983–2001. https://doi.org/10.1016/s0042-6989(03)00277-3

Cogan, A. I., Silverman, G., & Sekuler, R. (1982). Binocular summation in detection of contrast flashes. *Perception & Psychophysics*, *31*(4), 330–338. https://doi.org/10.3758/bf03202656

Cox, M. A., Dougherty, K., Westerberg, J. A., Schall, M. S., & Maier, A. (2019). Temporal dynamics of binocular integration in primary visual cortex. *Journal of Vision*, *19*(12), 13. https://doi.org/10.1167/19.12.13

Cox, M. A., Schmid, M. C., Peters, A. J., Saunders, R. C., Leopold, D. A., & Maier, A. (2013). Receptive field focus of visual area V4 neurons determines responses to illusory surfaces. *Proceedings of the National Academy of Sciences*, *110*(42), 17095–17100. https://doi.org/10.1073/pnas.1310806110

Cumming, B. G., & DeAngelis, G. C. (2001). THE PHYSIOLOGY OF STEREOPSIS. *Neuroscience*, *24*(1), 203–238. https://doi.org/10.1146/annurev.neuro.24.1.203

Dean, I., Harper, N. S., & McAlpine, D. (2005). Neural population coding of sound level adapts to stimulus statistics. *Nature Neuroscience*, *8*(12), 1684–1689. https://doi.org/10.1038/nn1541

DeAngelis, G. C., & Newsome, W. T. (1999). Organization of Disparity-Selective Neurons in Macaque Area MT. *The Journal of Neuroscience*, *19*(4), 1398–1415. https://doi.org/10.1523/jneurosci.19-04-01398.1999

Ding, J., Klein, S. A., & Levi, D. M. (2013a). Binocular combination in abnormal binocular vision. *Journal of Vision*, *13*(2), 14. https://doi.org/10.1167/13.2.14

Ding, J., Klein, S. A., & Levi, D. M. (2013b). Binocular combination of phase and contrast explained by a gain-control and gain-enhancement model. *Journal of Vision*, *13*(2), 13. https://doi.org/10.1167/13.2.13

Ding, J., & Levi, D. M. (2017). Binocular combination of luminance profiles. *Journal of Vision*, *17*(13), 4. https://doi.org/10.1167/17.13.4

Ding, J., & Levi, D. M. (2021). A unified model for binocular fusion and depth perception. *Vision Research*, *180*, 11–36. https://doi.org/10.1016/j.visres.2020.11.009

Ding, J., & Sperling, G. (2006). A gain-control theory of binocular combination. *Proceedings of the National Academy of Sciences of the United States of America*, *103*(4), 1141–1146. https://doi.org/10.1073/pnas.0509629103

Dougherty, K., Carlson, B. M., Cox, M. A., Westerberg, J. A., Zinke, W., Schmid, M. C., Martin, P. R., & Maier, A. (2021). Binocular Suppression in the Macaque Lateral Geniculate Nucleus Reveals Early Competitive Interactions between the Eyes. *ENeuro*, *8*(2), ENEURO.0364-20.2020. https://doi.org/10.1523/eneuro.0364-20.2020

Dougherty, K., Cox, M. A., Westerberg, J. A., & Maier, A. (2019). Binocular Modulation of Monocular V1 Neurons. *Current Biology*, *29*(3), 381-391.e4. https://doi.org/10.1016/j.cub.2018.12.004

Dougherty, K., Schmid, M. C., & Maier, A. (2019). Binocular response modulation in the lateral geniculate nucleus. *Journal of Comparative Neurology*, *527*(3), 522–534. https://doi.org/10.1002/cne.24417

Douglas, R. J., & Martin, K. A. C. (2004). NEURONAL CIRCUITS OF THE NEOCORTEX. *Neuroscience*, *27*(1), 419–451. https://doi.org/10.1146/annurev.neuro.27.070203.144152

Felleman, D. J., & Essen, D. C. V. (1991). Distributed Hierarchical Processing in the Primate Cerebral Cortex. *Cerebral Cortex*, *1*(1), 1–47. https://doi.org/10.1093/cercor/1.1.1-a

Ferster, D. (1981). A comparison of binocular depth mechanisms in areas 17 and 18 of the cat visual cortex. *The Journal of Physiology*, *311*(1), 623–655. https://doi.org/10.1113/jphysiol.1981.sp013608

Fitzpatrick, D., Lund, J. S., Schmechel, D. E., & Towles, A. C. (1987). Distribution of GABAergic neurons and axon terminals in the macaque striate cortex. *Journal of Comparative Neurology*, *264*(1), 73–91. https://doi.org/10.1002/cne.902640107

Fleet, D. J., Heeger, D. J., & Wagner, H. (1997). *Modelling Binocular Neurons in the Primary Visual Cortex*. 103–130.

Fleet, D. J., Wagner, H., & Heeger, D. J. (1996). Neural encoding of binocular disparity: Energy models, position shifts and phase shifts. *Vision Research*, *36*(12), 1839–1857. https://doi.org/10.1016/0042-6989(95)00313-4

Fonta, C., Chapert, C., & Imbert, M. (2000). Effect of monocular deprivation on NMDAR1 immunostaining in ocular dominance columns of the marmoset Callithrix jacchus. *Visual Neuroscience*, *17*(3), 345–352. https://doi.org/10.1017/s0952523800173031

Freeman, R. D., & Ohzawa, I. (1990). On the neurophysiological organization of binocular vision. *Vision Research*, *30*(11), 1661–1676. https://doi.org/10.1016/0042-6989(90)90151-a

Gardner, J. C., & Raiten, E. J. (1986). Ocular dominance and disparity-sensitivity: why there are cells in the visual cortex driven unequally by the two eyes. *Experimental Brain Research*, *64*(3), 505–514. https://doi.org/10.1007/bf00340488

Georgeson, M. A., & Sengpiel, F. (2021). Contrast adaptation and interocular transfer in cortical cells: A re-analysis & a two-stage gain-control model of binocular combination. *Vision Research*, *185*, 29–49. https://doi.org/10.1016/j.visres.2021.03.004

Georgeson, M., Meese, T., & Baker, D. (2007). Binocular interaction: contrast matching and contrast discrimination are predicted by the same model. *Spatial Vision*, *20*(5), 397–413. https://doi.org/10.1163/156856807781503622

Ghose, G. M., & Ts'O, D. Y. (1997). Form Processing Modules in Primate Area V4. *Journal of Neurophysiology*, *77*(4), 2191–2196. https://doi.org/10.1152/jn.1997.77.4.2191

Gilbert, C. D., & Li, W. (2013). Top-down influences on visual processing. *Nature Reviews Neuroscience*, *14*(5), 350–363. https://doi.org/10.1038/nrn3476

Giuseppe, N., & Andrea, F. (1983). Binocular Interaction in Visual-Evoked Responses: Summation, Facilitation and Inhibition in a Clinical Study of Binocular Vision. *Ophthalmic Research*, *15*(5), 261–264. https://doi.org/10.1159/000265268

Godlove, D. C., Maier, A., Woodman, G. F., & Schall, J. D. (2014). Microcircuitry of Agranular Frontal Cortex: Testing the Generality of the Canonical Cortical Microcircuit. *Journal of Neuroscience*, *34*(15), 5355–5369. https://doi.org/10.1523/jneurosci.5127-13.2014

Gordon, J. A., & Stryker, M. P. (1996). Experience-Dependent Plasticity of Binocular Responses in the Primary Visual Cortex of the Mouse. *The Journal of Neuroscience*, *16*(10), 3274–3286. https://doi.org/10.1523/jneurosci.16-10-03274.1996

Grünau, M. V. (1979). Binocular summation and the binocularity of cat visual cortex. *Vision Research*, *19*(7), 813–816. https://doi.org/10.1016/0042-6989(79)90158-5

Grünau, M. W. von, & Singer, W. (1979). The role of binocular neurons in the cat striate cortex in combining information from the two eyes. *Experimental Brain Research*, *34*(1), 133–142. https://doi.org/10.1007/bf00238346

Haden, H. C. (1936). A Study of the Changes in the Optic Discs, Visual Fields, and Vision Following Bisection of the Optic Chiasm. *Transactions of the American Ophthalmological Society*, *34*, 208–216.

Haefner, R. M., & Cumming, B. G. (2008). Adaptation to Natural Binocular Disparities in Primate V1 Explained by a Generalized Energy Model. *Neuron*, *57*(1), 147–158. https://doi.org/10.1016/j.neuron.2007.10.042

Harter, M. R., Seiple, W. H., & Salmon, L. (1973). Binocular summation of visually evoked responses to pattern stimuli in humans. *Vision Research*, *13*(8), 1433–1446. https://doi.org/10.1016/0042-6989(73)90004-7

Hartline, H. K. (1948). Retinal action potentials of photoreceptor cells and the discharge of nerve impulses in their axones. *The American Journal of the Medical Sciences*, *215*(6), 714.

Haseltine, E. C., DeBruyn, E. J., & Casagrande, V. A. (1979). Demonstration of ocular dominance columns in Nissl-stained sections of monkey visual cortex following enucleation. *Brain Research*, *176*(1), 153–158. https://doi.org/10.1016/0006-8993(79)90878-3

Hawken, M. J., & Parker, A. J. (1984). Contrast sensitivity and orientation selectivity in lamina IV of the striate cortex of Old World monkeys. *Experimental Brain Research*, *54*(2), 367–372. https://doi.org/10.1007/bf00236238

Heeger, D. J. (1992a). Half-squaring in responses of cat striate cells. *Visual Neuroscience*, *9*(5), 427–443. https://doi.org/10.1017/s095252380001124x

Heeger, D. J. (1992b). Normalization of cell responses in cat striate cortex. *Visual Neuroscience*, *9*(2), 181–197. https://doi.org/10.1017/s0952523800009640

Heeger, D. J., & Mackey, W. E. (2019). Oscillatory recurrent gated neural integrator circuits (ORGaNICs), a unifying theoretical framework for neural dynamics. *Proceedings of the National Academy of Sciences*, *116*(45), 22783–22794. https://doi.org/10.1073/pnas.1911633116

Heeger, D. J., & Zemlianova, K. O. (2020). A recurrent circuit implements normalization, simulating the dynamics of V1 activity. *Proceedings of the National Academy of Sciences*, *117*(36), 22494–22505. https://doi.org/10.1073/pnas.2005417117

Hendrickson, A. E., & Wilson, J. R. (1979). A difference in [14C]deoxyglucose autoradiographic patterns in striate cortex between Macaca and Saimiri monkeys following monocular stimulation. *Brain Research*, *170*(2), 353–358. https://doi.org/10.1016/0006-8993(79)90113-6

Hendrickson, A. E., Wilson, J. R., & Ogren, M. P. (1978). The neuroanatomical organization of pathways between the dorsal lateral geniculate nucleus and visual cortex in Old World and New World primates. *The Journal of Comparative Neurology*, *182*(1), 123–136.

Henriksen, S., Tanabe, S., & Cumming, B. (2016). Disparity processing in primary visual cortex. *Philosophical Transactions of the Royal Society B: Biological Sciences*, *371*(1697), 20150255. https://doi.org/10.1098/rstb.2015.0255

Heravian, J. S., Jenkins, T. C. A., & Douthwaite, W. A. (1990). Binocular summation in visually evoked responses and visual acuity. *Ophthalmic and Physiological Optics*, *10*(3), 257–261. https://doi.org/10.1111/j.1475-1313.1990.tb00861.x

Hermes, D., Miller, K. J., Wandell, B. A., & Winawer, J. (2015). Stimulus Dependence of Gamma Oscillations in Human Visual Cortex. *Cerebral Cortex*, *25*(9), 2951–2959. https://doi.org/10.1093/cercor/bhu091

Hess, R. F., & Thompson, B. (2015). Amblyopia and the binocular approach to its therapy. *Vision Research*, *114*, 4–16. https://doi.org/10.1016/j.visres.2015.02.009

Hess, R. F., Thompson, B., & Baker, D. H. (2014). Binocular vision in amblyopia: structure, suppression and plasticity. *Ophthalmic and Physiological Optics*, *34*(2), 146–162. https://doi.org/10.1111/opo.12123

Heuer, H. W., & Britten, K. H. (2002). Contrast Dependence of Response Normalization in Area MT of the Rhesus Macaque. *Journal of Neurophysiology*, *88*(6), 3398–3408. https://doi.org/10.1152/jn.00255.2002

Hitchcock, P. F., & Hickey, T. L. (1980). Ocular dominance columns: evidence for their presence in humans. *Brain Research*, *182*(1), 176–179. https://doi.org/10.1016/0006-8993(80)90841-0

Holt, C. J., Miller, K. D., & Ahmadian, Y. (2023). The stabilized supralinear network accounts for the contrast dependence of visual cortical gamma oscillations. *BioRxiv*, 2023.05.11.540442. https://doi.org/10.1101/2023.05.11.540442

Home, R. (1978). Binocular summation: A study of contrast sensitivity, visual acuity and recognition. *Vision Research*, *18*(5), 579–585. https://doi.org/10.1016/0042-6989(78)90206-7

Horton, J. C. (2006). Ocular integration in the human visual cortex. *Canadian Journal of Ophthalmology / Journal Canadien d'Ophtalmologie*, *41*(5), 584–593. https://doi.org/10.1016/s0008-4182(06)80027-x

Horton, J. C., & Adams, D. L. (2005). The cortical column: a structure without a function. *Philosophical Transactions of the Royal Society B: Biological Sciences*, *360*(1456), 837–862. https://doi.org/10.1098/rstb.2005.1623

Horton, J., & Hocking, D. (1996a). Anatomical Demonstration of Ocular Dominance Columns in Striate Cortex of the Squirrel Monkey. *The Journal of Neuroscience*, *16*(17), 5510–5522. https://doi.org/10.1523/jneurosci.16-17-05510.1996

Horton, J., & Hocking, D. (1996b). Intrinsic Variability of Ocular Dominance Column Periodicity in Normal Macaque Monkeys. *The Journal of Neuroscience*, *16*(22), 7228–7339. https://doi.org/10.1523/jneurosci.16-22-07228.1996

Hou, C., Nicholas, S. C., & Verghese, P. (2020). Contrast Normalization Accounts for Binocular Interactions in Human Striate and Extra-striate Visual Cortex. *The Journal of Neuroscience*, *40*(13), 2753–2763. https://doi.org/10.1523/jneurosci.2043-19.2020

Howarth, M., Walmsley, L., & Brown, T. M. (2014). Binocular Integration in the Mouse Lateral Geniculate Nuclei. *Current Biology*, *24*(11), 1241–1247. https://doi.org/10.1016/j.cub.2014.04.014

Huang, C.-B., Zhou, J., Lu, Z.-L., & Zhou, Y. (2011). Deficient binocular combination reveals mechanisms of anisometropic amblyopia: Signal attenuation and interocular inhibition. *Journal of Vision*, *11*(6), 4–4. https://doi.org/10.1167/11.6.4

Huang, C.-B., Zhou, J., Zhou, Y., & Lu, Z.-L. (2010). Contrast and Phase Combination in Binocular Vision. *PLoS ONE*, *5*(12), e15075. https://doi.org/10.1371/journal.pone.0015075

Hubel, D. H., LeVay, S., & Wiesel, T. N. (1975). Mode of termination of retinotectal fibers in macaque monkey: An autoradiographic study. *Brain Research*, *96*(1), 25–40. https://doi.org/10.1016/0006-8993(75)90567-3

Hubel, D. H., & Wiesel, T. N. (1959). Receptive fields of single neurones in the cat's striate cortex. *The Journal of Physiology*, *148*(3), 574–591. https://doi.org/10.1113/jphysiol.1959.sp006308

Hubel, D. H., & Wiesel, T. N. (1962). Receptive fields, binocular interaction and functional architecture in the cat's visual cortex. *The Journal of Physiology*, *160*(1), 106–154. https://doi.org/10.1113/jphysiol.1962.sp006837

Hubel, D. H., & Wiesel, T. N. (1968). Receptive fields and functional architecture of monkey striate cortex. *The Journal of Physiology*, *195*(1), 215–243. https://doi.org/10.1113/jphysiol.1968.sp008455

Hubel, D. H., & Wiesel, T. N. (1969). Anatomical Demonstration of Columns in the Monkey Striate Cortex. *Nature*, *221*(5182), 747–750. https://doi.org/10.1038/221747a0

Hubel, D. H., & Wiesel, T. N. (1972). Laminar and columnar distribution of geniculo-cortical fibers in the macaque monkey. *Journal of Comparative Neurology*, *146*(4), 421–450. https://doi.org/10.1002/cne.901460402

Hubel, D. H., Wiesel, T. N., & LeVay, S. (1976). Functional Architecture of Area 17 in Normal and Monocularly Deprived Macaque Monkeys. *Cold Spring Harbor Symposia on Quantitative Biology*, *40*(0), 581–589. https://doi.org/10.1101/sqb.1976.040.01.054

Hubel, D. H., Wiesel, T. N., LeVay, S., Barlow, H. B., & Gaze, R. M. (1977). Plasticity of ocular dominance columns in monkey striate cortex. *Philosophical Transactions of the Royal Society of London. B, Biological Sciences*, *278*(961), 377–409. https://doi.org/10.1098/rstb.1977.0050

Hubel, D., & Livingstone, M. (1987). Segregation of form, color, and stereopsis in primate area 18. *The Journal of Neuroscience*, *7*(11), 3378–3415. https://doi.org/10.1523/jneurosci.07-11-03378.1987

Humphrey, A. L., Albano, J. E., & Norton, T. T. (1977). Organization of ocular dominance in tree shrew striate cortex. *Brain Research*, *134*(2), 225–236. https://doi.org/10.1016/0006-8993(77)91069-1

Hupé, J. M., James, A. C., Payne, B. R., Lomber, S. G., Girard, P., & Bullier, J. (1998). Cortical feedback improves discrimination between figure and background by V1, V2 and V3 neurons. *Nature*, *394*(6695), 784–787. https://doi.org/10.1038/29537

Johnson, R. R., & Burkhalter, A. (1996). Microcircuitry of forward and feedback connections within rat visual cortex. *Journal of Comparative Neurology*, *368*(3), 383–398. https://doi.org/10.1002/(sici)1096-9861(19960506)368:3<;383::aid-cne5>3.0.co;2-1

Jones, R. K., & Lee, D. N. (1981). Why two eyes are better than one: The two views of binocular vision. *Journal of Experimental Psychology: Human Perception and Performance*, *7*(1), 30–40. https://doi.org/10.1037/0096-1523.7.1.30

Kaas, J. H. (2015). Principles of Organization of the Dorsal Lateral Geniculate Nucleus. *Brain, Behavior and Evolution*, *85*(3), 137–138. https://doi.org/10.1159/000382030

Kaas, J. H., Huerta, M. F., Weber, J. T., & Harting, J. K. (1978). Patterns of retinal terminations and laminar organization of the lateral geniculate nucleus of primates. *Journal of Comparative Neurology*, *182*(3), 517–553. https://doi.org/10.1002/cne.901820308

Katz, L. C., & Crowley, J. C. (2002). Development of cortical circuits: Lessons from ocular dominance columns. *Nature Reviews Neuroscience*, *3*(1), 34–42. https://doi.org/10.1038/nrn703

Kay, K. N., Naselaris, T., Prenger, R. J., & Gallant, J. L. (2008). Identifying natural images from human brain activity. *Nature*, *452*(7185), 352–355. https://doi.org/10.1038/nature06713

Kay, K. N., Winawer, J., Rokem, A., Mezer, A., & Wandell, B. A. (2013). A Two-Stage Cascade Model of BOLD Responses in Human Visual Cortex. *PLoS Computational Biology*, *9*(5), e1003079. https://doi.org/10.1371/journal.pcbi.1003079

Kennedy, C., Rosiers, M. H. D., Sakurada, O., Shinohara, M., Reivich, M., Jehle, J. W., & Sokoloff, L. (1976). Metabolic mapping of the primary visual system of the monkey by means of the

autoradiographic [14C]deoxyglucose technique. *Proceedings of the National Academy of Sciences of the United States of America*, *73*(11), 4230–4234. https://doi.org/10.1073/pnas.73.11.4230

Kohn, A., & Whitsel, B. L. (2002). Sensory cortical dynamics. *Behavioural Brain Research*, *135*(1–2), 119–126. https://doi.org/10.1016/s0166-4328(02)00139-0

Kondo, S., & Ohki, K. (2016). Laminar differences in the orientation selectivity of geniculate afferents in mouse primary visual cortex. *Nature Neuroscience*, *19*(2), 316–319. https://doi.org/10.1038/nn.4215

Krnjević, K., Randić, M., & Straughan, D. W. (1966). Nature of a cortical inhibitory process. *The Journal of Physiology*, *184*(1), 49–77. https://doi.org/10.1113/jphysiol.1966.sp007903

Kuffler, S. W. (1953). DISCHARGE PATTERNS AND FUNCTIONAL ORGANIZATION OF MAMMALIAN RETINA. *Journal of Neurophysiology*, *16*(1), 37–68. https://doi.org/10.1152/jn.1953.16.1.37

Ledgeway, T., Zhan, C. Z. C., Johnson, A. P., Song, Y., & Baker, C. L. (2005). The direction-selective contrast response of area 18 neurons is different for first- and second-order motion. *Visual Neuroscience*, *22*(1), 87–99. https://doi.org/10.1017/s0952523805221120

Lee, J., & Maunsell, J. H. R. (2009). A Normalization Model of Attentional Modulation of Single Unit Responses. *PLoS ONE*, *4*(2), e4651. https://doi.org/10.1371/journal.pone.0004651

Legge, G. E. (1984a). Binocular contrast summation—I. Detection and discrimination. *Vision Research*, *24*(4), 373–383. https://doi.org/10.1016/0042-6989(84)90063-4

Legge, G. E. (1984b). Binocular contrast summation—II. Quadratic summation. *Vision Research*, *24*(4), 385–394. https://doi.org/10.1016/0042-6989(84)90064-6

Lehky, S. R., & Maunsell, J. H. R. (1996). No binocular rivalry in the LGN of alert macaque monkeys. *Vision Research*, *36*(9), 1225–1234. https://doi.org/10.1016/0042-6989(95)00232-4

LeVay, S., Connolly, M., Houde, J., & Essen, D. V. (1985). The complete pattern of ocular dominance stripes in the striate cortex and visual field of the macaque monkey. *The Journal of Neuroscience*, *5*(2), 486–501. https://doi.org/10.1523/jneurosci.05-02-00486.1985

LeVay, S., Hubel, D. H., & Wiesel, T. N. (1975). The pattern of ocular dominance columns in macaque visual cortex revealed by a reduced silver stain. *Journal of Comparative Neurology*, *159*(4), 559–575. https://doi.org/10.1002/cne.901590408

LeVay, S., & Voigt, T. (1988). Ocular dominance and disparity coding in cat visual cortex. *Visual Neuroscience*, *1*(4), 395–414. https://doi.org/10.1017/s0952523800004168

LeVay, S., Wiesel, T. N., & Hubel, D. H. (1980). The development of ocular dominance columns in normal and visually deprived monkeys. *Journal of Comparative Neurology*, *191*(1), 1–51. https://doi.org/10.1002/cne.901910102

Levelt. (1965). *On binocular rivalry.* Inst. Perception Rvo-Tno.

Ling, S., & Blake, R. (2012). Normalization Regulates Competition for Visual Awareness. *Neuron*, *75*(3), 531–540. https://doi.org/10.1016/j.neuron.2012.05.032

Ling, S., & Carrasco, M. (2006). Sustained and transient covert attention enhance the signal via different contrast response functions. *Vision Research*, *46*(8–9), 1210–1220. https://doi.org/10.1016/j.visres.2005.05.008

Liu, L., & Schor, C. M. (1995). Binocular combination of contrast signals from orthogonal orientation channels. *Vision Research*, *35*(18), 2559–2567. https://doi.org/10.1016/0042-6989(95)00009-o

Livingstone, M., & Hubel, D. (1984). Specificity of intrinsic connections in primate primary visual cortex. *The Journal of Neuroscience*, *4*(11), 2830–2835. https://doi.org/10.1523/jneurosci.04-11-02830.1984

Livingstone, M. S., & Tsao, D. Y. (1999). Receptive fields of disparity-selective neurons in macaque striate cortex. *Nature Neuroscience*, *2*(9), 825–832. https://doi.org/10.1038/12199

Logothetis, N. K., Kayser, C., & Oeltermann, A. (2007). In Vivo Measurement of Cortical Impedance Spectrum in Monkeys: Implications for Signal Propagation. *Neuron*, *55*(5), 809–823. https://doi.org/10.1016/j.neuron.2007.07.027

Longordo, F., To, M.-S., Ikeda, K., & Stuart, G. J. (2013). Sublinear integration underlies binocular processing in primary visual cortex. *Nature Neuroscience*, *16*(6), 714–723. https://doi.org/10.1038/nn.3394

Louie, K., & Glimcher, P. W. (2019). *Oxford Research Encyclopedia of Neuroscience*. https://doi.org/10.1093/acrefore/9780190264086.013.43

Louie, K., Grattan, L. E., & Glimcher, P. W. (2011). Reward Value-Based Gain Control: Divisive Normalization in Parietal Cortex. *The Journal of Neuroscience*, *31*(29), 10627–10639. https://doi.org/10.1523/jneurosci.1237-11.2011

MacEvoy, S. P., Tucker, T. R., & Fitzpatrick, D. (2009). A precise form of divisive suppression supports population coding in the primary visual cortex. *Nature Neuroscience*, *12*(5), 637–645. https://doi.org/10.1038/nn.2310

Maier, A., Adams, G. K., Aura, C., & Leopold, D. A. (2010). Distinct Superficial and Deep Laminar Domains of Activity in the Visual Cortex during Rest and Stimulation. *Frontiers in Systems Neuroscience*, *4*, 31. https://doi.org/10.3389/fnsys.2010.00031

Maier, A., Aura, C. J., & Leopold, D. A. (2011). Infragranular sources of sustained local field potential responses in macaque primary visual cortex. *The Journal of Neuroscience : The Official Journal of the Society for Neuroscience*, *31*(6), 1971–1980. https://doi.org/10.1523/jneurosci.5300-09.2011

Maier, A., Cox, M. A., Westerberg, J. A., & Dougherty, K. (2022). Binocular Integration in the Primate Primary Visual Cortex. *Annual Review of Vision Science*, *8*(1), 345–360. https://doi.org/10.1146/annurev-vision-100720-112922

Maier, A., Wilke, M., Aura, C., Zhu, C., Ye, F. Q., & Leopold, D. A. (2008). Divergence of fMRI and neural signals in V1 during perceptual suppression in the awake monkey. *Nature Neuroscience*, *11*(10), 1193–1200. https://doi.org/10.1038/nn.2173

Mao, Y., Min, S. H., Chen, S., Gong, L., Chen, H., Hess, R. F., & Zhou, J. (2020). Binocular Imbalance in Amblyopia Depends on Spatial Frequency in Binocular Combination. *Investigative Ophthalmology & Visual Science*, *61*(8), 7. https://doi.org/10.1167/iovs.61.8.7

Martínez-Trujillo, J. C., & Treue, S. (2002). Attentional Modulation Strength in Cortical Area MT Depends on Stimulus Contrast. *Neuron*, *35*(2), 365–370. https://doi.org/10.1016/s0896-6273(02)00778-x

Matin, L. (1962). Binocular Summation at the Absolute Threshold of Peripheral Vision*. *Journal of the Optical Society of America*, *52*(11), 1276. https://doi.org/10.1364/josa.52.001276

Maunsell, J. H., & Essen, D. C. V. (1983). Functional properties of neurons in middle temporal visual area of the macaque monkey. II. Binocular interactions and sensitivity to binocular disparity. *Journal of Neurophysiology*, *49*(5), 1148–1167. https://doi.org/10.1152/jn.1983.49.5.1148

McConnell, S. K., & LeVay, S. (1986). Anatomical organization of the visual system of the mink, Mustela vison. *Journal of Comparative Neurology*, *250*(1), 109–132. https://doi.org/10.1002/cne.902500110

Meese, T. S., Georgeson, M. A., & Baker, D. H. (2006). Binocular contrast vision at and above threshold. *Journal of Vision*, *6*(11), 7–7. https://doi.org/10.1167/6.11.7

Mendoza-Halliday, D., Major, A. J., Lee, N., Lichtenfeld, M. J., Carlson, B., Mitchell, B., Meng, P. D., Xiong, Y. (Sophy), Westerberg, J. A., Jia, X., Johnston, K. D., Selvanayagam, J., Everling, S., Maier, A., Desimone, R., Miller, E. K., & Bastos, A. M. (2024). A ubiquitous spectrolaminar motif of local field potential power across the primate cortex. *Nature Neuroscience*, *27*(3), 547–560. https://doi.org/10.1038/s41593-023-01554-7

Mitchell, B. A., Carlson, B. M., Westerberg, J. A., Cox, M. A., & Maier, A. (2023). A role for ocular dominance in binocular integration. *Current Biology*, *33*(18), 3884-3895.e5. https://doi.org/10.1016/j.cub.2023.08.019

Mitchell, B. A., Dougherty, K., Westerberg, J. A., Carlson, B. M., Daumail, L., Maier, A., & Cox, M. A. (2022). Stimulating both eyes with matching stimuli enhances V1 responses. *IScience*, *25*(5), 104182. https://doi.org/10.1016/j.isci.2022.104182

Mitzdorf, U. (1985). Current source-density method and application in cat cerebral cortex: investigation of evoked potentials and EEG phenomena. *Physiological Reviews*, *65*(1), 37–100. https://doi.org/10.1152/physrev.1985.65.1.37

Moradi, F., & Heeger, D. J. (2009). Inter-ocular contrast normalization in human visual cortex. *Journal of Vision*, *9*(3), 13–13. https://doi.org/10.1167/9.3.13

Naka, K. I., & Rushton, W. A. H. (1966). S-potentials from luminosity units in the retina of fish (Cyprinidae). *The Journal of Physiology*, *185*(3), 587–599. https://doi.org/10.1113/jphysiol.1966.sp008003

Nassi, J. J., Gómez-Laberge, C., Kreiman, G., & Born, R. T. (2014). Corticocortical feedback increases the spatial extent of normalization. *Frontiers in Systems Neuroscience*, *8*, 105. https://doi.org/10.3389/fnsys.2014.00105

Ng, C. J., & Purves, D. (2019). An Alternative Theory of Binocularity. *Frontiers in Computational Neuroscience*, *13*, 71. https://doi.org/10.3389/fncom.2019.00071

Nicholson, C., & Freeman, J. A. (1975). Theory of current source-density analysis and determination of conductivity tensor for anuran cerebellum. *Journal of Neurophysiology*, *38*(2), 356–368. https://doi.org/10.1152/jn.1975.38.2.356

Nikara, T. (1972). Neurophysiology of stereopsis; binocular vision of single units in the cat's striate cortex. *Iyodenshi To Seitai Kogaku*, *10*(2), 80–87. https://doi.org/10.11239/jsmbe1963.10.80

Nityananda, V., & Read, J. C. A. (2017). Stereopsis in animals: evolution, function and mechanisms. *The Journal of Experimental Biology*, *220*(14), 2502–2512. https://doi.org/10.1242/jeb.143883

Obeid, D., & Miller, K. D. (2021). Stabilized Supralinear Network: Model of Layer 2/3 of the Primary Visual Cortex. *BioRxiv*, 2020.12.30.424892. https://doi.org/10.1101/2020.12.30.424892

Ohshiro, T., Angelaki, D. E., & DeAngelis, G. C. (2011). A Normalization Model of Multisensory Integration. *Nature Neuroscience*, *14*(6), 775–782. https://doi.org/10.1038/nn.2815

Ohzawa, I., Deangelis, G. C., & Freeman, R. D. (1997). Encoding of Binocular Disparity by Complex Cells in the Cat's Visual Cortex. *Journal of Neurophysiology*, *77*(6), 2879–2909. https://doi.org/10.1152/jn.1997.77.6.2879

Ohzawa, I., & Freeman, R. D. (1986). The binocular organization of simple cells in the cat's visual cortex. *Journal of Neurophysiology*, *56*(1), 221–242. https://doi.org/10.1152/jn.1986.56.1.221

Ohzawa, I., Sclar, G., & Freeman, R. D. (1985). Contrast gain control in the cat's visual system. *Journal of Neurophysiology*, *54*(3), 651–667. https://doi.org/10.1152/jn.1985.54.3.651

O'Leary, J. L. (1940). A structural analysis of the lateral geniculate nucleus of the cat. *Journal of Comparative Neurology*, *73*(3), 405–430. https://doi.org/10.1002/cne.900730304

O'Leary, J. L. (1941). Structure of the area striata of the cat. *Journal of Comparative Neurology*, *75*(1), 131–164. https://doi.org/10.1002/cne.900750107

Olsen, S. R., Bhandawat, V., & Wilson, R. I. (2010). Divisive Normalization in Olfactory Population Codes. *Neuron*, *66*(2), 287–299. https://doi.org/10.1016/j.neuron.2010.04.009

Pachitariu, M., Sridhar, S., & Stringer, C. (2023). Solving the spike sorting problem with Kilosort. *BioRxiv*, 2023.01.07.523036. https://doi.org/10.1101/2023.01.07.523036

Pachitariu, M., Steinmetz, N., Kadir, S., Carandini, M., & D, H. K. (2016). *Kilosort: realtime spike-sorting for extracellular electrophysiology with hundreds of channels*. https://dx.doi.org/10.1101/061481

Pack, C. C., Born, R. T., & Livingstone, M. S. (2003). Two-Dimensional Substructure of Stereo and Motion Interactions in Macaque Visual Cortex. *Neuron*, *37*(3), 525–535. https://doi.org/10.1016/s0896-6273(02)01187-x

Pardhan, S., Gilchrist, J., Douthwaite, W., & Yap, M. (1990). Binocular Inhibition: Psychophysical and Electrophysiological Evidence. *Optometry and Vision Science*, *67*(9), 688–691. https://doi.org/10.1097/00006324-199009000-00006

Parker, A. J., & Cumming, B. G. (2001). Chapter 14 Cortical mechanisms of binocular stereoscopic vision. *Progress in Brain Research*, *134*, 205–216. https://doi.org/10.1016/s0079-6123(01)34015-3

Parker, A. J., Smith, J. E. T., & Krug, K. (2016). Neural architectures for stereo vision. *Philosophical Transactions of the Royal Society B: Biological Sciences*, *371*(1697), 20150261. https://doi.org/10.1098/rstb.2015.0261

Peirce, J. W. (2007). The potential importance of saturating and supersaturating contrast response functions in visual cortex. *Journal of Vision*, *7*(6), 13. https://doi.org/10.1167/7.6.13

Pettigrew, J. D., Nikara, T., & Bishop, P. O. (1968). Binocular interaction on single units in cat striate cortex: Simultaneous stimulation by single moving slit with receptive fields in correspondence. *Experimental Brain Research*, *6*(4), 391–410. https://doi.org/10.1007/bf00233186

Pirenne, M. H. (1943). Binocular and Uniocular Threshold of Vision. *Nature*, *152*(3867), 698–699. https://doi.org/10.1038/152698a0

Poggio, G. F. (1995). Mechanisms of Stereopsis in Monkey Visual Cortex. *Cerebral Cortex*, *5*(3), 193–204. https://doi.org/10.1093/cercor/5.3.193

Poggio, G. F., & Fischer, B. (1977). Binocular interaction and depth sensitivity in striate and prestriate cortex of behaving rhesus monkey. *Journal of Neurophysiology*, *40*(6), 1392–1405. https://doi.org/10.1152/jn.1977.40.6.1392

Poggio, G., Gonzalez, F., & Krause, F. (1988). Stereoscopic mechanisms in monkey visual cortex: binocular correlation and disparity selectivity. *The Journal of Neuroscience*, *8*(12), 4531–4550. https://doi.org/10.1523/jneurosci.08-12-04531.1988

Priebe, N. J. (2008). The relationship between subthreshold and suprathreshold ocular dominance in cat primary visual cortex. *The Journal of Neuroscience : The Official Journal of the Society for Neuroscience*, *28*(34), 8553–8559. https://doi.org/10.1523/jneurosci.2182-08.2008

Priebe, N. J., & Ferster, D. (2008). Inhibition, Spike Threshold, and Stimulus Selectivity in Primary Visual Cortex. *Neuron*, *57*(4), 482–497. https://doi.org/10.1016/j.neuron.2008.02.005

Priebe, N. J., & Ferster, D. (2012). Mechanisms of Neuronal Computation in Mammalian Visual Cortex. *Neuron*, *75*(2), 194–208. https://doi.org/10.1016/j.neuron.2012.06.011

Qian, C. S., & Brascamp, J. W. (2017). How to Build a Dichoptic Presentation System That Includes an Eye Tracker. *Journal of Visualized Experiments : JoVE*, *127*. https://doi.org/10.3791/56033

Rathjen, S., Schmidt, K. E., & Löwel, S. (2002). Two-dimensional analysis of the spacing of ocular dominance columns in normally raised and strabismic kittens. *Experimental Brain Research*, *145*(2), 158–165. https://doi.org/10.1007/s00221-002-1086-9

Ray, S., Ni, A. M., & Maunsell, J. H. R. (2013). Strength of Gamma Rhythm Depends on Normalization. *PLoS Biology*, *11*(2), e1001477. https://doi.org/10.1371/journal.pbio.1001477

Read, J. (2005). Early computational processing in binocular vision and depth perception. *Progress in Biophysics and Molecular Biology*, *87*(1), 77–108. https://doi.org/10.1016/j.pbiomolbio.2004.06.005

Read, J. C. A., & Cumming, B. G. (2003). Testing Quantitative Models of Binocular Disparity Selectivity in Primary Visual Cortex. *Journal of Neurophysiology*, *90*(5), 2795–2817. https://doi.org/10.1152/jn.01110.2002

Read, J. C. A., & Cumming, B. G. (2004). Ocular Dominance Predicts Neither Strength Nor Class of Disparity Selectivity With Random-Dot Stimuli in Primate V1. *Journal of Neurophysiology*, *91*(3), 1271–1281. https://doi.org/10.1152/jn.00588.2003

Read, J. C. A., Parker, A. J., & Cumming, B. G. (2002). A simple model accounts for the response of disparity-tuned V1 neurons to anticorrelated images. *Visual Neuroscience*, *19*(6), 735–753. https://doi.org/10.1017/s0952523802196052

Rubin, D. B., Van Hooser, S. D., & Miller, K. D. (2015). The Stabilized Supralinear Network: A Unifying Circuit Motif Underlying Multi-Input Integration in Sensory Cortex. *Neuron*, *85*(2), 402–417. https://doi.org/10.1016/j.neuron.2014.12.026

Said, C. P., & Heeger, D. J. (2013). A Model of Binocular Rivalry and Cross-orientation Suppression. *PLoS Computational Biology*, *9*(3), e1002991. https://doi.org/10.1371/journal.pcbi.1002991

Salthouse, T. A., & Ellis, C. L. (1980). Determinants of eye-fixation duration. *The American Journal of Psychology*, *93*(2), 207–234.

Sawada, T., & Petrov, A. A. (2017). The divisive normalization model of V1 neurons: a comprehensive comparison of physiological data and model predictions. *Journal of Neurophysiology*, *118*(6), 3051–3091. https://doi.org/10.1152/jn.00821.2016

Schroeder, C. E., Tenke, C. E., Arezzo, J. C., & Vaughan, H. G. (1990). Binocularity in the lateral geniculate nucleus of the alert macaque. *Brain Research*, *521*(1–2), 303–310. https://doi.org/10.1016/0006-8993(90)91556-v

Schroeder, C. E., Tenke, C. E., Givre, S. J., Arezzo, J. C., & Vaughan, H. G. (1991). Striate cortical contribution to the surface-recorded pattern-reversal vep in the alert monkey. *Vision Research*, *31*(7–8), 1143–1157. https://doi.org/10.1016/0042-6989(91)90040-c

Schwartz, O., & Simoncelli, E. P. (2001). Natural signal statistics and sensory gain control. *Nature Neuroscience*, *4*(8), 819–825. https://doi.org/10.1038/90526

Schwarzkopf, D. S., Schindler, A., & Rees, G. (2010). Knowing with Which Eye We See: Utrocular Discrimination and Eye-Specific Signals in Human Visual Cortex. *PLoS ONE*, *5*(10), e13775. https://doi.org/10.1371/journal.pone.0013775

Sclar, G., Ohzawa, I., & Freeman, R. D. (1986). Binocular summation in normal, monocularly deprived, and strabismic cats: visual evoked potentials. *Experimental Brain Research*, *62*(1), 1–10. https://doi.org/10.1007/bf00237398

Sengpiel, F., Baddeley, R. J., Freeman, T. C. B., Harrad, R., & Blakemore, C. (1998). Different mechanisms underlie three inhibitory phenomena in cat area 17. *Vision Research*, *38*(14), 2067–2080. https://doi.org/10.1016/s0042-6989(97)00413-6

Sengpiel, F., & Blakemore, C. (1994). Interocular control of neuronal responsiveness in cat visual cortex. *Nature*, *368*(6474), 847–850. https://doi.org/10.1038/368847a0

Sengpiel, F., & Blakemore, C. (1996). The neural basis of suppression and amblyopia in strabismus. *Eye*, *10*(2), 250–258. https://doi.org/10.1038/eye.1996.54

Shatz, C. J., Lindstro¨m, S., & Wiesel, T. N. (1977). The distribution of afferents representing the right and left eyes in the cat's visual cortex. *Brain Research*, *131*(1), 103–116. https://doi.org/10.1016/0006-8993(77)90031-2

Shatz, C. J., & Stryker, M. P. (1978). Ocular dominance in layer IV of the cat's visual cortex and the effects of monocular deprivation. *The Journal of Physiology*, *281*(1), 267–283. https://doi.org/10.1113/jphysiol.1978.sp012421

Sherman, S. M., & Guillery, R. W. (2002). The role of the thalamus in the flow of information to the cortex. *Philosophical Transactions of the Royal Society of London. Series B: Biological Sciences*, *357*(1428), 1695–1708. https://doi.org/10.1098/rstb.2002.1161

Sincich, L. C., Jocson, C. M., & Horton, J. C. (2012). Neuronal projections from V1 to V2 in amblyopia. *The Journal of Neuroscience : The Official Journal of the Society for Neuroscience*, *32*(8), 2648–2656. https://doi.org/10.1523/jneurosci.4799-11.2012

Smith, E. L., Chino, Y., Ni, J., & Cheng, H. (1997). Binocular Combination of Contrast Signals by Striate Cortical Neurons in the Monkey. *Journal of Neurophysiology*, *78*(1), 366–382. https://doi.org/10.1152/jn.1997.78.1.366

Somers, D. C., Todorov, E. V., Siapas, A. G., Toth, L. J., Kim, D. S., & Sur, M. (1998). A local circuit approach to understanding integration of long-range inputs in primary visual cortex. *Cerebral Cortex (New York, N.Y. : 1991)*, *8*(3), 204–217. https://doi.org/10.1093/cercor/8.3.204

Sparks, D., Mays, L., Gurski, M., & Hickey, T. (1986). Long- and short-term monocular deprivation in the rhesus monkey: effects on visual fields and optokinetic nystagmus. *The Journal of Neuroscience*, *6*(6), 1771–1780. https://doi.org/10.1523/jneurosci.06-06-01771.1986

Stryker, M. P. (1978). Postnatal development of ocular dominance columns in layer IV of the cat's visual cortex and the effects of monocular deprivation. *Archives Italiennes de Biologie*, *116*(3–4), 420–426.

Supèr, H., & Roelfsema, P. R. (2005). Chronic multiunit recordings in behaving animals: advantages and limitations. In *Development, Dynamics and Pathiology of Neuronal Networks: from Molecules to Functional Circuits* (Vol. 147, pp. 263–282). Elsevier. https://doi.org/10.1016/s0079-6123(04)47020-4

Swindale, N. V. (1981). Absence of ocular dominance patches in dark-reared cats. *Nature*, *290*(5804), 332–333. https://doi.org/10.1038/290332a0

Tanabe, S., & Cumming, B. G. (2008). Mechanisms Underlying the Transformation of Disparity Signals from V1 to V2 in the Macaque. *Journal of Neuroscience*, *28*(44), 11304–11314. https://doi.org/10.1523/jneurosci.3477-08.2008

Tanaka, K. (1985). Organization of geniculate inputs to visual cortical cells in the cat. *Vision Research*, *25*(3), 357–364. https://doi.org/10.1016/0042-6989(85)90060-4

Tao, C., He, Z., Chen, Y., Zhou, J., & Hess, R. F. (2020). Can ocular dominance plasticity provide a general index to visual plasticity to personalize treatment in amblyopia? *MedRxiv*, 2020.03.26.20044701. https://doi.org/10.1101/2020.03.26.20044701

Thiele, A., Pooresmaeili, A., Delicato, L. S., Herrero, J. L., & Roelfsema, P. R. (2009). Additive Effects of Attention and Stimulus Contrast in Primary Visual Cortex. *Cerebral Cortex (New York, NY)*, *19*(12), 2970–2981. https://doi.org/10.1093/cercor/bhp070

Tieman, D. G., McCall, M. A., & Hirsch, H. V. (1983). Physiological effects of unequal alternating monocular exposure. *Journal of Neurophysiology*, *49*(3), 804–818. https://doi.org/10.1152/jn.1983.49.3.804

Tootell, R., Hamilton, S., Silverman, M., & Switkes, E. (1988). Functional anatomy of macaque striate cortex. I. Ocular dominance, binocular interactions, and baseline conditions. *The Journal of Neuroscience*, *8*(5), 1500–1530. https://doi.org/10.1523/jneurosci.08-05-01500.1988

Troyer, T. W., Krukowski, A. E., Priebe, N. J., & Miller, K. D. (1998). Contrast-Invariant Orientation Tuning in Cat Visual Cortex: Thalamocortical Input Tuning and Correlation-Based Intracortical Connectivity. *The Journal of Neuroscience*, *18*(15), 5908–5927. https://doi.org/10.1523/jneurosci.18-15-05908.1998

Truchard, A. M., Ohzawa, I., & Freeman, R. D. (2000). Contrast gain control in the visual cortex: monocular versus binocular mechanisms. *J Neurosci*, *20*, 3017–3032. https://www.ncbi.nlm.nih.gov/pubmed/10751454

Tsang, E. K. C., & Shi, B. E. (2008). Normalization Enables Robust Validation of Disparity Estimates from Neural Populations. *Neural Computation*, *20*(10), 2464–2490. https://doi.org/10.1162/neco.2008.05-07-532

Tyler, C. W., & Apkarian, P. A. (1985). Effects of contrast, orientation and binocularity in the pattern evoked potential. *Vision Research*, *25*(6), 755–766. https://doi.org/10.1016/0042-6989(85)90183-x

Vanni, S., Hokkanen, H., Werner, F., & Angelucci, A. (2020). Anatomy and Physiology of Macaque Visual Cortical Areas V1, V2, and V5/MT: Bases for Biologically Realistic Models. *Cerebral Cortex*, *30*(6), 3483–3517. https://doi.org/10.1093/cercor/bhz322

Vastola, E. F. (1960). Binocular inhibition in the lateral geniculate body. *Experimental Neurology*, *2*(3), 221–231. https://doi.org/10.1016/0014-4886(60)90010-8

Wallace, M. T., Roberson, G. E., Hairston, W. D., Stein, B. E., Vaughan, J. W., & Schirillo, J. A. (2004). Unifying multisensory signals across time and space. *Experimental Brain Research*, *158*(2), 252–258. https://doi.org/10.1007/s00221-004-1899-9

Westerberg, J. A., Cox, M. A., Dougherty, K., & Maier, A. (2019). V1 microcircuit dynamics: altered signal propagation suggests intracortical origins for adaptation in response to visual repetition. *Journal of Neurophysiology*, *121*(5), 1938–1952. https://doi.org/10.1152/jn.00113.2019

White, C. T., & Bonelli, L. (1970). BINOCULAR SUMMATION IN THE EVOKED POTENTIAL AS A FUNCTION OF IMAGE QUALITY*. *Optometry and Vision Science*, *47*(4), 304–309. https://doi.org/10.1097/00006324-197004000-00007

Wiesel, T. N. (1982). Postnatal development of the visual cortex and the influence of environment. *Nature*, *299*(5884), 583–591. https://doi.org/10.1038/299583a0

Wiesel, T. N., & Hubel, D. H. (1963). SINGLE-CELL RESPONSES IN STRIATE CORTEX OF KITTENS DEPRIVED OF VISION IN ONE EYE. *Journal of Neurophysiology*, *26*(6), 1003–1017. https://doi.org/10.1152/jn.1963.26.6.1003

Wiesel, T. N., Hubel, D. H., & Lam, D. M. K. (1974). Autoradiographic demonstration of ocular-dominance columns in the monkey striate cortex by means of transneuronal transport. *Brain Research*, *79*(2), 273–279. https://doi.org/10.1016/0006-8993(74)90416-8

Wilming, N., Onat, S., Ossandón, J. P., Açık, A., Kietzmann, T. C., Kaspar, K., Gameiro, R. R., Vormberg, A., & König, P. (2017). An extensive dataset of eye movements during viewing of complex images. *Scientific Data*, *4*(1), 160126. https://doi.org/10.1038/sdata.2016.126

Wong-Riley, M. (1979). Changes in the visual system of monocularly sutured or enucleated cats demonstrable with cytochrome oxidase histochemistry. *Brain Research*, *171*(1), 11–28. https://doi.org/10.1016/0006-8993(79)90728-5

Yang, Y., Liu, S., Chowdhury, S. A., DeAngelis, G. C., & Angelaki, D. E. (2011). Binocular Disparity Tuning and Visual-Vestibular Congruency of Multisensory Neurons in Macaque Parietal Cortex. *Journal of Neuroscience*, *31*(49), 17905–17916. https://doi.org/10.1523/jneurosci.4032-11.2011

Yehezkel, O., Ding, J., Sterkin, A., Polat, U., & Levi, D. M. (2016). Binocular combination of stimulus orientation. *Royal Society Open Science*, *3*(11), 160534. https://doi.org/10.1098/rsos.160534

Zhang, S.-H., Zhao, X.-N., Jiang, D.-Q., Tang, S.-M., & Yu, C. (2024). Ocular dominance-dependent binocular combination of monocular neuronal responses in macaque V1. *ELife*, *13*, RP92839. https://doi.org/10.7554/elife.92839

Zhao, X., Liu, M., & Cang, J. (2013). Sublinear Binocular Integration Preserves Orientation Selectivity in Mouse Visual Cortex. *Nature Communications*, *4*(1), 2088–2088. https://doi.org/10.1038/ncomms3088

Zhou, H., & Desimone, R. (2011). Feature-Based Attention in the Frontal Eye Field and Area V4 during Visual Search. *Neuron*, *70*(6), 1205–1217. https://doi.org/10.1016/j.neuron.2011.04.032

Zhou, J., Liu, R., Feng, L., Zhou, Y., & Hess, R. F. (2016). Deficient Binocular Combination of Second-Order Stimuli in Amblyopia. *Investigative Opthalmology & Visual Science*, *57*(4), 1635. https://doi.org/10.1167/iovs.15-18253